Prediction
Of
Earthquakes

Euan Macpherson Fraser

Submitted for the Degree of M.Sc. at The University of Glasgow
in the Department of Mathematics,
October 1997.

ProQuest LLC.
789 East Eisenhower Parkway
P.O. Box 1346
Ann Arbor, MI 48106 – 1346

Abstract

We start by introducing the reader to the mechanisms behind earthquake production, including the Elastic Rebound Theory and the theory of Plate Tectonics. We also discuss the quantification of earthquakes in terms of magnitude, intensity and energy released. A short review of the history of earthquake prediction is also given, along with a discussion of some of the latest attempts at discovering seismic precursors. The VAN method, and the controversy surrounding it are discussed in some depth in chapter 5, while the theory of Seismic Gaps is introduced in chapter 6. Experiments using cellular automata to model earthquake production are performed in chapter 7, and the resulting analysis presented. The use of mechanical models is explored in chapter 8, where the slider block model is analysed. The Hurst analysis of a time series is introduced, and real earthquake data analysed in detail. A short discussion of fractal dimensions is given in chapter 10, where we present some classic fractals such as the Sierpinski gasket and the Koch curve. The Hausdorff dimension is introduced, and the idea of Box counting dimension discussed. The calculation of the correlation dimension is then presented. This is then used in chapter 11, where we present a new prediction method, based upon fluctuations in the correlation dimension. The results obtained using this method are outlined, as are some hopes for the future of earthquake prediction.

Contents

Chapter 1

Introduction

"If I were a brilliant scientist, I would be working in Earthquake Prediction"
Los Angeles talk show host(1994).

In 1964, Charles Richter, of Richter Scale fame, made the following quote: *"Claims to predict earthquakes usually come from cranks, publicity seekers, or people who pretend to foresee the future in general".*

The aim of this thesis is to discuss a variety of different techniques used for the prediction of earthquakes. These techniques range from the measurement of geophysical data and the inferences to be made from the resulting information, to the use of statistical techniques and finally, the use of mathematical models. We then extend the work, proposing a new technique, and giving examples of any predictions made and their successes and/or failures.

1.1 History

Throughout the history of mankind, earthquake prediction has been the focus of myths, folklore and sorcery. Earthquake prediction has always created controversy, with many people claiming that the mechanism is so complicated that earthquakes will never be predicted. The opposite viewpoint states that we have learnt so much about the earth, and progressed so far that, if we only do more research and perform more experiments, then we will eventually be able to predict them.

1.2 The reasons for earthquake prediction

World-wide, there are on average, 18 earthquakes every year with a magnitude of 7.0 or larger. These earthquakes, if they occur in highly populated areas, can be very destructive and cause great loss of life. In many parts of the world earthquakes represent severe natural hazards, and thus earthquake prediction could save human life. Earthquakes have, throughout history, been responsible for a huge number of deaths. It is estimated that, world-wide, there have been in excess of 7,000,000 deaths. Many of these deaths have occurred in the last 100 years, as populations and population densities have increased. In many cases, it is not the actual earthquake that causes the fatalities, but rather the after-effects of the quake, such as tsunamis, fires, landslides, and floods.

1.3 Where?

The distribution of earthquakes has a distinct spatial pattern. The reasons for this distribution will be discussed fully in the next chapter. The main areas which have earthquake problems are those countries which lie on the Pacific Rim, i.e. Japan, Chile, USA etc. Other nations affected include the old USSR, the Middle East and Greece.

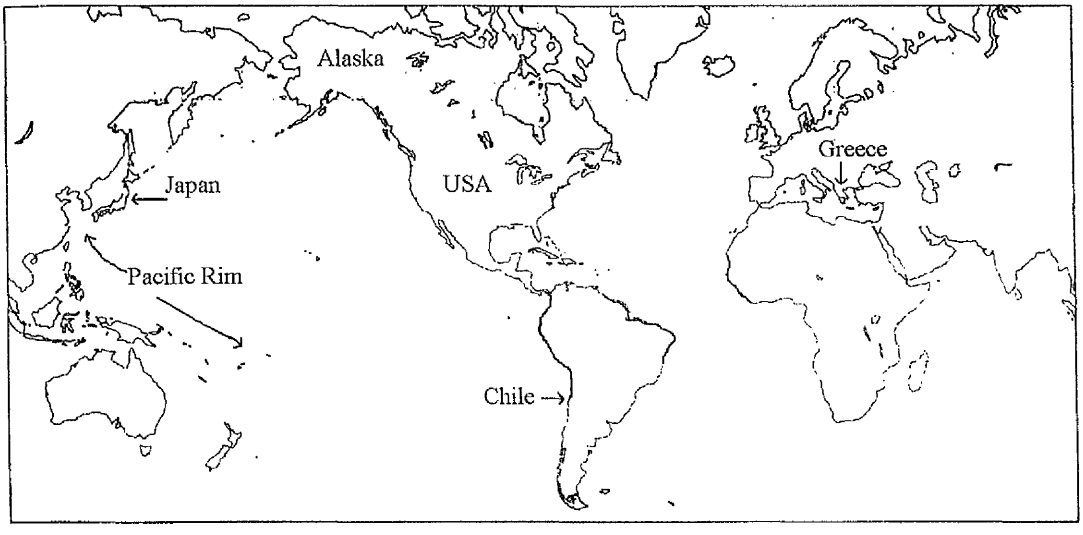

(Figure 1.1 World Map)

Most of the countries which are affected by earthquakes have some form of earthquake prediction programme. For example, Japan spends millions of dollars, or billions of Yen, every year in an attempt to predict earthquakes. Since 1965 it has spent over $1 Billion on its earthquake prediction schemes. The old USSR, China, the United States of America and Greece all have substantial programmes of earthquake research. In the USA, earthquakes result in 70 million people living with a significant risk to their lives and property. In Los Angeles, a great earthquake could take 15,000 lives, and cause damage of over $25 Billion.

1.4 What constitutes a prediction?

When making a valid prediction, we need to specify certain quantities, ensuring that they are within narrow limits. We need to state the following :

1. The period within which the event will occur.
2. The Location of the Earthquake, within a specified tolerance.
3. The Magnitude range.
4. The odds that an earthquake of this type could occur purely by chance.

All of the above must be stated with an accuracy sufficient to ensure that the ultimate success or failure may be judged. See *Rundle, Turcotte & Klein*[1996] for more information.

1.5 Warnings and Predictions

A *prediction* is a neutral statement that accumulated observations seem to signal clearly the occurrence of an earthquake. A *warning* is a declaration that normal life routines should be changed for a period of time due to an impending danger. It should also advise the public of what procedures to follow. These two definitions are different: predictions are based purely on science, while warnings are interpretations of predictions based on current public policy.

Chapter 2

Earthquake Theory

2.1 Introduction

In this section we shall give a brief explanation of the theory underlying earthquake occurrence. The structure of the Earth, the theory of Plate Tectonics and crustal faults are all discussed. We shall also list some of the key definitions and terminology which will be used throughout the remainder of this thesis.

2.2 Earth Structure

For simplicity, the earth can be thought of as a sphere. In reality, it is an oblate spheroid, as it is flattened at the poles and bulges at the equator. This squashing is due to the forces resulting from the Earth's rotation. We can split the interior of the Earth into a number of sections, including the mantle, the core and the crust. In figure 2.1, below, a schematic of the Earth's interior is given.

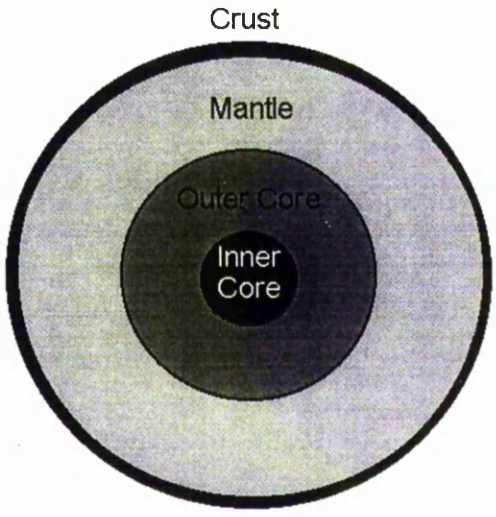

(Figure 2.1- Schematic of Earth's Interior)

The inner core is solid, due to the intense pressure it is under, while the outer core is liquid. The mantle can be thought of as a very viscous fluid, which is capable of plastic flow. The crust is a shell of cold, solidified rock on the outside of the sphere. We are interested in the Earth's crust, its movements, and the theory of Plate Tectonics.

2.3 The Earth's Crust

The Earth's crust has been formed over time by the cooling of molten rock from the mantle. The crust is not one solid object, and does not have a uniform thickness, or density. In fact, the thickness of the crust can vary significantly, from over 50 kilometres thick beneath the continents, while only a few kilometres thick under the ocean. Figure 2.2, below, illustrates some of the points discussed above. Note that the crust "floats" on top of the mantle.

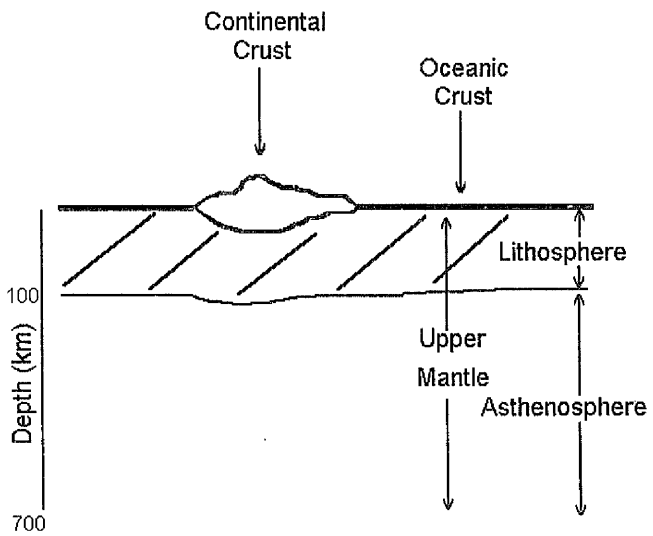

(Figure 2.2 The Earth's Crust and Upper Mantle)

The uppermost layer of the mantle and the crust, approximately 100 kilometres in depth, is usually called the *Lithosphere*. It is a rigid zone, and is stronger than the *Asthenosphere*, which lies directly beneath it. The Asthenosphere is a ductile solid, and can flow plastically. It is usually thought of as being a "weak zone".

The crust is formed from a variety of different types of minerals and rocks. The rock type is dependent upon the chemical composition and the conditions under which the rocks were formed. This explains the variation in the densities of the rocks. As the crust is not one solid body, there are a number of fractures or ruptures in the structure. They are known as faults, and at these locations, rock movement can occur.

2.4 Faults

In this section, we will describe the different types of faults that occur, but first we must make a number of definitions. These definitions are adapted from those given by Lapidus[1987].

Definition 2.1

A *fault* is a fracture in earth materials, along which the opposite sides have been relatively displaced parallel to the plane of movement. That is, a break in the Earth's crust.

Definition 2.2

The surface along which movement takes place is known as the *fault plane* (or *fault surface*, as it is not necessarily a plane).

Movement along a fault occurs in two ways, by continuous creep, or in abrupt jumps. As the name suggests, continuous creep is a gradual process, with the two portions of rock sliding past each other bit by bit. If we have a series of abrupt jumps, then the crust may move in steps of a few metres over a time scale of several seconds.

It is believed that most earthquakes are caused by this mechanism. There are three main types of fault, a normal fault, a reverse fault and a strike-slip fault, see *Kearey & Vine*[1996]. These three faults are illustrated below, in figures 2.3 - 2.5.

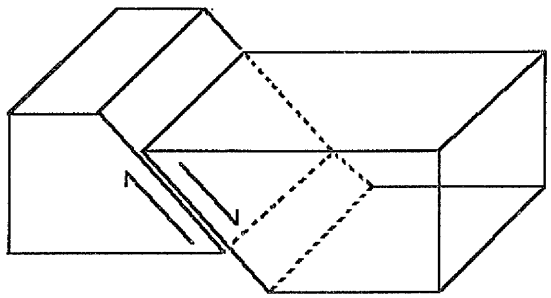

(Figure 2.3 A Normal Fault)

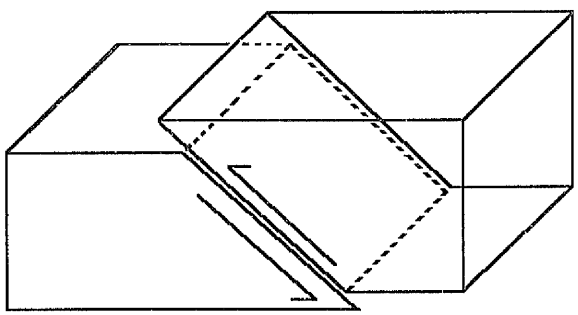

(Figure 2.4 A Reverse Fault)

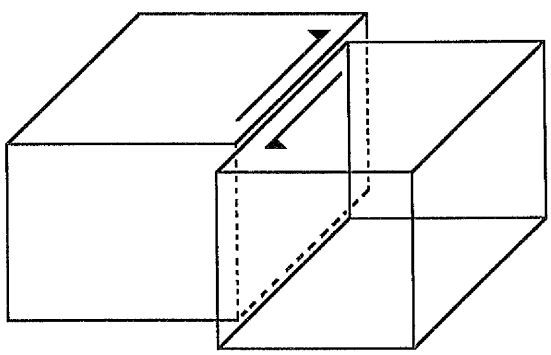

(Figure 2.5 Strike Slip Faults)

2.5 Plate Tectonics

The theory of Plate Tectonics states that the Earth's lithosphere is not one solid object, but instead is composed of a series of interlocking "plates", which cover the entire surface of the planet, see *Kearey & Vine*[1996] and *Bolt*[1993]. The plates move relative to each other, with the main driving force being convection currents in the mantle. The lithospheric plates slide over the weak, and ductile, asthenosphere. Figure 2.6, below, is an illustration of the world-wide distribution of earthquakes. The epicentre of each earthquake is represented by a black dot drawn on a world map. Earthquakes do not occur everywhere, but are restricted to certain narrow regions. These strips define the positions of the plate boundaries.

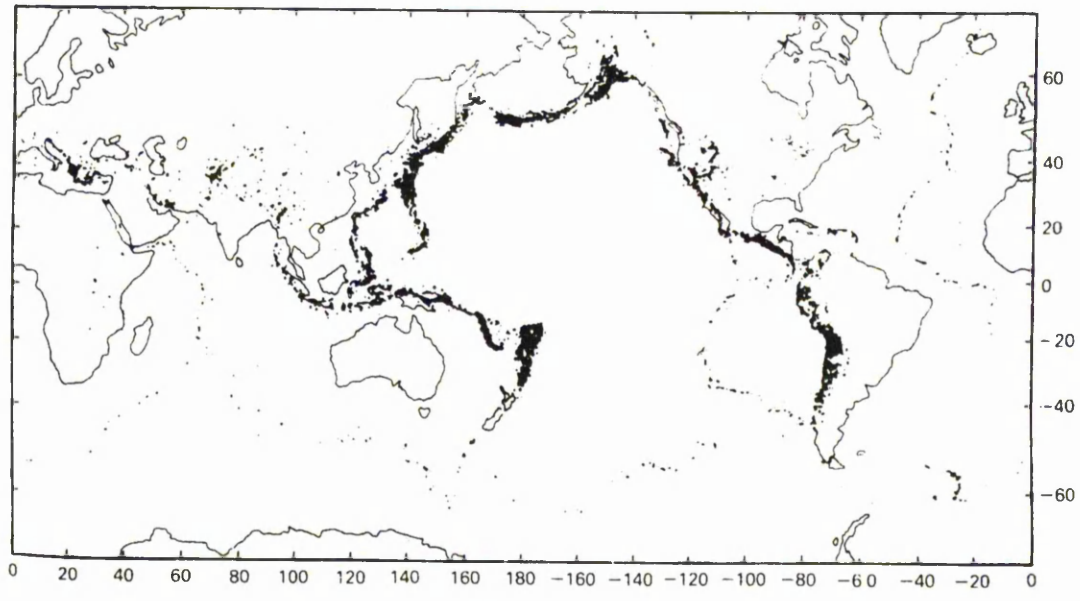

(Figure 2.6 World-wide Earthquake Distribution 1993-1996)

It is in these boundary areas that almost all the seismic activity is concentrated, and in which we are most interested. It was also postulated that away from the boundaries, in the middle of the tectonic plates, we would have aseismic regions, with almost no earthquake activity. The theory states that there are 3 different types of boundary. Figure 2.7, below shows the main tectonic plates, and their boundaries.

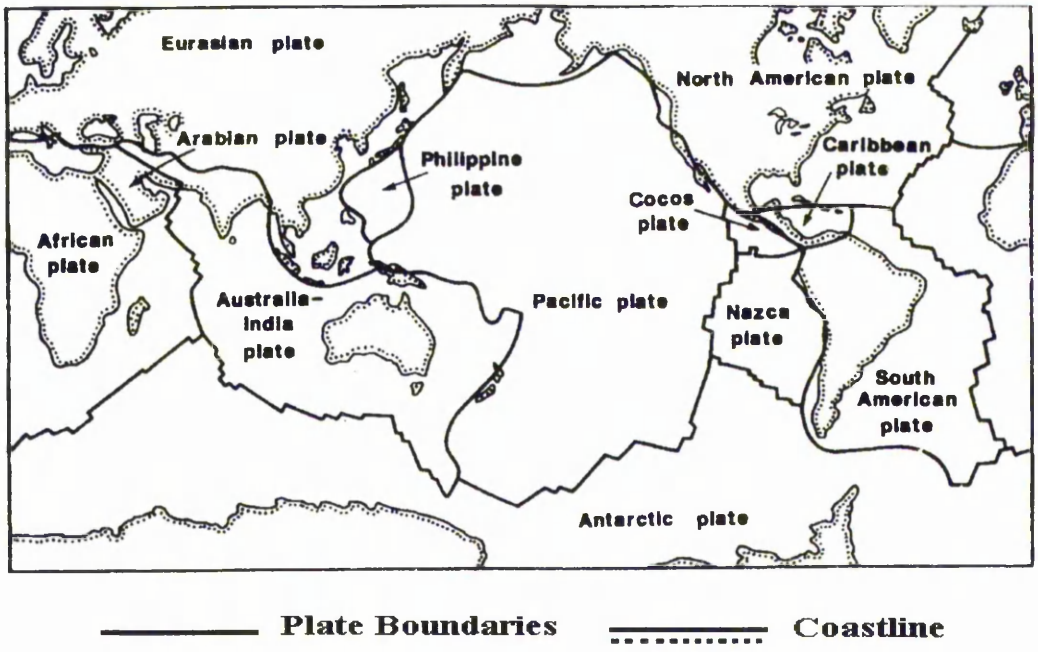

(Figure 2.7 Tectonic Plates)

2.5.1 Constructive Boundaries or Mid-Oceanic Ridges

A *mid-ocean ridge* is a continuous feature which extends through all the oceans of the Earth. It occurs within the Earth's oceans, at places where two tectonic plates are moving away from each other. At these points, new lithosphere is grown by the solidification of molten rock from the Earth's interior. Where the two plates are separating, molten rock, or magma, wells up into the resultant gap. This material slowly cools to produce a new sliver of sea floor. A simplified diagram of this process is shown below, see figure 2.8.

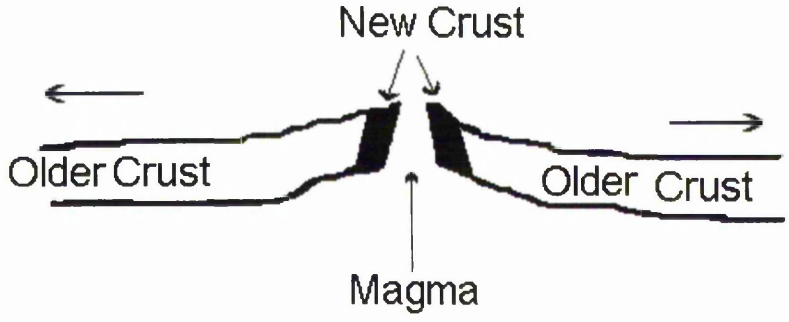

(Figure 2.8 Sea Floor Spreading)

This mechanism is known as sea-floor spreading and occurs at a rate of approximately 4 centimetres per year. In these regions, there are a large number of earthquakes, caused by the plate movements. Once again see *Kearey & Vine*[1996].

2.5.2 Destructive Boundaries or Subduction Zones

A *subduction zone* is a region where two tectonic plates are moving towards each other slowly. The denser plate is forced under the other, and the under-riding plate is gradually re-absorbed in to the mantle, i.e. the plate is destroyed. Hence, subduction zones are also known as *destructive boundaries*. In figure 2.9, below, a schematic of the process involved is given. The bottom plate is absorbed as it is forced down into a high pressure and temperature environment. The angle of subduction depends upon the composition of the bottom plate (*Kearey & Vine*[1996]). Earthquakes are also produced in this area, due to the stresses being applied to deform the bottom plate. Volcanic activity occurs as a result of these subduction zones. As the lower plate is absorbed into the mantle, partially melted rocks can separate from the plate, and rise to the surface, resulting in the appearance of a volcano at a point on the top plate.

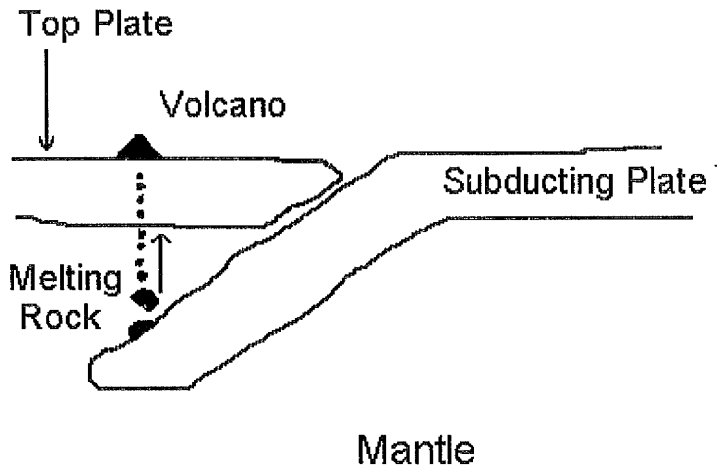

(Figure 2.9 Subduction Zone)

2.5.3 Conservative Plate Boundaries

At conservative plate boundaries, crust is neither created nor destroyed. These boundaries are called transcurrent, or strike-slip faults, see figure 2.5. As stated before, at these faults we have two plates which are sliding past each other. Earthquakes occur at these boundaries when we have a sudden movement along the fault.

2.6 Earthquakes

An earthquake is defined as: "A rumbling or trembling of the ground produced by the sudden breaking of rocks in response to geological forces within the Earth" This trembling is caused by the sudden release of large quantities of energy which have been stored in the Earth's crust. The elastic properties of the rocks in the crust allow energy to be stored during deformation caused by tectonic forces. When the strain in the rock exceeds the strength of the crust in a critically weak area, i.e. a geological fault, then we get slippage, and the two plates jump, releasing the elastic energy. This energy is released as seismic waves, and it is these waves which constitute an earthquake. This process is described more fully in the next section.

Earthquakes are usually assumed to have originated from a single point, known as the *hypocentre,* within the Earth. It is the initial rupture point of the earthquake. This is a simplification, as most earthquakes do not occur at a single point, but originate from a "focal region" which may extend over a few kilometres. The *epicentre* is the point on the Earth's surface directly above the hypocentre.

2.7 Elastic Rebound Theory

The majority of the world's earthquakes are believed to occur according to the *elastic rebound theory*, which was proposed by *Reid*[1911]. It was developed due to observations made after the 1906 San Francisco earthquake. In essence, this theory proposes that an earthquake, or movement along a fault, is due to a sudden release of elastic strain energy. This elastic strain is built up by deformation caused by the tectonic process over a period of time. It postulates that this release of energy returns the rocks to a state with very little elastic strain. A set of diagrams representing the main points of the elastic rebound theory is given below, in figure 2.10. The figures below all represent a block of rock in which there is a pre-existing fault. Note that, in figure 2.10(a), the broken line XY represents the fault, and the arrows represent the direction in which the two blocks are moving. This movement introduces the elastic strain to the system, and results in movement along the direction of the fault. The line PQ is a marker, which allows us to demonstrate the increasing strain in the system.

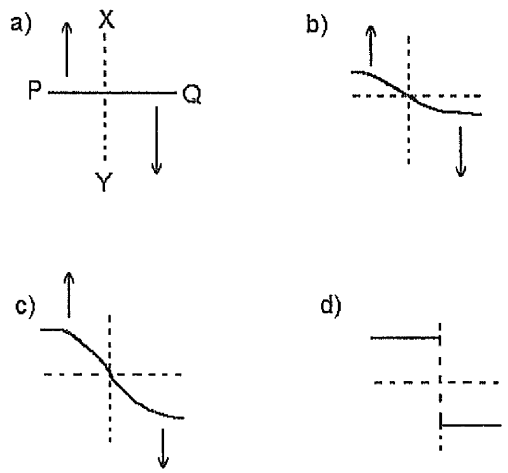

(Figure 2.10 The Elastic Rebound Theory)

As the build up in stress continues, at some point the elastic strain will exceed a critical value, and will be greater than the frictional and cementing forces, which are preventing movement. This is represented by figure 2.10(c), above. When this happens, fault movement occurs instantaneously, and we progress to figure 2.10(d).

The movement of the fault reduces the strain in the crust to almost zero, but if the forces acting on the crustal blocks persist, then eventually we will get a further build-up of strain energy, which will result in further fault movement. In essence, what the theory proposes is that we go through a continuous cycle of building up strain slowly, releasing it suddenly through an earthquake, then gradually increasing the strain again.

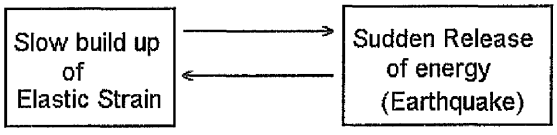

(Figure 2.11 Earthquake Cycle)

2.8 Seismic Waves

Part of the energy released by an earthquake is released in the form of seismic waves. There are a number of different types of seismic waves, but they are all propagated by elastic deformation of the medium through which they travel. To fully discuss the production, and transmission, of seismic waves requires a detailed knowledge of continuum mechanics and elasticity. Therefore, we will restrict ourselves to give a general overview of seismic waves.

There are two categories of waves: *body waves*, which travel through the interior of the Earth, and *surface waves*, which travel at, or close to, the Earth's surface. Within these categories, there are a number of different types of waves.

2.8.1 Body Waves

There are two different types of body waves, namely *P-waves* and *S-waves*. These two waves correspond to the different ways that an elastic solid can be deformed to produce waves. A P-wave, or primary wave, so called because it travels faster than the other waves, is produced by compression of the medium. The particles

of the rock are made to vibrate along the direction of propagation. What results is a series of compressions and rarefactions. Note that this type of wave is equivalent to a sound wave through air. Figure 2.12 is a diagram illustrating the movement of particles in the medium through which the wave is travelling. A secondary, or S-wave, is produced by shear deformation, perpendicular to the direction of propagation. Again this is illustrated in figure 2.12. Fluids cannot support shear, thus S waves cannot be transmitted through a fluid. Consequently, S waves are unable to pass through the Outer Core of the Earth, as this is a liquid. In fact, this is the main evidence that the Outer Core is a fluid.

2.8.2 Surface Waves

When earthquakes occur close to the surface of the Earth, then some of the seismic energy is constrained to travel close to the surface, and it is emitted as surface waves. As with body waves, there are two types of surface waves. *Rayleigh waves* result in the particles of the rock following an elliptical path in a vertical plane, while *Love waves* are horizontal shear waves.

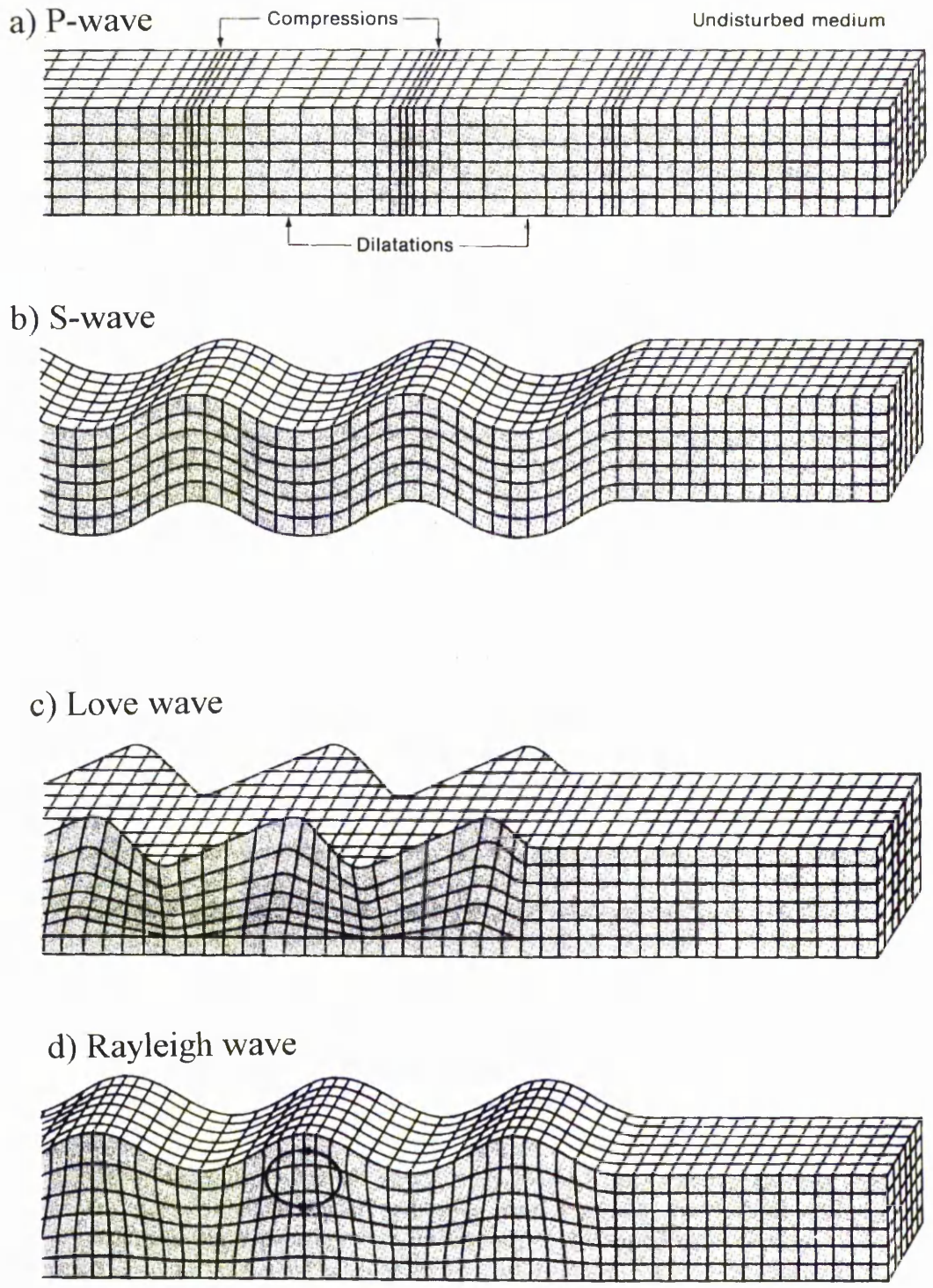

(Figure 2.12 Particle movement in Seismic Waves)

2.9 Seismometers

The different types of wave outlined in the previous section can all be detected by an instrument known as a *seismometer*. This instrument is the basis for much of modern day seismology. Almost all seismometers are based on the principle of inertia. They consist of two main parts, a frame and a heavy pendulum. The frame is secured to the rock, while the pendulum is allowed to swing freely, but is constrained to move in only one plane. When a seismic wave passes our measuring station, it causes the ground to move. This results in the frame of the instrument moving. As the pendulum is free to swing, and because of the inertial properties of the heavy mass, the pendulum tends to stay still. As a result, we have relative motion between the pendulum and the frame. This motion can be recorded by attaching a pen to the end of the pendulum. The resulting trace is known as a *seismogram*. Figure 2.13, below, illustrates the main elements of a simple seismometer.

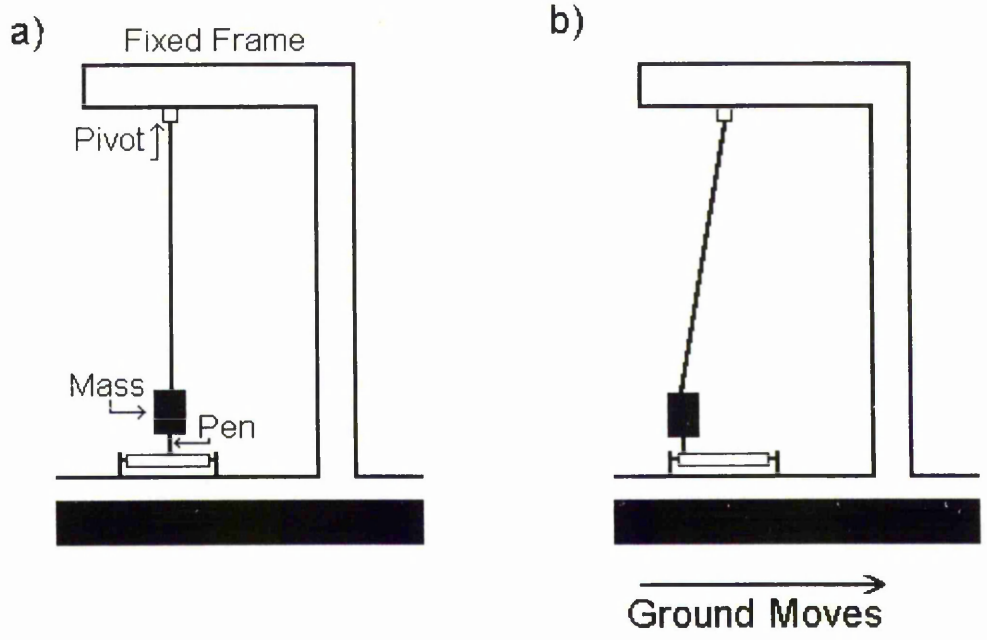

(Figure 2.13 A Simple Seismometer)

Modern seismometers tend to be based on a moving coil in an electric field. Note that we need a seismometer for each direction under consideration, i.e. we need one

instrument measuring North-South motion, and another measuring East-West movement. Vertical motion can also be measured using the same principle, but with the use of a spring, instead of a pendulum.

The output from these seismometers appears as a "squiggly line. The different types of seismic waves are easily identifiable on a seismogram. An example of the output from a typical seismometer is given below, figure 2.14.

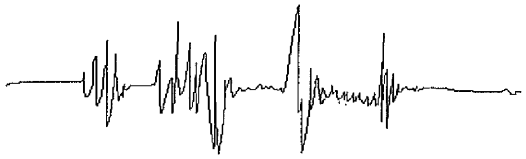

(Figure 2.14 A Seismogram)

The seismogram can be used for a variety of purposes, the most important of which being the determination of the strength and location of the earthquake.

2.10 The Size of an Earthquake

The size, or magnitude, of an earthquake is defined on the Richter scale. The Richter scale provides a quantitative method of describing the size of an earthquake, based on the seismogram recorded by seismometers. Prior to this, a qualitative method was used to describe the earthquake *intensity*.

2.10.1 Earthquake Intensity

The intensity of an earthquake is an estimate, at one particular place, of the amount of vibration, damage, etc.. There are a number of different scales used to measure the earthquake intensity, with two of the main examples being the *Rossi-Forel* scale and the *Modified Mercalli* scale. These scales depend upon observations made by people at a particular location. The Mercalli scale runs from I to XII, and is dependent upon the effects of the earthquake. Effects such as the disturbance of windows, standing cars rocking noticeably and heavy furniture moving, all determine

the value for the intensity. The Modified Mercalli Scale is given in Appendix A. Obviously this scale is subjective, and will depend upon the observer, and the distance from the source of the earthquake. Recently, the Mercalli Scale has been superseded by the European Macroseismic Scale (EMS), which tries to avoid subjectivity by defining terms precisely and relying on objective phenomena.

2.10.2 Earthquake Magnitude

The Richter scale is named after Charles Richter, who introduced the term to seismology around 1935. It is entirely based upon the instrumental record made by seismometers, and hence is reproducible and consistent. The Richter Scale was made logarithmic in nature, to allow for the huge range of energies emitted by earthquakes. It results in a single number being determined for each earthquake. These values are normally within the range -3 to +9. The magnitude scale is not limited to this range, these are just the practical measurement limits. Note that negative or small values represent smaller quakes, i.e. the bigger the Richter value, the bigger the quake. Richter defined his magnitude scale as follows:

The maximum trace on a seismogram, as measured in thousandths of a millimetre (1 micron), is used to determine the magnitude. An earthquake with a magnitude of 0.0 produces a maximum trace of 0.001 millimetres on a standard seismogram, 100 kilometres from the epicentre. Magnitude increases logarithmically (base 10) with the size of the maximum trace. For example, a maximum trace of 10 millimetres would imply that we have an earthquake of magnitude 4.0. A distance correction determined from actual measurements was used to allow the magnitude to be determined from seismograms at distances other than 100 km. This magnitude scale is known as the Richter scale or, since the introduction of other similar scales, the local magnitude M_L.

Richter's scale was based on earthquakes in California, which are relatively small and shallow. Hence, an extension of Richter's work was necessary to allow his definition of magnitude to be used in other areas, with larger earthquakes, and with

other instruments. Correspondingly, these different magnitudes have a general formula which is based upon the amplitude of seismic waves, but with corrections for epicentral distance, depth and other regional factors. The general formula can be represented thus:

$$M = Log\left[\frac{A}{T}\right] + f(d,h) + C_s + C_r,$$

(Equation 2.1)

where A is the amplitude of the wave and T is the period. Two magnitude scales have emerged as the most frequently used, *surface-wave magnitude*, M_s, and *body-wave magnitude*, m_b. The Surface-wave magnitude scale is determined using the amplitude of the Rayleigh waves, which were discussed earlier. The body-wave magnitudes are based on calculations made using the first few cycles of the P-waves.

2.11 Earthquake Energy

The main aim of defining a magnitude scale is to facilitate an approximation of the amount of energy released by an earthquake. The relationship between energy and magnitude has been approximated by a number of parties, by far the most important of which is that of *Gutenberg & Richter*[1954]. They approximated the energy released as :

$$Log\, E = 1.5\, M_s + 11.8$$

(Equation 2.2)

The energy released, E, is given in ergs. It is essential to realise the full impact that the logarithmic factor has on the quantity of energy released. For example, an increase in magnitude by 1, results in an increase by a factor of over 30 in the energy released. Thus, an earthquake of magnitude 5.0 releases 2×10^{19} ergs of energy. To put this in perspective, the atomic bomb dropped on Hiroshima released approximately this amount of energy, while 1 ton of chemical explosive releases only

4×10^{16} ergs. If we consider a great earthquake (magnitude > 8), of which there are on average one per year, then the energy is equivalent to over 30,000 Hiroshima bombs. This statistic puts the power of the Earth and earthquakes into perspective. Note that over 80% of all seismic energy comes from earthquakes with a magnitude greater than 7.9, even allowing for the fact that there are many more small shocks than there are large ones.

2.12 Miscellaneous Terms

We also define two important terms which will be used frequently. An *aftershock* is an earthquake following a larger earthquake and originating at or near the focus of the larger one. Generally, large earthquakes have quite a number of aftershocks. The aftershocks may extend over a period of days or even months, with the number decreasing as time passes. A *foreshock* is a small tremor which precedes a larger earthquake by an interval ranging from seconds to weeks or even longer.

Chapter 3

History of Earthquake Prediction

In this chapter we review some of the previous attempts at earthquake prediction. We also discuss the different ideologies behind the various different methods of prediction.

3.1 Ideologies

The current state of the art in earthquake forecasting suggests that there are three main ways in which we can proceed with prediction research. These three methods can be described as follows:

1) Precursory Phenomena

The fundamental assumption of this method is that the Earth emits "warning signals" which we must only decipher, to enable us to predict the earthquakes.

2) Statistical Analysis of Earthquake Catalogues

Once all the earthquake information is collected and recorded in an earthquake catalogue, these catalogues can then be analysed statistically. This analysis allows us to discover any patterns in the seismicity data. This prediction method can be summarised as "what happened in the past is the key to the future".

3) Physical Models

In this method, we create a physical model of the earthquake based on the laws of physics, and our current understanding of the mechanisms involved in earthquake occurrence. Using the model, computer simulations can be performed and predictions made from these.

3.2 Types of Prediction

As with weather forecasting, there are a number of different types of prediction. We classify the various types according to the time scales under consideration. We regard long-term predictions as those which deal with time scales of the order of decades, and intermediate term predictions as those which deal with time scales of years. Short-term predictions we will regard as discussing time frames of the order of days and weeks.

Long-term predictions are very useful in terms of improving urban planning, setting up legislation to improve building codes (ensuring new buildings are earthquake resistant etc) and increasing public awareness of safety procedures, risks involved and what to do when the "big one" strikes. A programme such as this should help to minimise loss of life and produce acceptable damage levels. Short-term predictions could be useful in terms of saving lives, as they would allow a state of emergency to be called and for appropriate action to be taken for a short period of time.

3.3 Legends

Historically, all sorts of legends have been associated with the prediction of earthquakes. Abnormal animal behaviour has regularly been cited as a forerunner of major earthquakes. In Japan, catfish and carp jumping out of ornamental ponds has often been "recognised" as a precursor to a major earthquake. The appearance of large numbers of deep-sea fish has often been reported prior to large events. Other animals which feature in reports on earthquake precursors include rats, frogs and snakes.

The appearance of mysterious lights in the sky have also been reported prior to the occurrence of large earthquakes. Other suggested phenomena include cases of magnets losing their magnetism and the position of celestial bodies.

3.4 Conclusion

The history of earthquake prediction is riddled with false claims and false claimants. The different methods outlined above are a selection of those which have been used historically to predict earthquakes. We argue that any claims made should be backed up with solid scientific evidence, and should be subjected to rigorous statistical tests. Claims should not be based on hearsay, or reports from untrained members of the general public, alone. For more background information on the material contained in chapters 1 to 3 see *Bolt*[1993], *Doyle*[1995], *Mogi*[1985], *Rikitake*[1976], *Ritter*[1971] and *Yeats et al.*[1997].

Chapter 4

Precursory Phenomena

Precursory phenomena were the first of our three ideologies for earthquake prediction outlined in the last chapter. The basic premise of precursors is that, prior to an earthquake, an event occurs which we are able to observe, or measure in some way. We can then decipher this event, based on our previous knowledge, and can predict the occurrence of an earthquake. These precursors act as warning signals, to inform us of a forthcoming earthquake.

There have been many claims regarding the discovery of reliable precursors which would enable us to predict major earthquakes. Unfortunately, these claims have been, on the whole, inaccurate. Once the precursor has been identified, and measurements of this quantity taken, the tendency has been for the precursor not to recur immediately before the next earthquake. This supposed unreliability of precursory phenomena is the main problem for earthquake prediction research. For reliable prediction methods we need consistent precursors; precursors which signal the onset of an earthquake *every* time.

To date, no precursor has been identified which pre-empts every earthquake. Precursors have been identified which occur before some quakes, but then are missing before others. As above, this may be due to the complex nature of the phenomena involved, and perhaps *no* precursor will ever be discovered which occurs before every earthquake. The solution to this could be the measurement of a number of different precursors. For example, if we measure five possible precursors, and three of our five showed a deviation from the norm, then we could base our prediction on these three changes.

In the following sections, we will discuss a number of the most popular, and realistic, precursors.

4.1 IASPEI Committee

In 1989, a sub-committee on earthquake prediction was set up by IASPEI, the International Association for Seismology and Physics of the Earth's Interior. Its function was to evaluate claims of earthquake precursors. The committee asked for nominations of geophysical precursors to be made, for inclusion in a preliminary list of significant earthquake precursory phenomena. These nominations must fulfil a number of criteria before they can be accepted. The criteria include presentation of a realistic physical model, definition of the anomaly being considered, and rules for associating these anomalies with earthquakes. The nominations are then reviewed rigorously, by experts, before being accepted or rejected. See *Wyss*[1997].

At the time of writing, over 40 nominations had been reviewed by the committee. Of these, only 5 have been accepted as possible earthquake precursors. Three of the five phenomena refer to changes in patterns of seismicity, while one refers to variations in ground water levels. The other phenomena is based on ground water chemistry.

Exclusion from the list does not imply that a precursor is not valid, it merely shows that there is not yet sufficient evidence to confirm, or refute conclusively the nomination. Similarly, acceptance to the list does not imply that the precursor is valid, but implies that there is enough evidence for the precursor to be considered.

4.2 Japanese Precursors

Japanese scientists have performed experiments on a wide range of precursory phenomena, and much research has been performed in a range of disciplines associated with geology and the earth sciences. Table 4.1 below lists some of the different precursors identified by the Japanese research, and the number of recorded occurrences of the phenomena, see *Rikitake*[1987].

Table 4.1 Japanese Precursors

Precursor Type	Number of Data	Precursor Type	Number of Data
Gravity	1	Q-Value	1
Geodetic Survey	12	Tilt (Horizontal Pendulum)	46
Tide Gauge Observation	9	Tilt (Water-Tube)	11
Foreshock	128	Strain (extensometer)	17
b-Value	15	Strain (bore-hole strain meter)	24
Micro earthquake	10	Geomagnetic Field	5
Focal Mechanism	1	Earth Currents	10
Change in Seismic Wave Velocity	16	Resistivity (Variometer)	30
Change in Seismic Activity Pattern	14	Resistivity (Distant Electrodes)	9
Anomalous Seismicity	13	Electromagnetic Radiation	7
Seismic quiescence	12	Radon Gas	15
Seismic Wave Form	2	Underground water / Hot Spring	10

Note that the table contains a whole variety of different precursors, from different branches of the science. We have precursors which stem from earthquake statistics, to geochemistry and geophysics.

4.3 Seismic Velocities

One of the many precursory phenomenon that has been reported is the change in the ratio of the *P-wave* velocity, V_p, to the *S-wave* velocity, V_s, prior to an earthquake. The different types of seismic waves were discussed in Chapter 2. This change was first observed in Garm, USSR, but has since been identified in other countries.

We do not calculate V_p and V_S independently, as their ratio can be easily obtained from travel time data. We denote the arrival times of the P-waves, by t_p, and the S-wave arrival times by t_s. Note that, as outlined in Chapter 2, the P-wave travels faster than the S-wave, and always arrives first. Hence, t_s is always greater than t_p, and the difference between them increases as t_p increases.

If the graph of $(t_s - t_p)$ against t_p is plotted, then a straight line of gradient m is obtained. The gradient of the line is given by:

$$m = \frac{t_s - t_p}{t_p} = \frac{t_s}{t_p} - 1.$$

(Equation 4.1)

Note that this considers the Earth to be homogeneous and isotropic. If we assume that the path followed by the waves are identical then:

$$V_p\, t_p = V_s\, t_s$$

$$\text{i.e. } \frac{t_s}{t_p} = \frac{V_p}{V_s}.$$

(Equation 4.2)

Therefore, by substituting into equation 4.1, we get that

$$m = \frac{V_p}{V_s} - 1$$

$$\text{i.e. } \frac{V_p}{V_s} = m + 1$$

(Equation 4.3)

The original experiments in the USSR showed that the $\frac{V_p}{V_s}$ ratio decreased markedly, some time before a large earthquake, and then recovered to the "normal" level immediately afterwards. The "normal" value for the ratio was about 1.75, and anomalies of approximately 10% to 15% were experienced. It is now thought that the original Garm results were caused by the peculiarities in the method employed by the original experimenters, see *Nersesov et al*[1971,1979].

Work in this area has also been performed in the United States. At Blue Mountain Lake, in New York State, *Aggarwal et al.*[1973] reported that they had found variations in $\frac{V_p}{V_s}$ before earthquakes of magnitude 3.

Unfortunately, our familiar problems reappeared. *Bakun et al.*[1973] showed that no changes in $\frac{V_p}{V_s}$ occurred before the 1972 earthquake in Bear Valley, on the San Andreas fault. It seems that, once again, we have an example of a phenomenon which occurs before some earthquakes, and not before others. However, this method could be used as one of our basket of methods.

4.4 Seismicity Precursors

Due to the increasing interest in earthquakes, and the improvements in seismic monitoring equipment, many areas of the world are now closely monitored by local seismic networks. Hence, we can now produce detailed catalogues, recording most earthquakes.

It has been suggested that changes in the pattern of seismicity occur before an earthquake. These changes could be characterised by a period of seismic quiescence, where the seismic activity in a certain area appears to diminish for a period, or by an increase in seismic activity, as if the Earth were "winding up" for some large event. Unfortunately, the seismicity patterns that are measured, are so complex, that it is nigh on impossible to associate a changing pattern with any imminent earthquake. A seismicity pattern which shows the main points of the theory of seismic quiescence is given below, figure 4.1. In figure 4.1, we can see that there are "gaps" with no seismic activity, and immediately after these gaps we have a major earthquake.

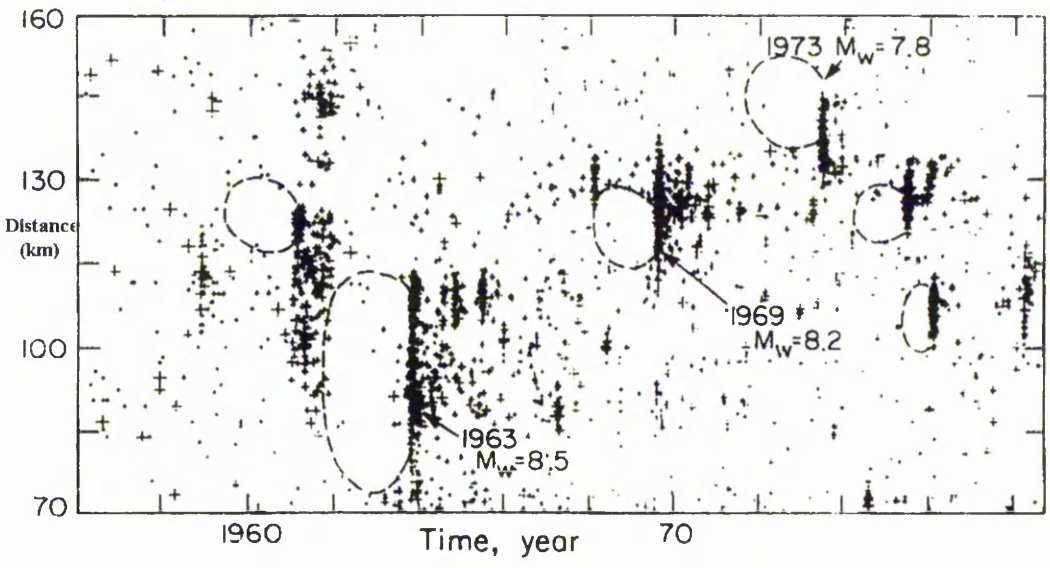

(Figure 4.1)

Figure 4.1 illustrates the distribution of seismicity for the Kurile Islands region. The dashed regions represent periods of seismic quiescence. See *Kanamori*[1981].

We can see that the sizes of the "gaps" are different along both axes. It is also felt that *other* gaps could be drawn on the map, but as it is known where and when the large earthquakes occur, the proposers only mark on the "correct" gaps. Figure 4.2 below, shows additional areas for which gaps could feasibly have been drawn.

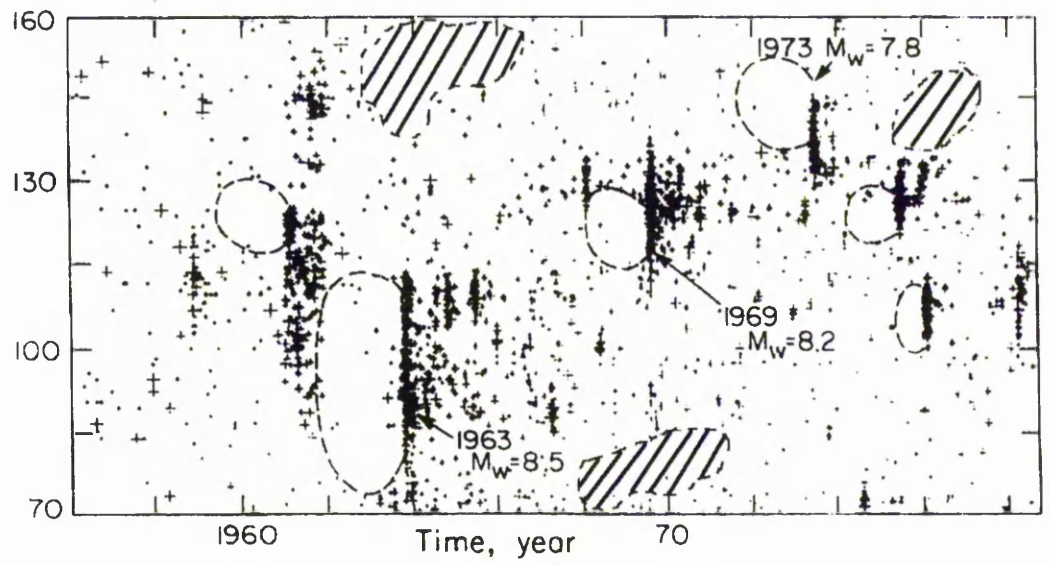

(Figure 4.2)

The author believes, however, that this sort of *postdiction*, or proof after the fact, is a very dangerous practice, and that *prediction*, is completely different. Projecting forward in time is much more difficult. If we are trying to predict earthquakes, then we must be very careful when applying this postdictive technique. *Schreider*[1990] proposed a statistical method for making reliable predictions based upon seismic quiescence.

Other possible seismic precursors are thought to include the appearance of foreshocks. Note that the definition of a foreshock was given at the end of chapter 2. Foreshocks occur before approximately one quarter of all large earthquakes. Apart from the obvious problem that foreshocks do not occur before every event, there is another major problem with this method: it is generally impossible to determine whether an earthquake is a foreshock until *after* the main shock occurs. A method was proposed by *Kagan*[1996], whereby after every moderately large earthquake, a warning would be issued, just in case this was the forerunner of some larger earthquake. Obviously, this is not going to be a very accurate prediction method, but it could form the basis of a more advanced method, i.e. it could be used in conjunction with other factors.

4.5 Water Levels

There are many reportedly precursory phenomena which are related to changing water levels. Variations in the water level in underground wells, changes in the flow rates of springs and general phenomena associated with the height of the local water table, have all been associated with earthquake forecasting.

The physical basis behind these phenomena is thought to be the process called *dilatancy*. Linear elasticity predicts that the volume of an object decreases *linearly* with increasing pressure. Dilatancy describes a deviation from this situation, the volume of the rock, during deformation by *squeezing*, changes but not in the linear way expected. The volume of the rock is *greater* than predicted by the linear

elasticity law. This deviation is due to the opening and extension of small cracks in the rock. This effect has been the subject of many experiments in laboratories throughout the world. It is thought that dilatancy could explain the occurrence of many precursory seismic phenomena. Recently, however, there has been some controversy as to the validity of directly applying laboratory results to the Earth's crust. Active research is still being carried out into dilatancy, ground water levels, and associated phenomena.

A significant problem with basing any forecasts on these phenomena is the possibility of results being affected by rainfall, precipitation and irrigation. These effects would need to be accounted for in some way before a reliable prediction method could be proposed for this precursor.

Other phenomena associated with water include changes in underground water temperature and water chemistry.

4.6 Geochemical Precursors

It has been reported that high levels of radon may appear in spring waters prior to an earthquake. Radon is a daughter product in the radioactive decay of Uranium 238. The radioactive decay process is:

$$^{238}U \rightarrow {}^{230}Th \rightarrow {}^{226}Ra \rightarrow {}^{222}Rn$$

(Equation 4.4)

See *Sears[1987]*. The half-life of Radon is approximately 4 days, and hence the radioactivity can be measured easily.

Results from deep well monitoring stations in Japan showed that, before the 1995 Kobe earthquake, the radon concentration in the water increased markedly. Unfortunately, this was not noticed until *after* the earthquake had occurred.

4.7 Electromagnetic Precursors

Precursory variations in measurements of electrical currents in the Earth have been recorded in a number of places. Most significantly, a number of important discoveries have been made in Greece, by Professor Varotsos of the University of Athens.

His method has resulted in a great deal of media interest, and has caused controversy amongst the geophysical community. As a result, the next chapter is devoted entirely to the discussion of his method.

There have also been numerous historical reports of major changes in geomagnetism around the time of a large earthquake. *Rikitake*[1968] showed that since the advent of modern measuring apparatus, the number of reports of this nature has declined sharply. This suggests that previous evidence should be treated as extremely unreliable.

Changes to the resistivity of rocks due to saturation and pressure effects have also been suggested as precursors.

4.8 Geodetic Surveys

It is well known large earthquakes are often accompanied by land deformation, but it has also been shown that some deformation occurs *before* an earthquake. It appears that the build up of strain, by tectonic forces, causes the land to flex at certain places. This movement, although small, can be measured with very high precision. The techniques involved in making these measurements use modern satellite technology and more traditional triangulation surveys.

The tilting effect can be used as a precursor, and with the use of previously collected data, can be used to form the basis of a prediction method.

4.9 Conclusion

Many precursors have been postulated, from many different sources, using various techniques. Unfortunately, no precursor has been found to be foolproof. The problem still remains unsolved, and much further research is needed. As stated previously, it may be possible to use a collection of different precursors to help improve prediction.

Chapter 5

The VAN Prediction Method

5.1 Introduction

Since 1981, continuous measurements of the Earth's electric field have been made in Greece. These measurements were used by a group of Greek scientists as the basis of a method for the prediction of earthquakes. The VAN prediction method (after the initials of its proposers Varotsos, Alexopoulos and Nomicos) was originally postulated in 1981, and is a method for detecting Seismic Electrical Signals, hereafter referred to as SES. It is claimed by this group, and others, that this method can be used for the successful prediction of earthquakes. Varotsos *et al.[1988]* made a significant claim, that "every sizable earthquake is preceded by an SES, and inversely every SES is always followed by an earthquake, the magnitude and epicentre of which can be reliably predicted". Its supporters have recently claimed to have achieved a number of notable successes, and as a result have had an entire journal issue dedicated to them (see Tectonophysics, Volume 224, 1993). This method, which has a large number of sympathizers, also has a vast array of sceptics. *Geller*[1996] and *Kagan*[1996] suggest that the results obtained by the VAN method are not statistically significant. In this chapter, we shall discuss the VAN proposals, and the controversy surrounding it. The information in this chapter can be obtained in the following references [17], [34-36], [41], [48-52], [70,71], [83] and [105-122].

5.2 Overview of Methodology

The VAN method uses an array of conducting wires and electrodes, which are buried underground. These wires, and the potential differences, produced across

them, are then monitored at a number of permanent monitoring stations. The hypothesis of Varotsos *et al.*, states that if a transient change, or disturbance, in the electric field is detected by one, or more, of the monitoring stations, and if this signal is greater than the background noise level, then this may be a precursor to a large earthquake.

Definition

A *signal* is defined to be a transient change, ΔV, in the potential difference registered between the two electrodes. The electrodes are separated by a short distance.

Many hours before an earthquake occurs, a signal, as defined above, is recorded by the apparatus. This variation has a finite duration, of length τ, before the voltage recovers its initial value. If these signals are sufficiently large, and can be distinguished from the usual background noise, then an earthquake will occur within the area of sensitivity of the station, and within a certain time span, called the lead-time. Varotsos' method uses past experience to predict the earthquake, with the magnitudes of the earthquakes predicted being $M_s > 5.0$. Each prediction forecasts the epicentre and the magnitude of the impending earthquake as well as a time window, within which the earthquake is expected.

5.3 Apparatus

The VAN method uses a pair of nonpolarized lead/lead chloride electrodes ($Pb/PbCl_2$), although copper or brass electrodes have been used previously. The lead electrodes have been selected because of their low noise and long-term stability. The lead electrode is surrounded by a mass made from mixing a solution of lead chloride with plaster of Paris. The electrode is then fixed into the hole by setting in a further mixture of plaster of Paris. The electrodes are buried in the earth to a depth of 2 metres. It has been noted that the noise produced by different types of electrode can

vary. The electrodes are separated by a distance, L, of between 30 and 200 metres. See *Varotsos & Lazaridou*[1991].

The electric field is determined by measuring the potential difference between these two electrodes. We require at least two perpendicular lines to determine the electric field at a particular station. In the VAN experiment, at each station, one line was oriented in an East - West direction, while another was oriented in a North - South direction. The potential difference, V, is measured after amplifying and filtering out frequencies above 0.3 Hz. The results obtained are displayed on a strip chart recorder.

The siting of a particular recording station is crucial, as we wish to minimise the amount of "noise" in the circuit. Varotsos *et al.* claim that the noise should not exceed 0.1 - 0.2 mV for a line of length 100m. This implies that the station must be situated away from any electrical power sources (power cables, etc.) and obviously places severe restrictions upon where a station can be situated. Local disturbances due to the introduction of strong currents into the earth, e.g. by factories, must also be avoided. The telluric electric field can be disturbed by magnetic variations, but these can be excluded from the analysis if the magnetic field at the station is monitored continuously. During strong magnetic storms, the electrical variations produced are so large, that a SES cannot be recognised if the earthquake is weak (small SES), or the epicentral distance is large. Other problems incurred include the production of anomalous discontinuities produced by metal electrodes after rain. These electrochemical effects may be confused with SES. In total, 18 recording stations are used, with each station being linked to Athens via a telephone link. The distribution of these stations can be seen below, in figure 5.1.

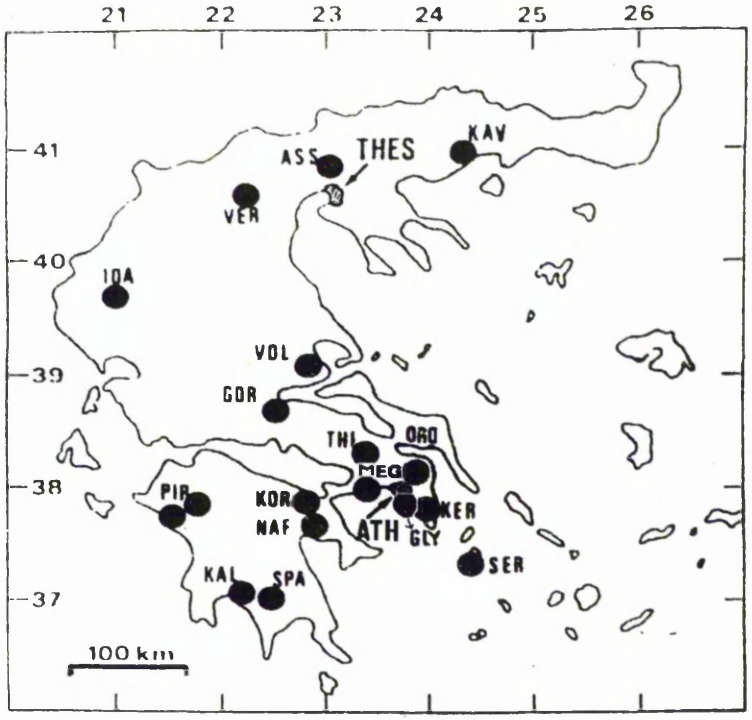

(Figure 5.1 - Map showing the Distribution of Greek Monitoring Stations)

Above, we can see a map of Greece with the 18 permanent measuring stations marked, with each station labeled with a three letter code word. The two largest cities in Greece, Athens (ATH) and Thessaloniki (THES), are also marked on the map.

The names of the stations are given below:-

ASS = Assiros

GLY = Glyfada

GOR = Gorgopotamos

IOA = Ioannina

KAL = Kalamata

KAV = Kavala

KER = Keratea

KOR = Korinthos

MEG = Megara

NAF = Nauplio

ORO = Oropos

PIR = Pirgos

SER = Serifos

VER = Veroia

VOL = Volos

THI = Thiva

5.4 Selectivity

A controversial aspect of the VAN method is "selectivity". This permits an easy explanation if there is failure to identify, or predict an earthquake.

Given a particular monitoring station, S_A, situated at position A, this station may be able to detect SES from seismic area B, but not from area C, even if the distance AC is less than AB (see figure 5.2).

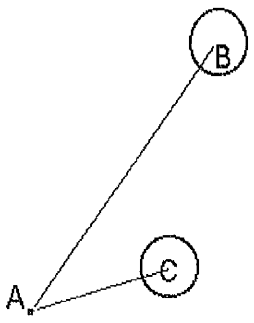

(Figure 5.2 Selectivity)

Varotsos also states that this "selectivity" is not reversible and that, although S_A may be able to record events at B, that a station at B may not be able to record signals at A. Varotsos goes further still, and states that even if all 3 points lie on a straight line, then station S_A may be able to record SES from B, but not from C (see figure 5.3).

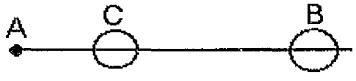

(Figure 5.3 Selectivity)

He claims this because, selectivity is not only a directional phenomenon, but that it depends on other factors.

a) Physical Properties

This selectivity depends on the physical properties of the *path* between the site of the SES and the monitoring station. For example, he claims that the conductivity of the Earth between the two positions determines whether we get a signal.

b) Source Properties

Varotsos also claims that the *source* of the SES affects the detectability of the signal. For example, the directional properties of the emitted current affect the detection.

c) Geological Structure at Station

He also makes the claim that any *inhomogeneities* in the Earth's crust, in the vicinity of the recording station, which result in different resistivities along various azimuths, will determine whether or not we can detect an SES. In a strongly inhomogeneous area, there are "sensitive localities", i.e. small sub-areas that amplify the SES signal. This local effect is superimposed on the regional characteristics.

Varotsos makes one final claim regarding this selectivity. He proposes that once a station has been shown to be sensitive to a particular seismic area, then it will be sensitive to all future events in this area.

Utada[1993], he gives a possible explanation of the selectivity effect. The model requires that there exists a planar path between the source region and the sensitive monitoring site, through which the electric current can travel. This path must have a higher conductivity than the surroundings, which allows the electric current to be concentrated on this path. If there is a highly resistive anomaly on this path, then the electric field will be further amplified here, and this would be our sensitive area. This model accounts for all 3 of the properties postulated by Varotsos, see figure 5.4 below. We do not claim that this is *the* only model or that it is actually

feasible, we simply claim that it provides a *possible* reason for the appearance of these properties.

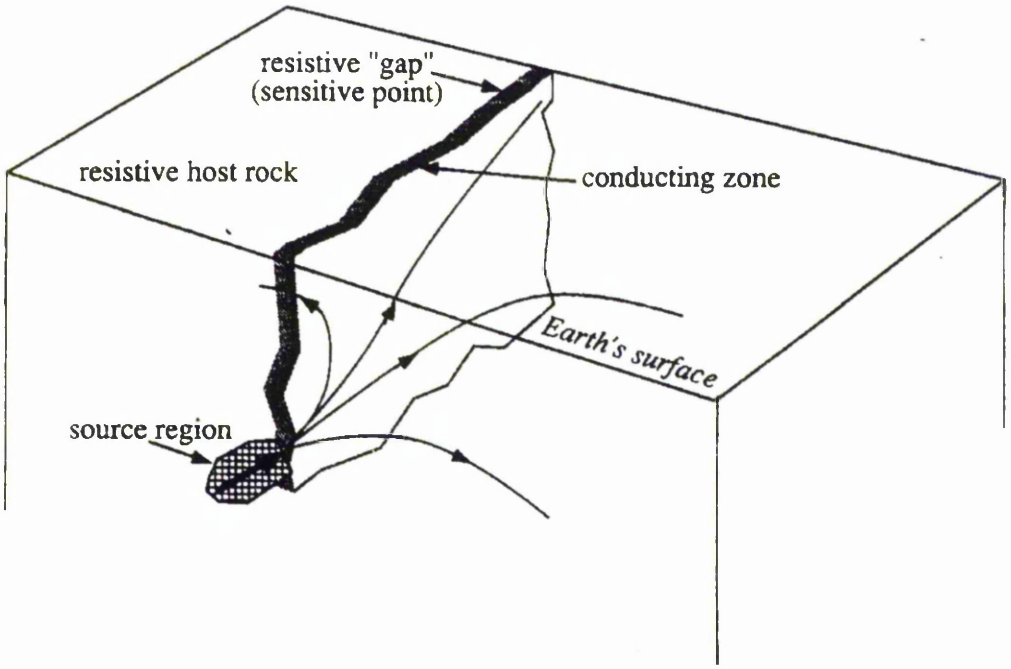

(Figure 5.4 Selectivity Model)

5.5 Method of Prediction

The potential difference for each pair of electrodes is recorded as it varies with time. When a transient change in this potential difference occurs, we say that a signal has been detected, and the next step is to determine the origin of the signal. By a transient change we mean that the potential difference deviates from its normal value for a short period of time. Usually, this is of the order of minutes, but in some cases, the deviation can remain for over an hour. This is the position we shall use as the epicentre of the impending earthquake. We must then predict the magnitude of the earthquake. The methods used employ a process of elimination, based upon previous experience, to determine the desired quantities.

5.5.1 Determination of Epicentre

As stated above, the epicentre is determined by a process of elimination based upon the following criteria:

a) Selectivity Effect.

Using the knowledge gained from previous events which were not measured at this station, regions to which this station is *not* sensitive, are excluded immediately. This restriction limits the number of areas which we must consider to places which have produced an SES, and earthquake, before.

b) Polarity Effect.

From the restricted set of seismic areas obtained above, it is also possible to exclude those areas to which the station is sensitive, but which emit SES with polarity opposite to those of the signal recorded. For example, if a particular area is known to emit signals with a positive change to the potential difference, and the signal we have obtained has a negative sign, then we can eliminate this area.

c) Ratio of the two components of the SES.

The ratio of the East-West component to the North-South component of the signal, given by $\left(\frac{\Delta V}{L}\right)_{EW} : \left(\frac{\Delta V}{L}\right)_{NS}$, can be determined and compared with previous SES from the remaining seismic areas. This ratio is used to identify the epicentre, based upon previously active regions. Unfortunately, if the ratio under consideration does not match that of a previous event, then a prediction has to be based upon interpolation, using the values of neighbouring areas.

This method allows us to predict the position of the epicentre of the earthquake.

5.5.2 Determination of Magnitude

The method used to calculate the magnitude of the earthquake is, again, based upon past events. The predicted magnitude depends, not only upon the strength of the signal, but also the station the signal is recorded at, and the predicted region the signal originates from. Using previous data, the graph of $\log\left(\frac{\Delta V}{L}\right)$ versus M can be plotted. This yields a straight line, with equation :

$$\log\left(\frac{\Delta V}{L}\right) = a\,M + b$$

(Equation 5.1)

where the gradient typically takes a value of between 0.34 and 0.37, and the intercept, b, takes a variety of values depending upon the area under consideration. Therefore, for every area that a station is sensitive to, we must have a calibration, before any prediction of magnitude can be given. Using equation 5.1 and the value for $\frac{\Delta V}{L}$ a prediction for the magnitude of the imminent event can be issued.

5.6 Mechanisms for Signal Production

One of the main problems with the VAN method is the difficulty in understanding the physical basis for the production of these seismic signals. In a number of recent papers, it has been claimed that the generation of these signals can be explained by various physical models, for example, *Gershenzon & Gokhberg*[1993]; *Lazarus*[1993]; *Slifkin*[1993]. According to Lazarus, any model would need to fulfill a number of criteria, and answer a number of important questions. These questions include :

1) Why are SES detected only prior to earthquakes, and not during them, when deformation would be larger?

2) Why is there such a large variability in the time intervals between the detection of the SES and the earthquake occurrence?

3) Why are SES only detected from certain sensitive regions, and only from earthquakes arising in certain areas?

4) How can the SES propagate over hundreds of kilometres to some detectors and yet not at all by much closer detectors?

It is claimed that, in principle, seismic electric signals could be generated by an array of different mechanisms. There are a number of theories which have been postulated as explanations for the appearance of these SES, these are mainly based upon mechanoelectric occurrences. For example, piezoelectric effects due to excess crystal polarities in one direction. A number of these theories are summarised below.

5.6.1 Piezoelectric Effect

It is a well known phenomenon that some anistropic materials polarize upon the application of mechanical stress. This effect is known as the *piezoelectric effect.* For example, a quartz crystal will polarize along one direction if compressed along another at right angles. The production of the SES is based on this piezoelectric effect. At a geological fault, or where we have crustal movement, or deformation, any piezoelectric material if compressed could give rise to a voltage, see figure 5.5 below.

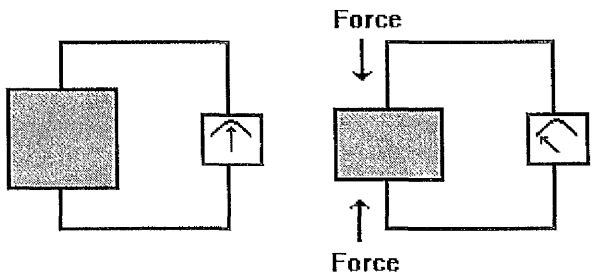

(Figure 5.5 Piezoelectric Effect)

Quartz is a rock forming mineral, as well as a piezoelectric material, and could produce our SES. If the signal is large enough, then it can be detected by our monitoring stations.

5.6.2 Crystal Deformation

Another possible method of SES production is caused by defects in the crystal structure. In general, crystals of rock-forming minerals contain defects in their lattice structures. From Solid State Physics, it is known that these defects can form electric dipoles, because of non-uniformities in the charge distribution. These dipoles can change their orientation under an applied stress, resulting in an abundance of dipoles aligned in one direction. This method is similar to the piezoelectric effect, but has a different physical basis.

5.6.3 Charge Separation by Rock Fracture

Laboratory experiments have revealed that the deformation of some crystalline materials generates an electromagnetic field. The main cause of this appears to be the movement of charge dislocations. *Gershenzon et al.*[1989], showed that during crustal fracturing, charged dislocations are produced. These dislocations result in measurable voltage differences being produced at crack tips.

5.6.4 Miscellaneous

Other methods of SES production involve the use of more complex solid state properties based on local changes in stress. They also make use of electrokinetic effects, local changes in crustal conductivity, moving source models, the Stepanov effect and many other effects obtained during rock failure experiments conducted in the laboratory.

5.6.5 Overview

It would appear that there are many different ways in which these SES could be produced, the methods outlined above are a selection of those currently being proposed. The opinion of this author is that, at this stage in the development of the VAN technique, the exact process through which these SES are produced is, while important, not the most important consideration. It is sufficient that we have a *possible* model for the production of the signals, ensuring that the technique does have a physical basis. One final point to consider is the possibility that more than one method of production is at work. It may be possible for a number of the mechanisms outlined in this section to contribute to the overall SES.

At this juncture, the most important research is the collection and publication of more reliable data, and the statistical analysis of the resulting data, proving that there is a significant statistical correlation between the SES and earthquake occurrence. If it is shown that there is a significant statistical link, then the correct model would need to be discovered, but this must be a secondary consideration.

5.7 Results

In this section, we give a summary of the VAN group's results from 1988 and 1989. These results are presented as an example of the type of predictions and results presented by the VAN group. They were chosen for analysis because they consist of a manageable amount of data, and because they form the basis for the bulk of the discussions in the appropriate geophysical journals. In the following table (Table 5.1), we list the predictions made by the VAN group, as they themselves present them. These predictions are sent to the Greek government by means of a telegram. They consist of the date on which the telegram was sent, and the magnitude and position of the earthquake epicentre. The position of the epicentre is given in terms of a bearing and direction from the central monitoring station, near Athens. For example, an entry such as NW330, implies that the epicentre will be at a position 330 kilometres to the North West of the central station. Note that, in some cases two possible sites for the earthquake are predicted. This occurs as a result of similarities in previous signals form these areas.

Table 5.1 Summary of Van Predictions

Date of Telegram	Prediction Epicentre	Prediction Magnitude	Earthquake Date	Earthquake Time	Earthquake Epicentre	Earthquake Magnitude
15-May-88	NW330 (W300)	5.0 5.3	18-May-88	5:17	W310	5.8
21-May-88	W300 (NW350)	5.3 5.0	22-May-88	3:44	W290	5.5
30-May-88	W300 (NW350)	5.4 5.0	2-Jun-88	10:35	W300	5.0
4-Jun-88	W300	5.0	6-Jun-88	5:57	W300	5.0
10-Jun-88	SW200	5.1	13-Jun-88	20:32	SW240	4.3
21-Jun-88	W300 (NW350)	5.0 4.8	26-Jun-88	6:05	W300	4.5-4.7
10-Jul-88	W170 (WSW240)	4.7 5.2	12-Jul-88	2:27	NNW95	5.0
13-Jul-88	W70	5.0	16-Jul-88	1:54	SW100	4.9
18-Jul-88	NNW80 (SW100)	Uncertain	23-Jul-88	9:20	SW200	4.4
1-Sep-88	W240 (NW300)	5.8 5.3	22-Sep-88	12:05	W250	5.1-5.5
30-Sep-88	W240 (NW330)	5.3 5.0	30-Sep-88 15-Oct-88	13:03 7:00	W215 W235	4.9 4.9
3-Oct-88	W235		16-Oct-88	12:34	W240	6
21-Oct-88	Several tens of km from W240	6.3-6.5	22-Oct-88 31-Oct-88 8-Nov-88 11-Nov-88	9:34 3:00 8:18 17:52	W250 W230 SW170 W270	4.9 4.9 5.3 5.0
2-Mar-89	W300 (NW330)	5.4 5.0	5-Mar-89 8-Mar-89	16:44 5:57	NW440 NW470	4.7 4.9
3-Jun-89	W300 (NW350)	5.5 5.0	7-Jun-89	19:45	W185	5.2-5.4
13-Jun-89	W200 (NW350)	5.2 4.8	17-Jun-89	20:56	W140	4.5
23-Jul-89	NE40	5.0	1-Aug-89	2:24	N130	5.0
16-Aug-89	WNW200	5	20-Aug-89	18:32	WSW245	5.9
24-Aug-89	WNW190-240	5.2-5.8	31-Aug-89	21:29	W170	4.8
11-Sep-89	WNW190-240	5.2-5.8	25-Sep-89	7:35 7:38	WSW220 WSW235	4.7 4.6
18-Oct-89	NW300 (W240)	4.8 5.5	29-Oct-89	19:36	NW280	4.5

5.8 Discussion of Claims

In this section we will discuss the success of the VAN method in the numerous papers. The main points of criticism against the VAN method will also be highlighted.

5.8.1 Selectivity

As discussed earlier, in section 5.4, the VAN group state that only seismic electric signals from certain areas are detectable at particular stations. While there is a possibility of a physical basis for this property existing, the Earth is clearly inhomogeneous (see chapter 2), it is felt that this explanation is too convenient, and easily susceptible to abuse. Again, we express our reservations regarding this claim.

5.8.2 Statement of Results

In Table 5.1, a summary of VAN's results is given. If we examine the column in which the epicentral position is predicted (column 2), we see that the position is expressed as a distance and bearing from the central station in Athens. We note that the bearing is expressed using 3 letters, for example, WSW is used to denote West-South-West. Using a system of three letters, we may split the compass into 16 different sections, which implies that the angle between each line is $\frac{360^\circ}{16} = 22.5^\circ$.

From Table 5.1, we see that *every* prediction consists of at most a 3 letter bearing; are we expected to believe that every prediction lies conveniently on one of the sixteen compass points? If not, are we to assume that the prediction is a region which subtends an angle of 22.5°? Actually, this statement is probably acceptable, since over the distances covered, i.e. a maximum of 400 km, this results in an error of at most 25km. As the VAN group claim a successful prediction if the error in epicentral distance is less than 100 km, this method of presentation is almost acceptable.

However, it is felt that the statement of results could be better presented if given in either standard latitude and longitude coordinates, or by the use of a proper bearing.

5.8.3 Missing Earthquakes

Varotsos *et al.* did not mention the earthquakes which they did not "predict". There are a number of earthquakes with a magnitude greater than 5 for which they did not receive seismic electric signals as precursors. For example, an earthquake with Ms = 5.8 occurred on March 19, 1989, with an epicentre at 39.3°N; 23.6°E. They failed to consider these unpredicted earthquakes, and did not seem to consider these "missed" events as important, or feel that they diminished the reliability of the prediction method.

5.8.4 Multiple Predictions

In many of the predictions issued by VAN, there were two possible solutions for each SES. This resulted in two predictions being issued for many of the SES, with one prediction being considered the primary one. These "double" predictions will clearly increase the probability of predicting the earthquake correctly. As is well known, earthquakes do not occur everywhere, but are mainly concentrated along faults. Therefore, there are a number of regions where the probability of earthquake occurrence is relatively high. By predicting two epicentral sites, in these "active" regions, the chances of success can be markedly increased. Therefore, the statistical significance of these multiple predictions must be questioned. Indeed, if we have a double prediction which predicts an earthquake, we should treat them separately as two different predictions. We should count one of them as being correct, and the other as being incorrect when we perform our statistical evaluation. Immediately, this drastically reduces the efficiency of Varotsos' method.

5.8.5 Probability beyond Chance

The background seismicity in Greece is relatively high, and as stated above, we know that earthquakes tend to occur on fault planes. These two factors imply that simply by choosing a highly active region on a fault plane, and predicting an earthquake at this point, we have a reasonable chance of forecasting the event. What must be considered is not only the number of correct predictions, but the number of predictions beyond chance. In his analysis, Varotsos fails to consider this, simply claiming that if he forecasts the event correctly then it must be as a result of his method. In *Mulargia and Gasperini* [1992], these issues are discussed more fully, although their analysis has proved almost as controversial as the VAN method itself. They employ a declustering, or aftershock removal algorithm to obtain the catalogue of main shocks which they claim should have been predicted by VAN. The removal of aftershocks is however, a dubious and non-trivial undertaking, and it is felt that this is an unsuitable way of proceeding.

5.8.6 Rules of the Game

It has been claimed by some that the so called "rules of the game" have been changed by Varotsos as the study has progressed. For example, in *Wyss*[1996], *Wyss and Allmann*[1993] and *Mulargia and Gasperini*[1992], the authors state that the Van group changed the lead time, the expected time until earthquake occurrence after arrival of SES, during the course of the study. They also claim that the allowable error in the predicted magnitude has been changed from 0.7 to 1.0, to improve the success rates. It is obvious that these post-event adjustments are not allowed, but it is felt that, while Varotsos' did not explicitly state the "laws of the game" beforehand, the claims made in these papers are, on the whole, unjustified. Throughout the course of the study, we could find no record of any alteration in the acceptable magnitude error, and that ΔM had remained constant at 0.7. The lead-time question is an altogether more difficult one to resolve. The lead time has changed during the course of the experiment, but Varotsos has claimed that this is due to the discovery of a

different type of SES. It is necessary that the procedure, including any parameters, be stated explicitly beforehand to enable us to perform a complete evaluation of the method, and that statements of the following three criteria be given:

a) A list of all precursory seismic electric signals.

b) A list of all predictions issued.

c) A list of all earthquake's occurring in region under study.

5.8.7 Earthquake Magnitudes

As described in chapter 2, there are a number of ways to define the magnitude of an earthquake. In the VAN experiment the magnitude of the earthquakes predicted are given in Ms, which appears to be the standard form in this area. VAN's opponents claim that they do not state clearly which scale they are using, and that they have not used the final earthquake catalogues. It is again felt that this criticism of VAN is unfair, and we feel that he has recently stated accurately the magnitude scales he has used. Regarding the use of earthquake catalogues; Varotsos did indeed use the preliminary catalogues for Greece, but as these were the only ones available to him at the time, it is felt that this should be allowed. We now come to possibly the most controversial, and difficult, question surrounding the VAN method. Varotsos states that he is able to predict earthquakes with a magnitude in excess of 5.0, and claims that the error in this magnitude is $\Delta M = \pm 0.7$. Thus, he claims that if he predicts an earthquake with M=5.0, and an earthquake with magnitude 4.3 occurs then this is a successful prediction, in terms of the magnitude. So far this would seem to be perfectly acceptable, but *Mulargia and Gasperini* (hereafter known as MG) state that if he claims this earthquake as a successful prediction, then he must also counts as *failures*, the number of events which he fails to predict with an earthquake magnitude > 4.3. Equation 5.2, below, shows the relationship between the magnitude and the number of earthquakes with that magnitude. Gutenberg and Richter showed that the number, N, of earthquakes with a magnitude greater than M is given by the following relationship:

$$Log\ N = 8.2 - M$$

(Equation 5.2)

As a result of the logarithmic scale, the number of earthquakes increase dramatically as we lower the magnitude. This result implies that if we accept MG's argument then we would have to include a large number of failures, which would obviously decrease our success rate. In fact, the number of earthquakes included by employing this method is so great that it completely swamps all the "correct" predictions made, and results in there being a very small success rate. For example, MG state that for the data set, where we have 20 "successful" predictions, we must also include 234 earthquakes with $4.3 < M < 5.0$. This means that the success rate drops to below 10%. It is felt, however, that this is not the correct way to proceed. The author does not believe that the lower magnitude earthquakes should be included when calculating the success rates. It is felt that they should be allowed to claim events of less than magnitude 5.0 as successes because of the complex nature of the earthquake mechanism. It is possible that a signal could be produced that gives the indications of a very large earthquake, but due to local considerations, may only result in a smaller event.

5.9 Analysis

We performed an analysis on the data given in table 3.1. For various different sets of rules we calculated the number of successful predictions made by VAN. A successful prediction is defined to be one which lies within the range of the variables set out in the rules of the game. We counted the number of successful predictions for various errors in the distance from the actual earthquake. The maximum allowable error in the distance between the predicted earthquake and the actual earthquake ranged from between 30 kilometres to 150 kilometres. We repeated this process for different values of the maximum allowable error in the magnitude. The success rates for the different rules are shown in the table 3.2, below.

Table 5.2 Success Rates for Various Rules

	Magnitude Range				
Distance	0.3	0.5	0.7	0.9	1.1
30	0.14	0.33	0.38	0.38	0.38
50	0.14	0.33	0.38	0.43	0.43
70	0.14	0.33	0.43	0.48	0.48
100	0.14	0.38	0.52	0.57	0.57
130	0.33	0.52	0.71	0.81	0.81
150	0.33	0.52	0.71	0.81	0.86

From the data above, and Graph 5.1, below, we see that by changing the rules we obtain different success rates. Obviously, the larger we make the acceptable error, the more likely we are to get "correct" predictions. We can see that if we allow a prediction to be up to 150km out, and 1.1 units off the magnitude, then we obtain a success rate of 86%. This, however, is slightly misleading. At the larger distances, we start to "cover" an area which is approximately half of the total area under consideration.

For the normal rules, $\Delta x = \pm 100$ km and $\Delta M = \pm 0.7$, we find a success rate of over 50%. It is felt that this result is quite reasonable at this stage of development of the method, and for the tolerances given.

Graph 5.1 Success Curves for Van Predictions using various "rules"

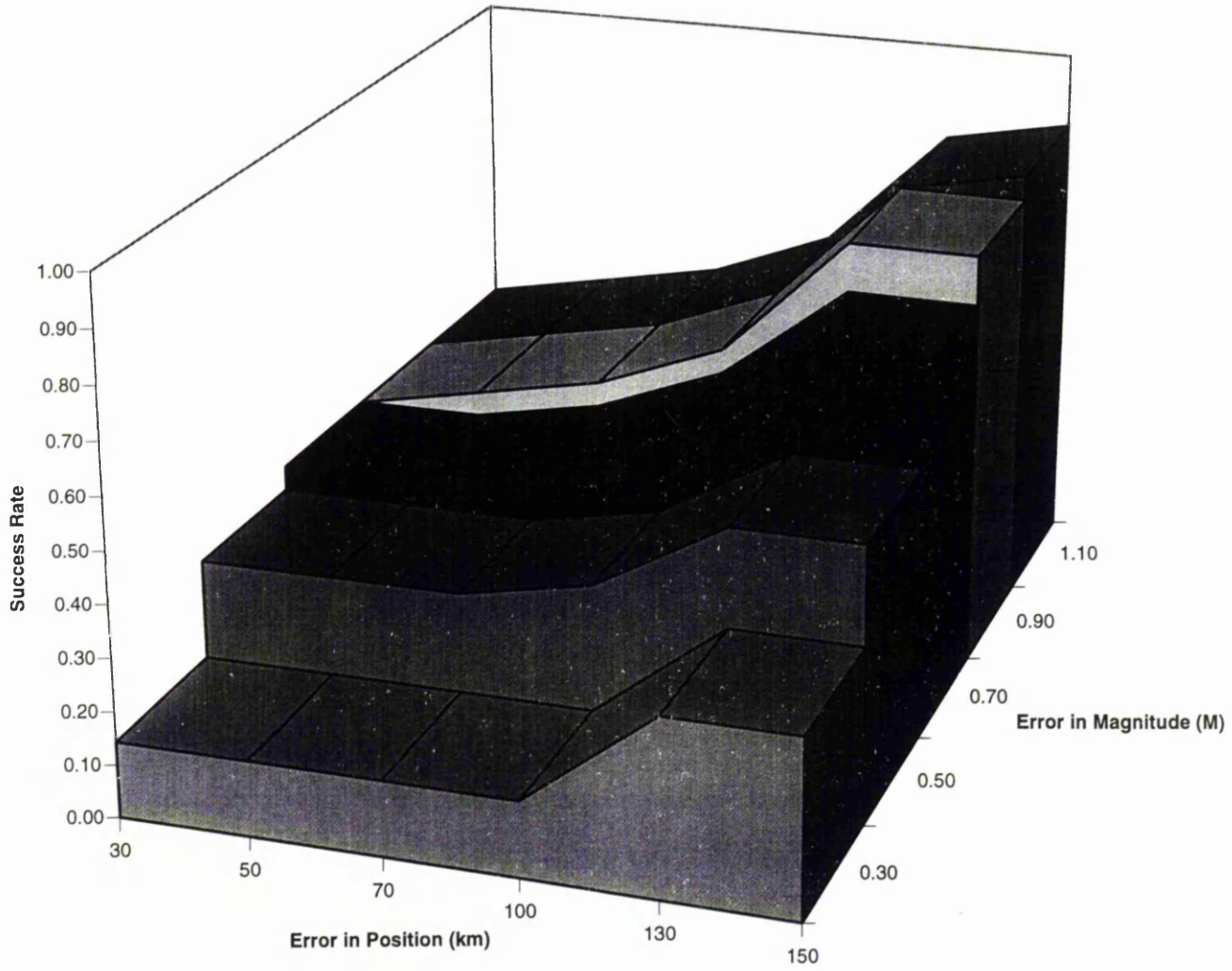

5.10 Considerations

In section 5.6.5, we discussed the possibility that a number of different mechanisms could be involved in the production of the seismic electric signals. If this is the case, then there is the possibility that two of the signals could *cancel each other out.* For example, if two different signals were similar in size, and opposite in polarity , i.e. one was positive and the other negative, then the resultant SES would be zero (or close enough for it to be regarded as noise). This is a very interesting thought, and could explain some of the cases where earthquakes were "missed". Although convenient for explaining the missing events, it would ultimately be a blow for the method, as it would mean that some events just could not be predicted.

Obviously, a lot more research needs to be carried out if we are to show whether this property is valid.

5.11 Conclusion

As yet there is no consensus amongst the geophysical community on what represents an earthquake prediction, or how claims should be evaluated. There is no definitive theory of earthquake occurrence and, hence, proposed techniques must be studied and validated statistically. The current state of play suggests that the VAN method for earthquake prediction is not perfect. If, however, further research resulted in a workable, and reliable, method then this could be of great benefit. The amount of warning given is sufficient to allow emergency measures to be taken, which could reduce the number of casualties.

The many controversies surrounding the method are mainly due to the poor reporting of the results, and the confusion that this has entailed. It is felt that the results obtained by Varotsos *et al.*, while not yet statistically significant, do provide a glimmer of hope. What is needed is a more rigorous test, with statements of the rules of the game and all appropriate parameters made beforehand, with no a posteriori adjustments allowed. Until this procedure is carried out, we cannot proclaim the VAN method as a success.

Chapter 6

Seismicity and Seismic Gaps

In this chapter we will discuss some of the main points of our second ideology for earthquake prediction, that of earthquake catalogues and statistics. In chapter 4, we highlighted some precursory effects gleaned from earthquake catalogues. Effects such as foreshocks and seismic quiescence, which we can think of as gaps in time, were outlined. Here, we will consider the theory of seismic gaps, which we can think of as gaps in space. We will also mention "Mogi's Doughnuts" and prediction using b-values.

6.1 Seismic Data

The collection of seismic data is a fundamental requirement for achieving any earthquake prediction. By recording earthquake occurrences world-wide, the distribution of earthquakes has been determined. Unfortunately, the records involved only stretch back about one hundred years. Historical earthquake catalogues of over 1000 years are available, although these are generally unreliable. With the time scales involved in earthquake prediction, we do not have enough data to produce a thorough statistical analysis.

The data that we have obtained can be used to provide rough forecasts of earthquake occurrence. These rough estimates are based on regularity, and effects such as periodicity and characteristic earthquakes. Characteristic earthquakes are defined as earthquakes in which the same segment of fault ruptures as in previous earthquakes. A great deal of research has been performed in Parkfield, California, where a characteristic earthquake is thought to occur approximately every 22 years, on average. It has done so for, at least, the last 150 years. See *Bakun & Lindh*[1985] for

more details. Unfortunately, the experimenters have overestimated the regularity of the Earth and, although predicted to occur a few years ago, the next characteristic Parkfield earthquake has yet to occur.

Seismicity data can still give us a rough estimate of where and when large earthquakes will occur.

6.2 The Seismic Gap Hypothesis

Large (M > 7), shallow earthquakes tend to occur in regions that have not been the site of such earthquakes for decades. The Seismic Gap Hypothesis was first proposed by *Fedotov*[1965], based on his work in the USSR and Japan. The essence of the theory is based on the premise that if a *large* earthquake has occurred in a specific region, along a fault, then the next large earthquake is more likely to occur in *another* region along this fault.

Fedotov estimated the size of the focal regions for each of the large earthquakes that had occurred in the seismic zone under consideration. That is, he calculated the size and position of the areas that had ruptured during major earthquakes. He used data from aftershocks, tsunami information and geodetic survey data to estimate the size of the ruptured area. He then plotted the different areas on a map of the seismic zone under consideration, the Kamchatka-Hokkaido Zone, which incorporates north-east Japan and the east coast of the former USSR. His original plot can be seen in figure 6.1, below. Fedotov noted that the focal areas cover large sections of the fault, and they do not overlap.

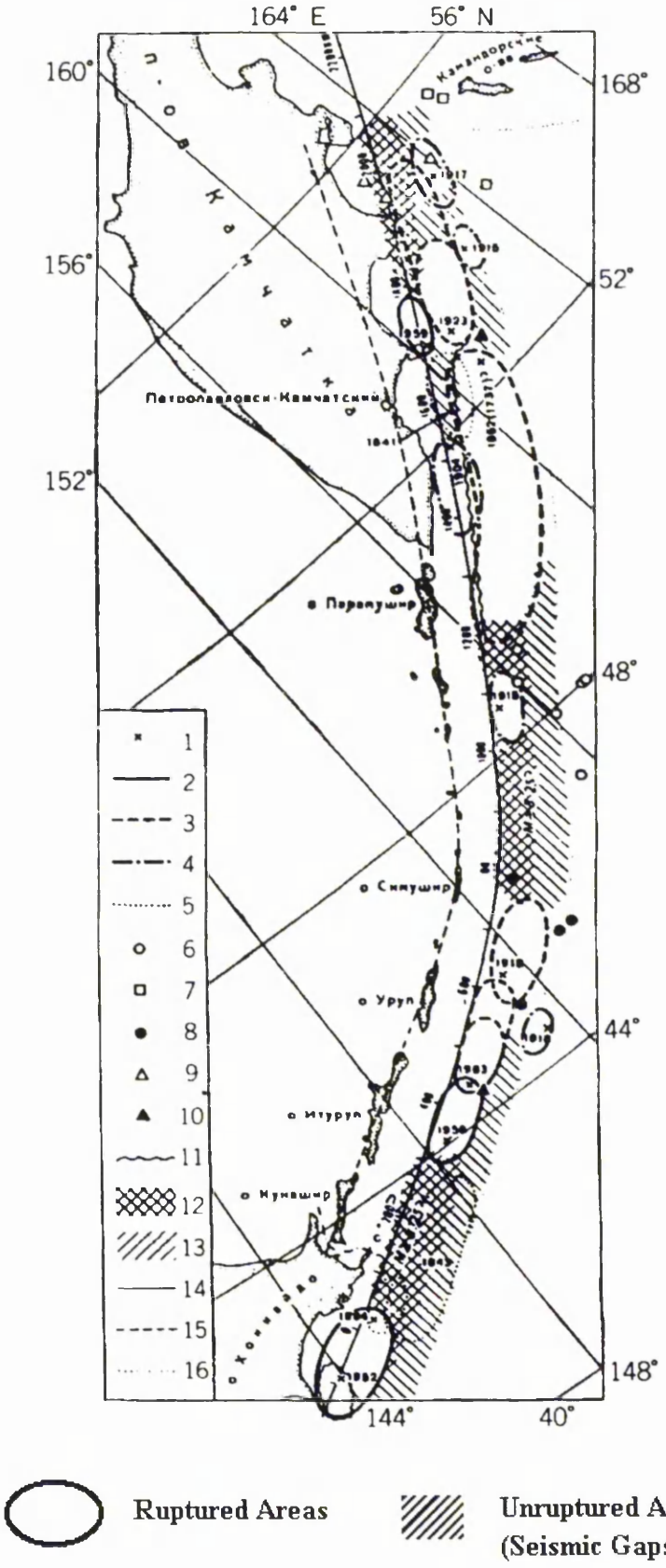

Ruptured Areas

Unruptured Areas (Seismic Gaps)

(Figure 6.1 Kamchatka - Hokkaido Seismic Zone with Seismic Gaps)

Fedotov's hypothesis stated that the next large earthquake should occur to fill in the remaining unruptured areas, or *gaps*. These unruptured areas are shaded in figure 6.1, above.

Using a similar technique, *Mogi*[1968 a,b] analysed the seismic zone that runs form Alaska to Russia. For each large earthquake, the ruptured area was estimated and plotted on a map of the area concerned. The ruptured zones are shown below, in figure 6.2. In this diagram, the *ruptured* areas are shaded.

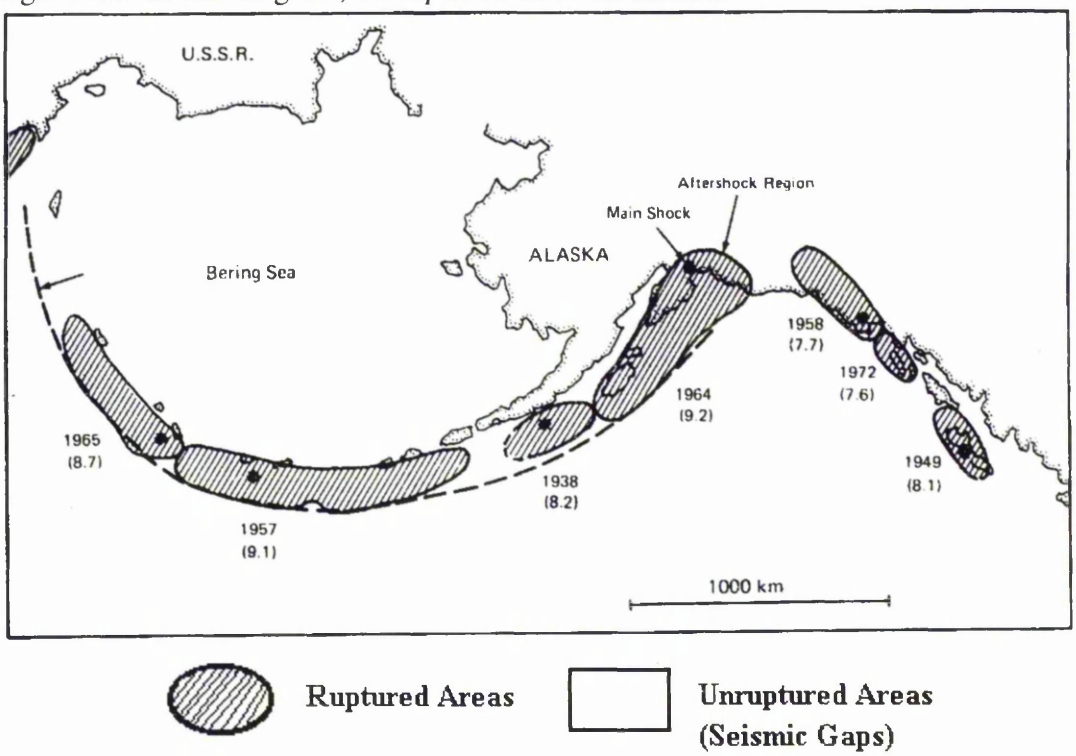

(Figure 6.2 Alaska-Russia Seismic Zone)

We can see that there is no overlapping of the ruptured regions. In fact, nearly all of the seismic zone has been "filled in" by these large earthquakes. It is assumed that once the zone is completely filled, we remove the first zone that ruptured, and go round the cycle again.

Results such as figure 6.2 are persuasive evidence as to the power of the seismic gap theory. It must be remembered that this is purely a long-term prediction method, as we are dealing with periods of decades. In recent years, work has been done to test the validity of the Seismic Gap Hypothesis.

6.3 Validation ?

Unfortunately, there is a major problem in validating the seismic gap hypothesis, hereafter referred to as the SGH. Once again, the problem lies in the length of the earthquake catalogue and the time scale involved in great earthquake occurrence. As stated in section 6.1, instrumental data only cover the last 100 years or so. Japan and China have historical catalogues which extend back over 2000 years, but it is difficult to assess their accuracy and reliability. More events are needed before we can show confidently that the SGH holds.

The Seismic Gap hypothesis assumes that large earthquakes are quasi-periodic in nature. A number of other assumptions about the process are implicit in the hypothesis. They can be summarised as:

a) The plate boundaries and major faults are subdivided into natural segments.

b) Tectonic stresses *within* a segment must be relieved by an *earthquake.*

c) Such an earthquake reduces the stress significantly below the point where successive large earthquakes are possible.

d) Within each segment, stress accumulates slowly, which implies that decades need to pass before the next great earthquake.

Some, or all, of these assumptions may be incorrect. For example, work done by *Bak & Tang*[1989] suggested that the Earth's crust is in a constant critical state. A state of "self-organised criticality". If this is true, then assumption (c) is invalid.

It must be remembered that we are only discussing large earthquake occurrence. As stated in section 2.11, the energy released by large earthquakes completely dominates the energy released by the multitude of smaller earthquakes.

Nishenko[1989] lists 13 earthquakes since 1968 which have occurred in previously identified seismic gaps. Thus many seismologists treat the Seismic Gap Hypothesis as confirmed by observation. According to *Kagan & Jackson*[1991], hereafter referred to as KJ, the procedure cannot be properly evaluated by considering only these successes. We must also consider its failures. Also, if we pick a series of

random gaps, then some earthquakes will occur by chance; we must consider this in any analysis.

KJ conclude that the SGH is false, and is not statistically significant as it currently stands. *Nishenko & Sykes*[1993] make a counter claim that KJ are incorrect in their analysis and that the SGH holds. However, KJ appear to be correct in this matter, as *Nishenko & Sykes* make retroactive changes to the proposals (see chapter 5). These changes to the proposition are based on our increasing knowledge of the Earth's crust. Changes to a model or theory are not allowed until after the testing is complete. Once the test is complete, changes can be made and a *revised* model tested. Kagan and Jackson's result does not mean that a revised Seismic Gap Hypothesis could not be accepted in the future, only that the current model is unacceptable.

6.4 Mogi's Doughnuts

A second type of seismic gap was proposed by *Mogi*[1979]. This is similar to seismic quiescence outlined in chapter 4. Mogi termed his gap a "seismic gap of the second kind", to distinguish it from the first kind of gap, outlined in the last section.

He discovered that prior to a large earthquake, not only did the focal region of the impending earthquake endure a period of quiescence, but the surrounding area had a period of higher seismic activity. The diagram below, figure 6.3, shows the main points of the proposition, with each dot representing an earthquake.

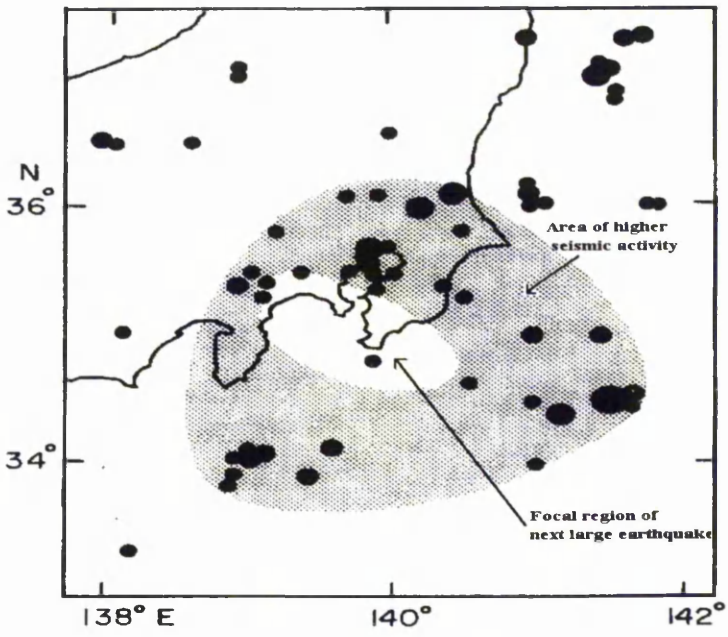

(Figure 6.3 Mogi's Doughnuts before Tokyo Earthquake)

Note that, in figure 6.3, the shaded area has high seismicity, while the unshaded, central area has almost no seismicity. As the shapes resemble ring doughnuts, this phenomena has been termed Mogi's Doughnuts.

After the large earthquake has occurred, the pattern reverses; we have high activity in the central portion and lower seismicity in the outer ring. Figure 6.4, below, illustrates this. This diagram is the "jam" in the middle of the doughnut!

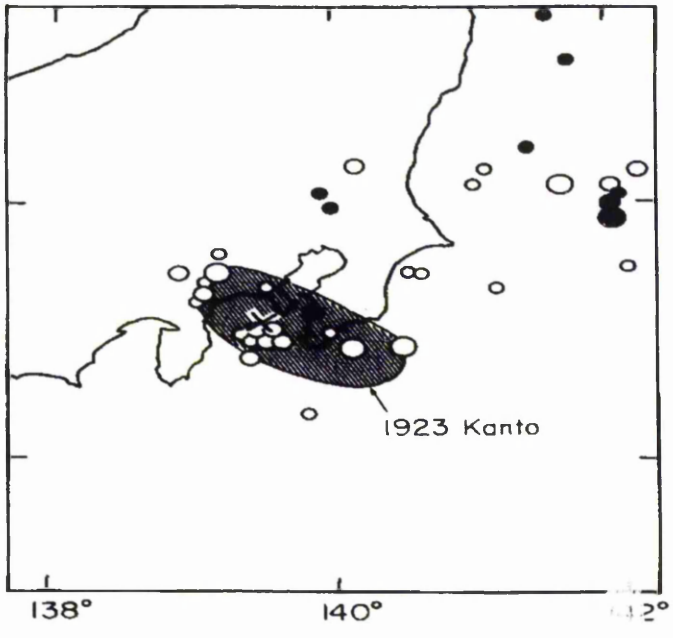

(Figure 6.4 Seismicity After Large earthquake(1923 Tokyo))

Ellsworth et al.[1981] pointed out that this type of phenomena occurred prior to the 1906 San Francisco earthquake. Other examples of this type have been found in different regions throughout the world.

How can we explain why activity decreases prior to a large earthquake? The explanation for this phenomenon is, once again, the theory of dilatancy. Cracks open in the crust due to increasing stress, causing an increase in volume. Hence, water pressure in the crack pores decreases, which results in crustal strength increasing and a decrease in seismic activity. This process is known as dilatancy hardening.

It remains to be seen, however, if this identification of seismicity patterns in the shape of doughnuts can produce predictions, as opposed to postdictions.

6.5 Forecasting using b-values

Gutenberg&Richter[1942,1944] used all the data at their disposal to produce a law relating the number of earthquakes and the magnitude. Their law states that:

$$Log\ N = a - b\,M$$

(Equation 6.1)

where N = the number of earthquakes with magnitude ≥ M

a = constant

b is a local variable but is normally approximately 1.

The *Gutenberg-Richter Law* (GR-Law) states that the number of earthquakes declines logarithmically with magnitude. The extent of the decline is given by the b-value. Figure 6.5, below illustrates this for Californian Earthquake Data from 1932-1971. Note that this relationship holds true at both regional and global scales.

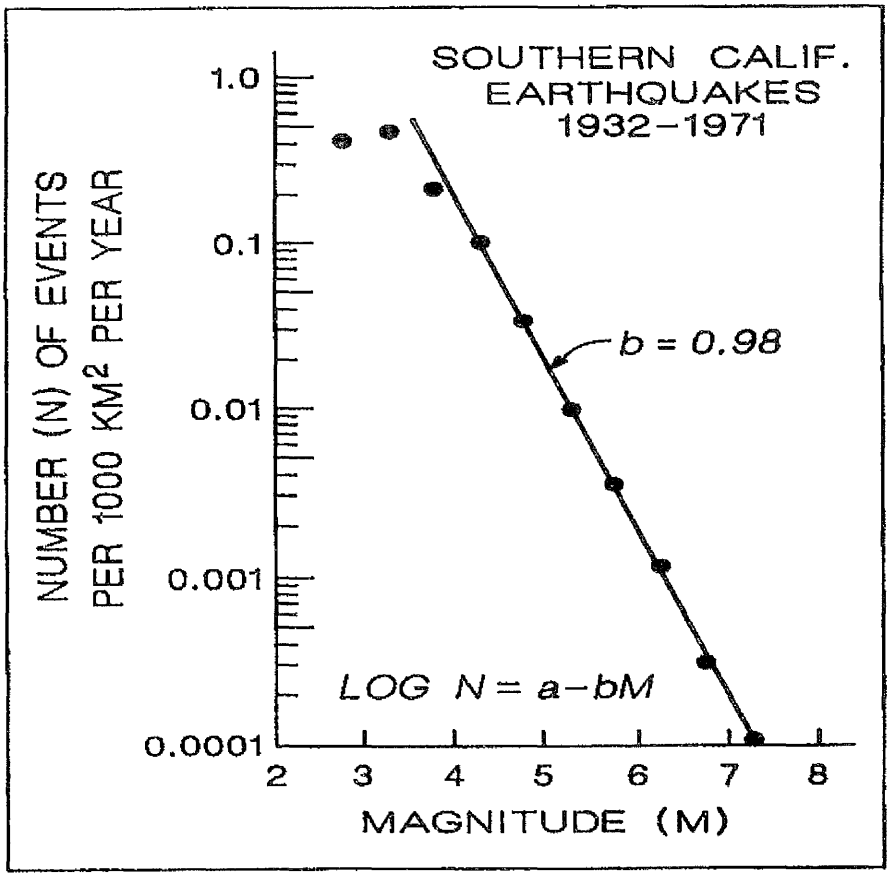

(Figure 6.5 GR-Law for Southern Californian Earthquakes)

Normally, *b* takes a value close to 1. However, it has been found that prior to large earthquakes, the b-value can drop significantly. *Suyehiro*[1966] analysed earthquake catalogues before the 1960 Chile earthquake. He found that the b-value dropped from its usual value of 1 to 0.55 before the great quake. *Scholz*[1968] claimed that the decline in the b-value is due to an increase in stress. This would be consistent with our model of stress increasing until failure.

As with other precursory phenomena, the problem is that a decrease in the b-value is not always followed by a large earthquake. This problem, allied to the fact that we must, as usual, notice the decline *before* any large earthquake makes this a difficult method for forecasting events.

6.6 Conclusion

As yet, not enough data have been accumulated to allow us to make accurate predictions based on seismic data alone. Perhaps the seismicity patterns will be so complex that we will never be able to predict earthquakes using this method alone.

At the moment, seismic data are only useful for identifying areas of high seismicity and high risk. This can help us to make rough forecasts, and allow the general public to be informed that they live in a high risk area.

We must continue collecting data in the hope that, one day, we will have enough of it to enable accurate forecasts to be made.

Chapter 7

Cellular Automata

7.1 Introduction

Many geological problems and phenomena possess properties of *scale invariance.* The observation of scale invariance in physics has tremendous importance, as scale invariance often indicates the existence of *power laws.* The advantage of power laws is that they are relatively easy to analyse and manipulate.

Mandelbrot[1967] introduced the idea of *fractals.* Fractals also deal with scale invariance. They may look the same, or similar, at different scales and different magnifications. The "Fractal" equation is a power law, and can be written as

$$N = \frac{C}{r^{D}}$$

(Equation 7.1)

where N = the number of objects with a characteristic linear dimension r,

C = a constant, and

D = the fractal dimension.

7.2 The Gutenberg-Richter Law

In section 6.5, the Gutenberg-Richter (GR) Law was outlined, along with its uses as a precursor of seismic events. The GR law can be formulated in two ways, cumulatively and non-cumulatively. In section 6.5 we expressed the cumulative form

of the GR law; here we give the non-cumulative version. The non-cumulative GR law states that the logarithm of the number, N, of earthquakes of a certain magnitude, M, is directly proportional to the magnitude. The equation is usually written as

$$Log\ N = a - bM\ .$$

(Equation 7.2)

From equation 2.2, we know that the energy, E, obeys a similar rule, i.e.

$$Log\ E = c + dM$$

$$\text{i.e. } M = \frac{Log\ E - c}{d}$$

(Equation 7.3)

Therefore, by substituting for the magnitude, M, in equation 7.2 we get that

$$Log\ N = a - \frac{b}{d} Log\ E - \frac{b\,c}{d} = K - \frac{b}{d} Log\ E\ ,$$

(Equation 7.4)

where K is some constant. This implies that

$$N \propto E^{-\frac{b}{d}}\ .$$

(Equation 7.5)

In essence, the Gutenberg-Richter Law is a power law relating the frequency of earthquakes with the energy released.

Another empirical relationship was given by *Utsu*[1969]. He found a relationship between the size, S, of the fractured zone of an earthquake and the magnitude, M. His rule can be stated as

$$M = Log\ S + 3.7$$

(Equation 7.6)

Substituting this into equation 7.2 yields

$$Log\ N(S) = a - b(\ Log\ S + 3.7)$$
$$i.e\ N(S) \propto S^{-b}$$

(Equation 7.7)

Once again, equation 7.7 represents a power law. This relationship will be used extensively throughout the rest of this chapter.

7.3 Real Earthquake Data

In order to check the validity of the Gutenberg-Richter law, real seismic data from the North California Earthquake Data Centre were downloaded from their information site on the world wide web. Earthquakes for the period 1990-1997 were used. All earthquakes with a magnitude greater than 1.5 were included in the catalogue. This provides us with a large earthquake catalogue, and a significant number of events.

Graph 7.1 was produced from the data. The two lines represent the cumulative and non-cumulative statistics. Note that for the non-cumulative data, in graph 7.1, we plot the logarithm of the number of earthquakes with magnitude M against the magnitude. For the cumulative data, we plot the logarithm of the total number of earthquakes *above* magnitude M, against the magnitude. This procedure is followed because the cumulative and non-cumulative Guttenberg-Richter Laws are mathematically equivalent (see *Main*[1995]). The gradients of the lines of best fit are also calculated.

Graph 7.1 Frequency-Magnitude Statistics for Californian Earthquakes 1990-1997

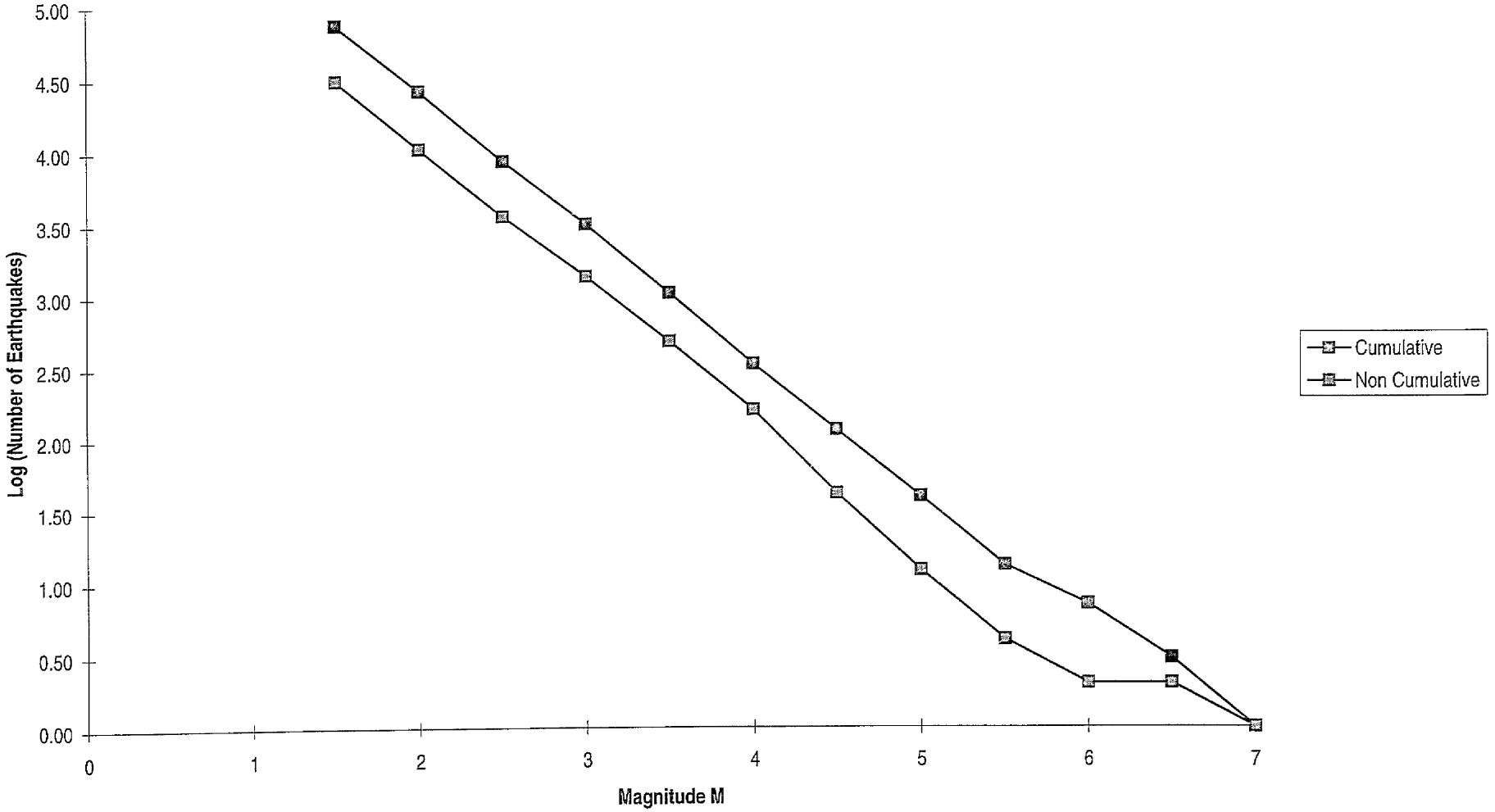

We can see that in the graphs obtained the data results in two straight lines, as expected. Note that the straight lines are very good, except at the upper limits of the magnitude scale. This effect is due to the relatively small number of events at these higher magnitudes. The gradient of the line of the best fit for the *non-cumulative* data is -0.97, while for the cumulative data the gradient is -0.94. These results imply b-values of 0.97 and 0.94 respectively.

These results are well within the accepted values for the GR Law. It has been found that, in general, the b value is approximately 1. Variations in the b value do occur, and it has been found that for a wide variety of different regions, the b value lies in the range 0.8 to 1.2.

7.4 Models

Traditional approaches to the production of physical models has tended to use a "from the bottom up" methodology. In many cases, behaviour on a macro scale has been derived from models on a micro scale. For example, the kinetic theory of gases derives large scale properties of an ideal gas from the motion of individual particles. Using well known, but admittedly idealised small scale physics, we are able to explain the macro properties such as pressure and volume.

A typical model often requires the solution of a set of differential equations which describe the general dynamics of the system. This however is a very complicated process, and as we do not fully understand the mechanism and physics of earthquake production, it is unlikely that a model such as this could be used. Perhaps this type of model could be our ultimate goal, but for the moment we will consider simpler models. The first type of model we will discuss is the "Sandbox Model".

According to *Bak, Tang & Weisenfeld*[1988], hereafter known as BTW, there is "little understanding of the spatio-temporal evolution of complex (spatially extended dynamical) systems". For example, the Earth's ecosystem cannot be

understood by the isolated study of each component. It is well known that many species are interdependent. This implies that the system will be susceptible to perturbations. As an example, consider a disease which results in a reduction in the number of ladybirds. Consequently, the number of green fly increases, and plants are damaged. This results in other animals not being able to feed properly, which results in... .

However, the system cannot be too sensitive to these perturbations, otherwise it would not be stable enough to have evolved into its present state. It is this type of balancing act which convinced BTW to term this sort of system "critical". The archetypal model for these critical systems is that of the "sandbox model". This was first proposed by BTW, and as the systems evolve themselves, naturally, with no outside tuning or tampering, they called these systems *self organised critical* systems. Information regarding self-organised critical systems can be found in the following references: [2-4], [16], [42-47], [56], [64], [72-75], [88-92], [96-98], [101-103].

7.5 Sandbox Models

The model we propose is similar to the one proposed by BTW, the main difference being the necessary adoption of different boundary conditions. We also visualise our model in a completely different way. Their model was based on a sand pile, to which sand was added randomly. Avalanches occurred when the slope of the sand pile exceeded a certain critical value. We propose a model which is based on small crustal blocks, and the strain in each block. Our model uses similar rules, but has different boundary conditions. Both models are easily represented using cellular automata, and can be simulated on a personal computer.

The essence of the model is this: when the strain in a block exceeds a critical value, then a "rupturing" is said to occur; this is equivalent to an earthquake. From chapter 2, where we outlined some of the aspects of earthquake theory, we can see that this model is a reasonable first approximation. We know that an earthquake

occurs when the strain in a particular region exceeds the strength of the rock, so the idea of strain and failure seems a natural one.

The main points of the model can be thought of as the following:

1) Divide the crust into small blocks.

2) The "strain" in each block is measured and recorded.

3) Strain is added *slowly and randomly* to the system by some process.

Note: It is essential that the rate of increase of strain is small compared with the speed of the earthquake. Otherwise we have problems with the redistribution of strain while strain is being added. In the real world, strain does indeed build up very slowly over tens or hundreds of years, while it is released in a matter of seconds by an earthquake. Also, the process by which the strain is added is assumed to be a tectonic process, caused by plate movements and mantle convection.

4) Consider the block to which strain has just been added. If the strain exceeds a critical value, then redistribute the strain to the nearest neighbours. This is the seed of the earthquake.

5) If the redistribution causes any other blocks to become unstable then, once again redistribute the strain to the nearest neighbours.

6) Repeat step 5 until there are no critical blocks remaining.

7) Go back to step 3 and repeat the process.

We begin with a one-dimensional model, and then extend it to further dimensions.

7.6 Definitions

Throughout the rest of this chapter we will be dealing with boxes or blocks which have a certain amount of strain in them. The amount of strain in a box is given by the value z for that box. We have a different name for blocks containing different amounts of strain. The classification used to describe a box depends on the strain in the box and its relation to the critical value.

In every model, the *critical value* z_c is defined as the value above which a box will rupture. Using this notion of the critical value, the 3 different types of boxes are:

a) Stable Block

This is the label we give to all blocks whose strain is less than the critical value, i.e. $z < z_c$.

b) Critical Block

This is the label given to all the blocks whose strain is equal to the critical value, i.e. $z = z_c$.

c) Unstable Block

This is the name given to any block whose strain exceeds the critical value, i.e. $z > z_c$.

Throughout the rest of this chapter these definitions will be used extensively.

7.7 The One-Dimensional Model

In this first model we will only consider one-dimension, and thus, we deal with a linear string of blocks. In this example, the number of blocks is L = 10. Figure 7.1, below, shows a schematic of the Earth's crust split up into a number of blocks. The height of each section denotes the amount of strain in the block, the higher the bar, the higher the strain. We have defined the critical value to be 3, i.e. z_c=3. In

figure 7.1, block number 6, the darker block, has too much strain, it is unstable. We can also see that blocks 2, 7 and 9 are critical blocks, while the rest are stable blocks. We must now redistribute the strain from block 6 to the two nearest neighbours, the blocks on either side.

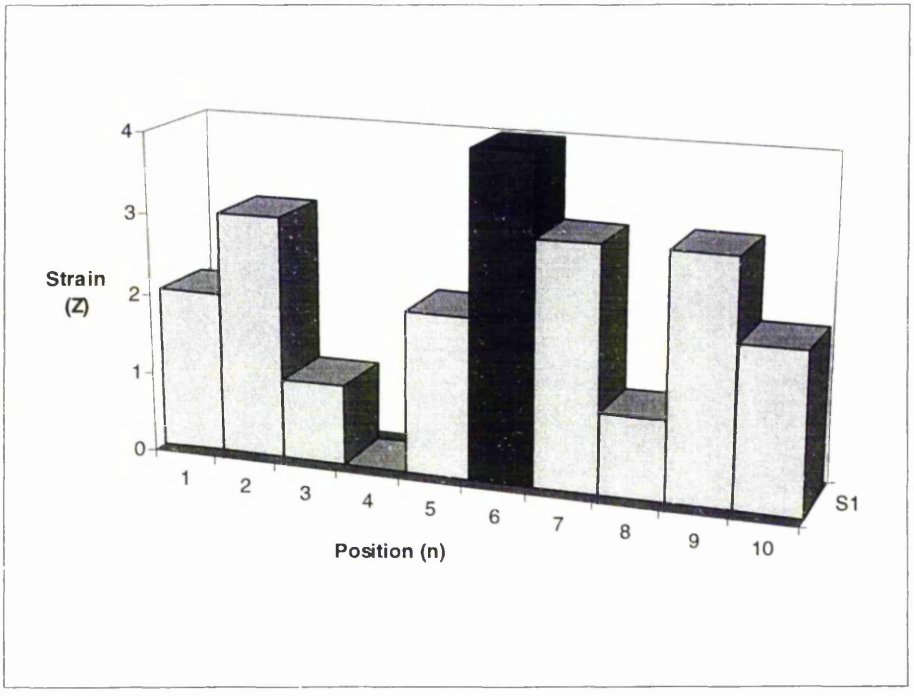

(Figure 7.1 One Dimensional Strain Model)

We can express adding strain and its redistribution in terms of a number of rules.

Rule 1 - Adding Strain

Choose a site, n, randomly. Note that $n = 1,2,...,L$. Then

$$z(n) \rightarrow z(n) + 1.$$

(Equation 7.8)

Rule 2 - Redistributing Strain

If $z(n) > z_c$ then

$$z(n) \rightarrow z(n) - 2$$
$$z(n-1) \rightarrow z(n-1) + 1$$
$$z(n+1) \rightarrow z(n+1) + 1$$

(Equation 7.9)

Note that z_c is the critical value for the strain; when z(n) exceeds z_c then we must redistribute the strain. In figure 7.1, z_c =3.

The boundary conditions we choose for our model can be expressed as :

$$z(0) = z_c$$
$$z(L+1) = 0$$

(Equation 7.10)

This implies that at one end of our linear set of blocks we enforce the condition that there is no strain, while at the other there is always strain, with the block at the critical point. This means that strain can only be "lost" from the system at one end of the blocks, i.e. at z(L). These boundary conditions are chosen deliberately to ensure that strain can only be lost at one end.

The model can be built up from scratch, i.e. $z(n) = 0 \quad \forall\, n$, or we can define an initial configuration and proceed from there.

7.8 Results

The results of this one dimensional model are fascinating. As a consequence of the simplicity of the model, we can work out the results exactly without actually performing the experiment.

For *any* initial configuration, the crustal blocks evolve into a *minimally stable state*. This terminology was introduced by *Weisenfeld, Tang & Bak*[1989]. The minimally stable state results in *every* block eventually obtaining a value equal to z_c, i.e. $z(n) = z_c \quad \forall\, n$. This situation is illustrated in figure 7.2 below.

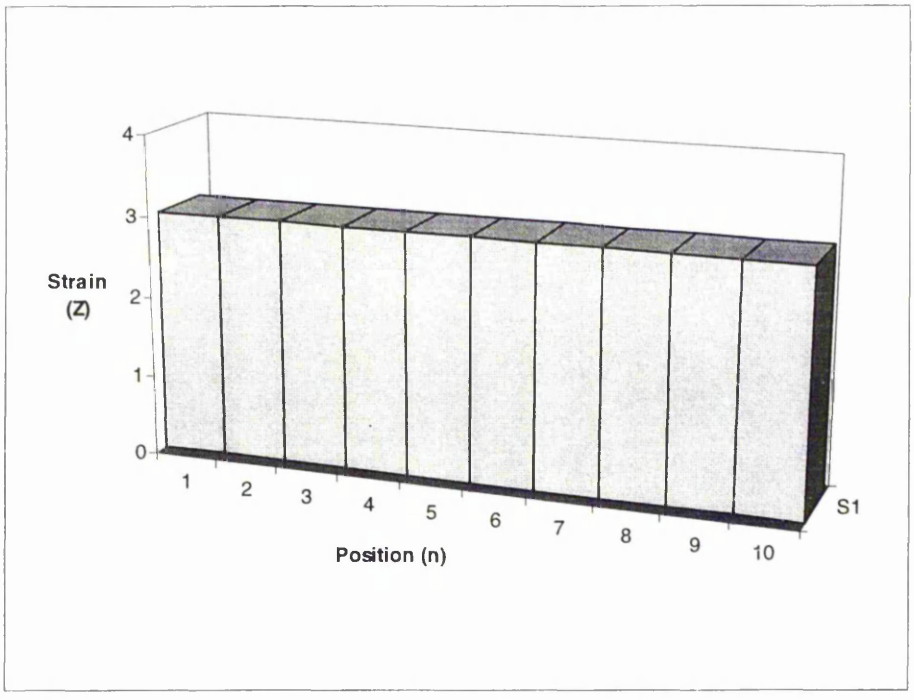

(Figure 7.2)

The effect of adding any strain to this configuration, no matter which position, is to cause a block to become unstable and hence cause a redistribution of the strain. Wherever the strain is added, we will exceed z_c, this is then redistributed using the rules outlined above, and eventually one unit of strain is "lost" at the edge of the system, block z(L). The configuration which remains is the minimally stable configuration, $z(n) = z_c \quad \forall\, n$. This state is, simultaneously, both sensitive and robust. According to *Weisenfeld, Bak & Tang*, it is sensitive because "a local perturbation propagates globally throughout the system" and robust because "the configuration is ultimately unaffected by the perturbation". Each time a unit of strain is added, the system reorganises itself and eventually loses one unit of strain at the edge of the system.

The minimally stable state is an amazing discovery. Unfortunately it is a freak, caused by the boundary conditions and the dimensionality of the model. Far more interesting is the two dimensional case.

7.9 Two Dimensional Models

In this section we extend the idea of the strain model to two dimensions. We split the crust up into small boxes in both the x and y directions. Figure 7.3, below, illustrates this procedure. The darker block is, once again, an unstable block.

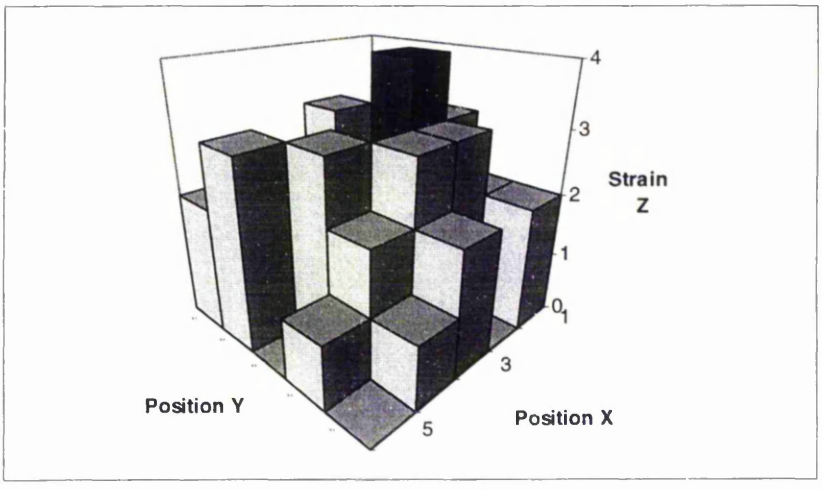

(Figure 7.3)

This model can be simulated easily using a computer program. The model can be thought of as a simple cellular automaton. We generalise the rules given in equations 7.7 and 7.8 to two dimensions.

Rule 1 - Adding Strain

A point on the grid is chosen randomly, and one unit of strain is added to this block.

$$z(i, j) = z(i, j) + 1$$

(Equation 7.11)

Rule 2 - Redistributing Strain

If the strain in any of the blocks exceeds the critical value then redistribute the strain to the 4 nearest neighbours. If $z(i, j) > z_c$ then

$$z(i,j) \rightarrow z(i,j) - 4$$
$$z(i+1,j) \rightarrow z(i+1,j) + 1$$
$$z(i-1,j) \rightarrow z(i-1,j) + 1$$
$$z(i,j+1) \rightarrow z(i,j+1) + 1$$
$$z(i,j-1) \rightarrow z(i,j-1) + 1$$

(Equation 7.12)

Figure 7.4, below, represents the redistributions given by equation 7.12.

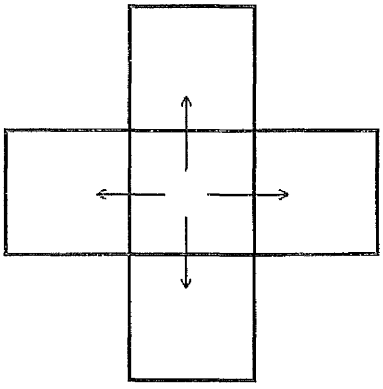

(Figure 7.4)

Again, we choose the critical value to be 3, i.e. $z_c = 3$. When the strain in any block is unstable, i.e. $z(x,y) \geq 4$, then we must redistribute the strain. The value 3 is chosen so that when we redistribute, the strain in our rupturing block is reduced to zero.

For the two dimensional model we alter the boundary conditions slightly. We change the conditions so that we have a free boundary all around the model. At every point on the boundary strain can be "lost", i.e. it is a dissipative boundary. In this case, we are dealing with a square L x L grid. We can express the boundary conditions as

$$z(i,0) = z(i,L+1) = 0 \qquad \forall i$$
$$z(0,i) = z(L+1,i) = 0 \qquad \forall i$$

(Equation 7.13)

As we are trying to simulate earthquakes, we assume that the rupturing of the blocks represents the rupturing of the crust, as in a real earthquake. How do we define the "size" of an earthquake in this model? The obvious way of doing this is to count the number of blocks which rupture after the addition of one unit of strain. Equation 7.7 showed that there is a relationship between the size of the ruptured zone and the number of earthquakes. This relationship was derived from the Gutenberg-Richter Law. Equation 7.7 can be rewritten as

$$Log\ N(S) = K - b\ Log\ S\ .$$

(Equation 7.14)

This implies that if we plot the logarithm of the number of earthquakes of size S against the logarithm of the size, then we should obtain a straight line of gradient -b.

A BASIC program was written which simulates the above model. The program is available in appendix B. The main features of the program are these:

1) We initially run the system for a very long time, to ensure that we have reached a statistically stationary state.

Note : We reach a statistically stationary state when, on average, the number of units of strain "lost" at the edge balances the number of units of strain added to the system.

2) We then add strain *randomly*, one unit at a time, to boxes on the grid.

3) We check to ensure that this box is not unstable.

4) If it is, then we redistribute the strain to the four nearest neighbours, using equation 7.11.

5) If any *new* boxes become unstable then we redistribute them.

6) We repeat step 5 until there are no more unstable boxes.

7) We count the number of boxes that were involved in the "earthquake". This is the size of our earthquake.

8) Go back to step 2 and repeat the process the desired number of times.

9) Output all the earthquake sizes to a data file for analysis.

The array used in the rest of this chapter was a 50 x 50 array. This gives us large events with over 2500 blocks rupturing, yet allows us to perform thousands of simulations relatively quickly.

7.10 Results

The computer program was executed and 10000 units of strain were added. This resulted in approximately 5000 earthquake events being recorded. Unfortunately, this gave us very poor results, as there were not enough earthquakes. We continued the experiment and performed a number of runs to give us a very large data sample. Overall, 30000 events were recorded. The reasons why this large sample is necessary will be explored later.

We denote the number of earthquakes of size S by the symbol N(S). These numbers are recorded, and a graph of Log N(S) against Log S plotted. The graphs obtained can be seen on the following page, Graphs 7.2 and 7.3. Note that the two graphs are different representations of the same data.

Graph 7.2 Frequency Size Data for Synthetic Earthquake Catalogues using Sandbox Model

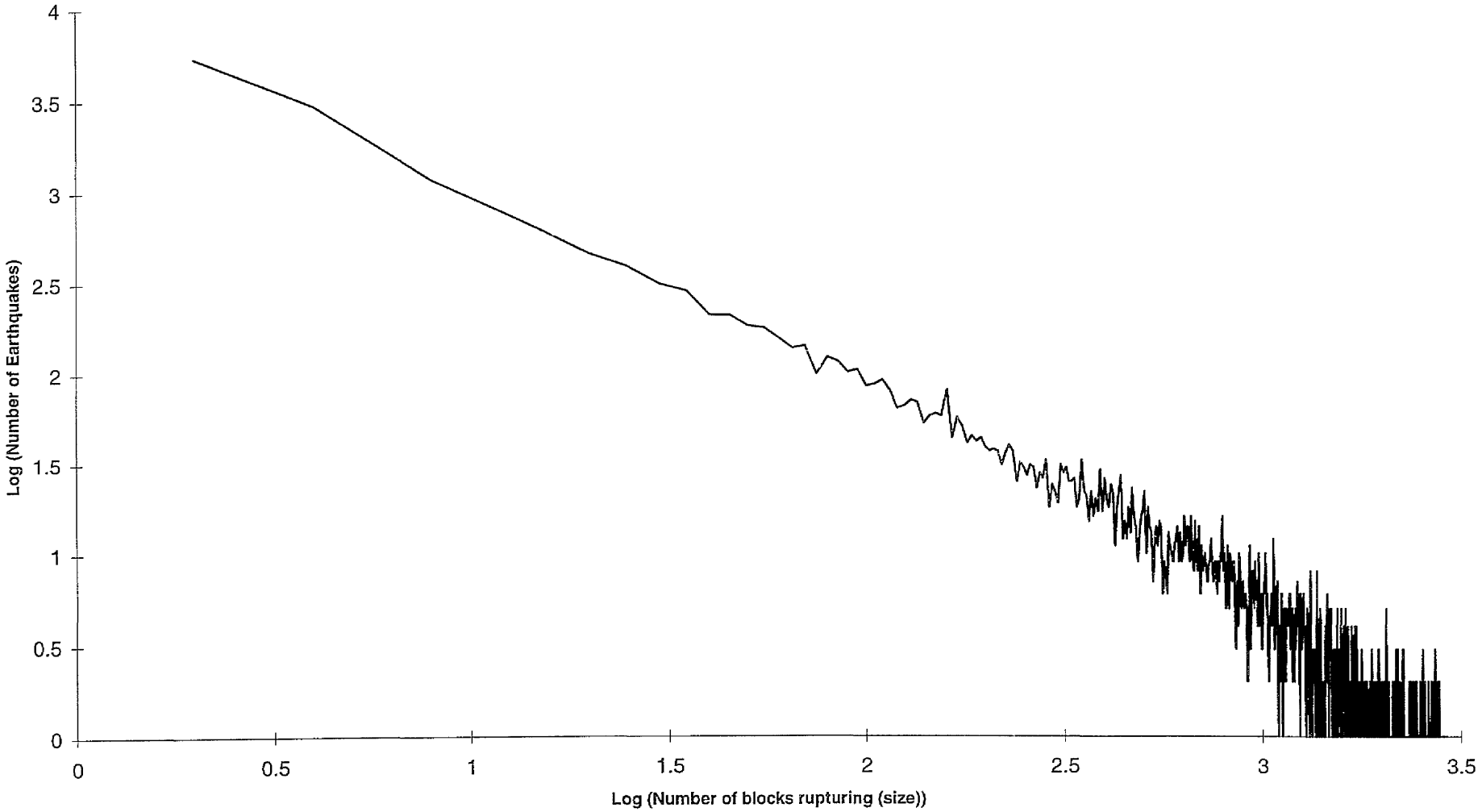

Graph 7.3 Frequency Size Data for Synthetic Earthquake Catalogues from Sandbox Model

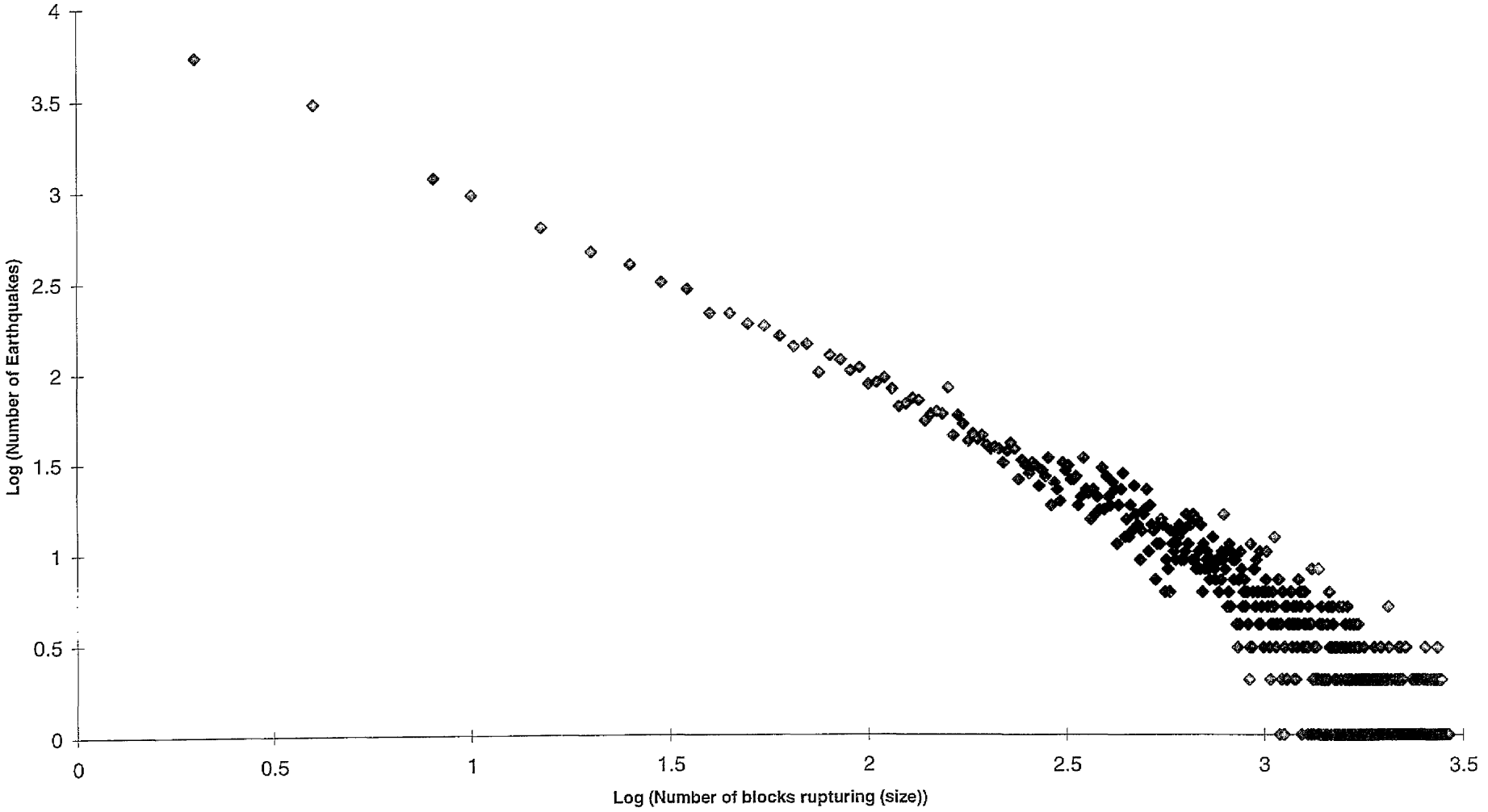

The most interesting fact to come form these experiments is the variation in the sizes of the earthquakes obtained. Obviously small events occur more often, and we have large numbers of events where only one block ruptures. The surprising aspect was the appearance of events on *all scales*. We obtained earthquakes which ruptured 1, 10 or 100 blocks. We even had earthquakes which ruptured over 1000 blocks. In fact, we had a number of earthquakes which ruptured every single block in the array. It is this *scale invariance* that is interesting.

Another interesting point to come from these experiments was the amazing "double rupturing" of some blocks. Some of the earthquakes resulted in over 2500 blocks (the size of the array) rupturing. Admittedly, there were very few events of this size, and it obviously requires a very special set of circumstances for this to happen. This result was very unexpected, but a simple analysis shows that it is feasible. For example, consider a 3 x 3 array. This small array is chosen for simplicity, but it can be thought of as a small subsection of a larger array, see figure 7.5.

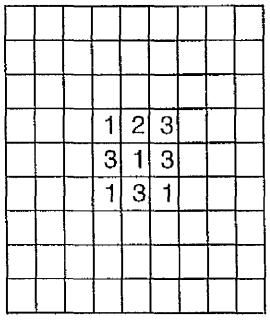

(Figure 7.5)

The diagrams below, figure 7.6 (a)-(f), represents what happens to a small array.

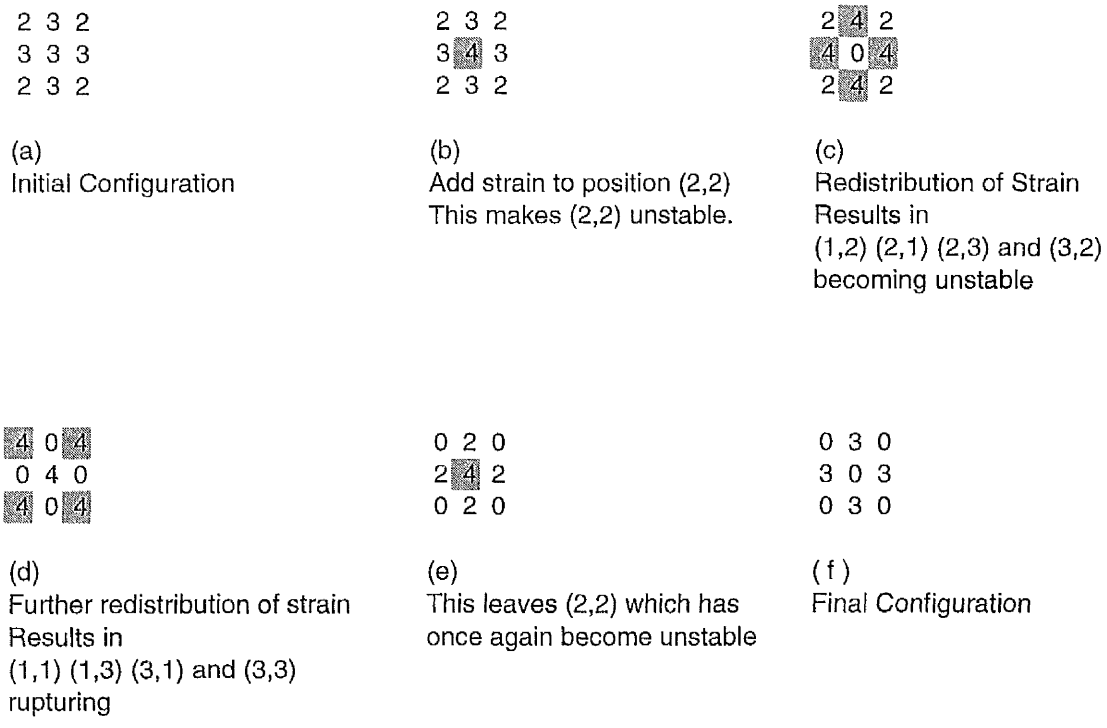

(Figure 7.6)

Once all the redistributions have been carried out, and there are no unstable blocks left, we can count the number of times each block has ruptured, and also the total number of blocks ruptured. From figure 7.6, above, we can see that the central block, (2,2), ruptured twice, and all the other blocks ruptured only once. In total we therefore have 10 "ruptures" from only 9 blocks. The same procedure works for larger scale arrays. The important point is that for "double rupturing", the 4 nearest neighbours need to be critical also, and this guarantees that the central block will rupture again. In fact, in larger arrays it is not necessary for all the nearest neighbours to be critical, as the earthquake could eventually spread round to the nearest neighbour that is not critical and make it unstable.

This multiple rupturing is a most interesting phenomenon, and more research could be devoted to this subject. Obviously this is probably unrealistic in terms of real earthquakes, as they are thought to propagate *out* from a focal region, but it is interesting nonetheless.

When analysing the graphs, it must be remembered that the larger "earthquakes" occur rarely, and hence even although we produced over 30000 events,

there are very few earthquakes at the bigger sizes. As a result, the graphs deteriorate badly at the larger magnitudes. This is identical to the results obtained for the real Gutenberg-Richter Law, where we found that because of the small number of large events, a few very large earthquakes affect the statistics.

What do we see in the graphs? The most important thing is that we obtain a linear relationship between the logarithm of the number of events of a certain size, S, and the size. This translates into there being a *power* law relationship between N(S) and S, i.e. $N(S) \propto S^b$, for some b. This is exactly what was expected from equations 7.2 - 7.7, and obtained in section 7.3, for real earthquake data. For real earthquake data we found that the b-value was approximately 1. The value for the non-cumulative statistics in section 7.3 gave a b-value of 0.97. For our sandbox model, it was found that the line of best fit, ignoring the higher magnitude sections where the data had deteriorated, had a gradient of -1.05. This translates to a b-value of 1.05. This is very close to the accepted value for real earthquakes, obtained by Gutenberg and Richter, which produced a b-value of approximately 1. This b value is also very close to the values we obtained ourselves from the Californian earthquake data. The only question mark could be the deterioration of the data at high magnitudes, but this also happens with real data, because of the rarity of large earthquakes, and therefore we do not feel that this is a significant problem. Perhaps the gradient and the graphs could be improved by taking more events into account, but this leads to problems with analysing such huge amounts of data.

What does this result tell us about our model? All of the above evidence suggests that the frequency distribution of events produced by our simplistic strain box model is similar to that produced by real earthquake mechanisms. Unfortunately, there are a number of problems with this simple cellular automaton model. The main problem with the events obtained by this model is the absence of *foreshocks* and *aftershocks*. These terms were defined in chapter 2. Perhaps by extending this model, we could achieve even better results.

7.11 Extensions

It has been suggested by *Barriere & Turcotte*[1994] that the model could be altered, and a different pattern of blocks used. Whereas our model uses a regularly spaced grid, with blocks of equal sizes, they suggest using a grid of boxes with a fractal distribution of sizes. This means that we would have boxes on all different scales, from large to small boxes. Figure 7.7 below compares the normal box layout, with one *possible* fractal box layout. Note that there are many different possibilities for our fractal distributions. This one is chosen because of its nice symmetry properties.

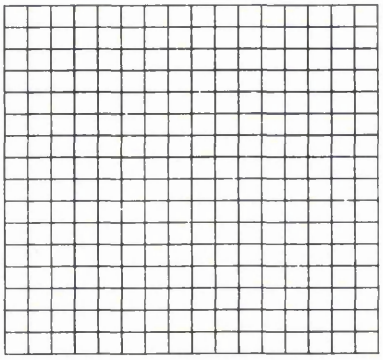

Normal Box Configuration

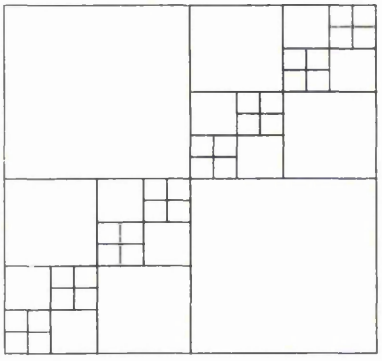

Fractal Box Configuration

(Figure 7.7)

The same rules as before are applied to this model. We add strain to the boxes in the model randomly; when the strain in a box exceeds the critical value then we must redistribute the strain. Note that the different sizes of boxes have different critical values. A large box requires more strain than a small box before it will rupture. Once again, the number of units of strain redistributed is a measure of the strength of the earthquake.

The advantage of this model is that it allows for *foreshocks* and *aftershocks*. The absence of these was one of the main deficiencies of our normal model. When a redistribution from a small box results in the instability of a larger box, then this is equivalent to a foreshock. The opposite is true for aftershocks. When a large box

redistributes, and produces instabilities in smaller boxes, then this is the analogue of a foreshock.

Other possible extensions include making our model three dimensional, or making it anisotropic. In our model we used a uniform redistribution of strain, with one unit being redistributed to each of the 4 nearest neighbours. This rule forces the model to be isotropic, but we know that the Earth is not, see Chapter 5. By altering the redistribution rules, we can make the model anisotropic. Any non-uniform redistributions will produce an anisotropic model. For example, adding 2 units of strain to the boxes above and below the rupturing block, while only adding 1 unit to the boxes to the left and right would make the model anisotropic. This would allow us to consider "faults" or "fault zones".

To make the model three dimensional, we follow the same procedure as before, only we think of z(i,j,k). Considering the speed of our program for a 50 x 50 array, the prospect of using a 50 x 50 x 50 array is not a pleasant one! This extension would, however, be relatively simple to perform if enough time was available.

7.12 Prospects for Prediction

So what do these results mean for our hopes of earthquake prediction? Unfortunately, the prognosis is not good. If the Earth's crust is constantly in a self-organised critical state, then it may be impossible to predict earthquakes.

One of the main problems we have encountered throughout this thesis is the shortness of earthquake catalogues when compared with the time scales involved in great earthquakes. This results in problems when we analyse the data statistically. The main advantage of these models is that we can produce huge amounts of data quickly, without having to wait around for events to happen. A few groups have performed similar experiments, and produced very long earthquake catalogues. Their analysis of the data gives us the following result: *there appears to be no seismic precursors.* From their data they did not discover any significant seismic patterns.

No periods of seismic quiescence were found and Mogi's doughnuts (outlined in chapter 6) were not identified. None of the other expected precursors were discovered either.

Bak & Tang [1989] analysed the temporal evolution of the energy released versus time during a typical earthquake created using their cellular automaton model. Their graph is given below, in figure 7.8.

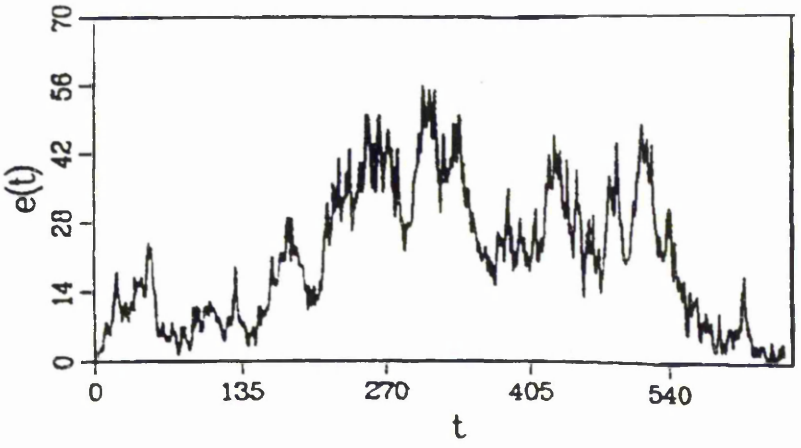

(Figure 7.8 Fluctuation of Energy release against time for a typical model earthquake)

As we can see from the above figure, at several points the amount of "energy" being released by the earthquake drops to very low levels, i.e. the earthquake is dying. The continued evolution depends on minor details in the model, or in the Earth's crust, far from the point of origin. Thus, in order to predict the size of an earthquake, we must have extremely detailed knowledge on very minor features of the crust, at large distances from the hypocentre.

These results do not auger well for earthquake prediction. Of course, it could well be that our model is too simple to produce these anticipated seismic precursors. Much further work is still required in this field.

Chapter 8

Slider-Block Models

In this chapter we discuss a mechanical model of the earthquake process. This section is based on the model originally postulated by *Burridge & Knopoff*[1967]. We will hereafter refer to them as BK. Their paper is an important one in the history of earthquake prediction; it was the first simple theoretical model of earthquake production. It has also been the basis for much further work in the modelling of earthquakes, but unfortunately little real progress has been made.

8.1 Introduction

In modelling earthquakes we wish to create an initially simple model, using physics that we understand, to produce an approximation of a real situation. Our model must explain, satisfactorily, the statistics of earthquake occurrence that we have collected at seismic monitoring stations. For example, we must explain the Gutenberg-Richter relation between frequency and magnitude.

When this model was originally postulated, most of the theories used in physics were linear theories. It is clear, however, that earthquakes with rock fracture, energy radiation and heat production are non-linear phenomena. The model which we discuss in this chapter is known as the Slider-Block model, and was originally proposed by BK in 1967. This model focuses on one aspect of earthquake production. It examines the idea that "friction between the two walls of an earthquake fault inhibits the relative displacement of the material on the two sides", *Burridge & Knopoff[1967]*. The model assumes that earthquakes are produced by the elastic rebound, or the stick-slip method, and that we have a normal fault (see chapter 2). See also *Kanamori & Anderson*[1981].

8.2 Laws of Physics

Throughout the rest of this chapter, we will use some underlying physics in the analysis of our model. The main laws that we use are Hooke's Law, and Newton's Second Law. Our model consists of blocks and springs, so we must understand some of the physics behind their movement.

8.2.1 Hooke's Law

Hooke's law is concerned with the relationship between the force required to stretch a spring and the amount of stretching. The diagram below, figure 8.1 illustrates this situation.

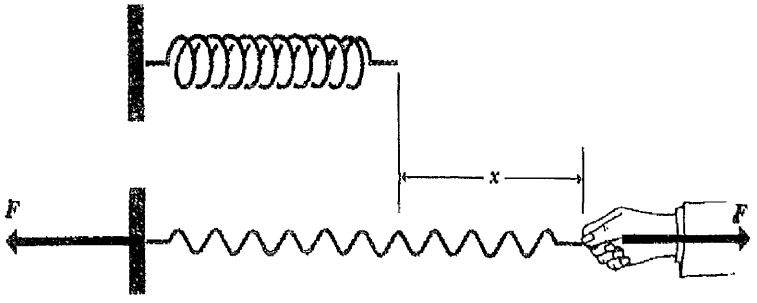

(Figure 8.1)

In figure 8.1, above, we show that to stretch the spring from its equilibrium, unstretched position by an amount x, we must apply a force of F newtons. Hooke's law states that the force, F, required to keep a string stretched an amount x beyond its unstretched length is directly proportional to the elongation x. That is $F \propto x$ or

$$F = k\,x\,.$$

(Equation 8.1)

The constant, k, in equation 8.1 is called the *force constant* or the *spring constant.* Note that Hooke's law only works for a limited range of forces and extensions. If we try to extend the spring too far, then the relationship is no longer one of direct

proportion. Throughout the rest of this analysis we will assume that we are working within the limits of the deformation of the spring, i.e. with Hookean springs.

We also need to calculate the energy, or the work done, in stretching the spring. The work done by a force, F, when stretching the spring from zero to a maximum value, X, is given by the area under the curve, i.e. the shaded area in figure 8.2, below.

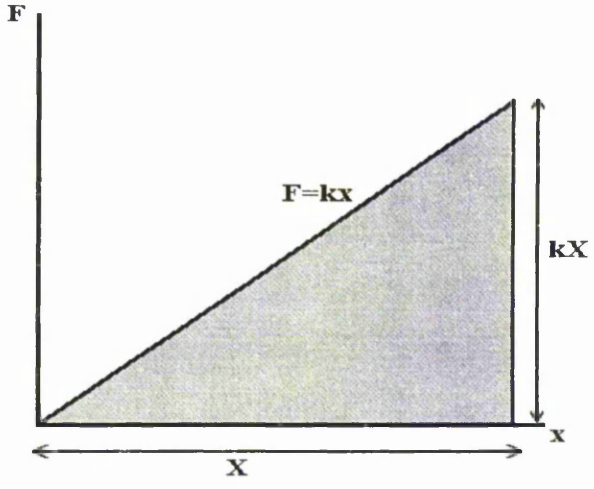

(Figure 8.2)

The area is a triangle, and the total work done is therefore given by

$$Work\ Done = \frac{1}{2} X . kX = \frac{1}{2} k X^2 .$$

(Equation 8.2)

8.2.2 Newton's Second Law

Newton's second law is one of the foundations of mechanics. It states that the acceleration of a body is directly proportional to the force exerted on the body. This can be expressed, in its familiar form, as

$$F = m a .$$

(Equation 8.3)

This law can be formulated in a number of ways, e.g. as the rate of change of momentum, but this formulation is by far the most common expression, and we will use this throughout the remainder of this chapter.

8.3 The Slider-Block Model

Our model consists of a linear array of blocks connected by springs to their nearest neighbours. The entire system lies on a rough horizontal surface. This situation can be seen in figure 8.3, below.

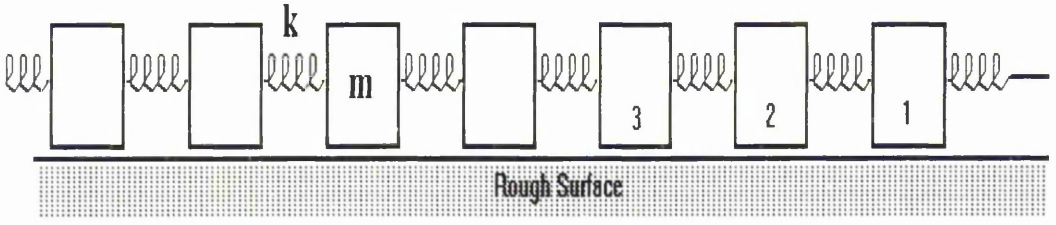

(Figure 8.3 Slider Block Model)

Note that in this section, all the springs between the blocks are identical, i.e. the springs are the same length, l, and the spring constants, k, are equal. Also note that the mass, m, of every block is the same. These conditions make the model spatially homogeneous. One other point of note is that the last block is left free.

The first block is connected to a spring which is then attached to a motor which extends the spring slowly. The first spring is stretched by the motor until the force applied to the first block is greater than the static frictional force on the first block. The first block then moves abruptly, reducing the extension in the first spring, but increasing the length of the second spring. It is this jerky movement of the blocks that we consider to be the earthquake. The string is extended slowly to ensure that the time between shocks is large compared to the duration of the shock, as in the case of real earthquakes.

The first spring is then stretched again, and the process continues. In some cases, after the movement of the first block, the increased tension in the second spring means that the force on the second block is greater than the static frictional force. This results in block 2 moving abruptly as well. The advantage of this model is that events of all sizes can be simulated. Obviously, there are more small events - where

only the first block moves - than there are large, catastrophic events, where the whole system realigns itself.

8.4 Procedure

The masses and springs are placed on the surface in some initial, random configuration and the motor is turned on. The whole system begins to stretch and moves in a series of jerky, impulsive motions. The positions of the blocks can be measured and recorded, and these data used to calculate useful statistical properties.

The potential energy of the system can be easily calculated from the positions of the blocks. In section 8.2.1, we discussed the energy required to stretch a spring (see equation 8.2). Using this relation, the potential energy of the whole system can be calculated simply by summing the potential energy of each block. Let the position of the nth mass be denoted by the symbol x_n, and the unstretched length of each spring to be l. Note that x_0 is taken to be the position of the front spring, even though there is no mass there. This allows the potential energy contribution from this spring to be calculated. Using equation 8.2, the potential energy of the system is given by the following equation:

$$P.E. = \frac{1}{2}k\left(x_0 - x_1 - l\right)^2 + \frac{1}{2}k\left(x_1 - x_2 - l\right)^2 + \ldots\ldots + \frac{1}{2}k\left(x_{N-1} - x_N - l\right)^2$$
$$= \sum_{i=1}^{N} \frac{1}{2}k\left(x_{i-1} - x_i - l\right)^2 .$$

(Equation 8.4)

In the quiet periods between shocks, the only variable that changes is x_0. The positions of the blocks are measured and the potential energy calculated as we drive the system. The results obtained are shown below.

8.5 Equations of Motion

Using Newton's law, equation 8.3 above, we can write down explicit forms for the equations of motion for the blocks in the model. We must first calculate the force on each block. We use Hooke's Law to calculate the forces acting on the blocks, based on the extension of the strings. Using the position of the two blocks and the length, l, of the spring between them, we can calculate the force acting on each block. By applying Newton's law to each block we can produce an equation for the motion of each block. Remember that the tension in one spring pulls the block to the right, while the other spring pulls the block to the left. We denote movements to the right as *positive* and movements to the left as *negative*. Note that $\dot{x}_j$ denotes the *velocity* of block j, while $\ddot{x}_j$ denotes the *acceleration* of block j. The force, $F(\dot{x}_j)$, in equation 8.5, below, is the frictional force acting on the block. Note that we assume that there is a component of static friction, and one of dynamic friction, which depends on the velocity of the block.

$$Force\ on\ block\ \ j = k(x_{j-1} - x_j - l) - k(x_j - x_{j+1} - l) + F(\dot{x}_j)$$

(Equation 8.5)

Using this expression for the force acting on the block, and Newton's law, the equation of motion for block j is :

$$\begin{aligned} m\ddot{x}_j &= k(x_{j-1} - x_j - l) - k(x_j - x_{j+1} - l) + F(\dot{x}_j) \\ &= k(x_{j-1} + x_{j+1} - 2x_j) + F(\dot{x}_j). \end{aligned}$$

(Equation 8.6)

We can repeat the above analysis for each of the blocks, and produce a system of coupled differential equations.

The solution of these equations depends upon the form of the friction law we assume acts upon the blocks. The normal law which is assumed takes the shape of the graph given in figure 8.4, below.

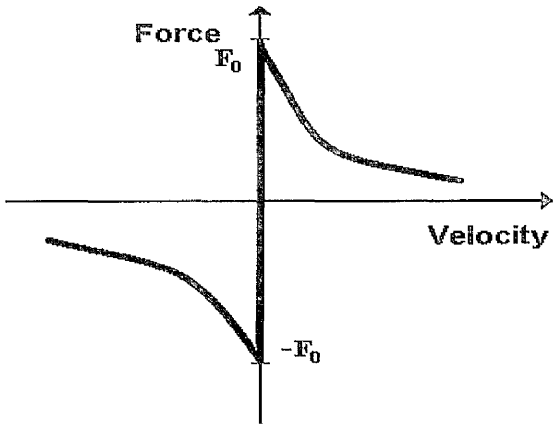

(Figure 8.4)

Figure 8.4 shows an idealised friction law which decreases monotonically with increased slipping speed. Obviously, the exact solution of these equations will depend upon the type and shape of the friction law assumed but, in principle, we can solve the equations numerically.

8.6 Results

In equation 8.4 we produced a formula for calculating the potential energy of the system from the positions of the blocks. These calculations were performed, and figure 8.5, below, shows the plot of the potential energy against time.

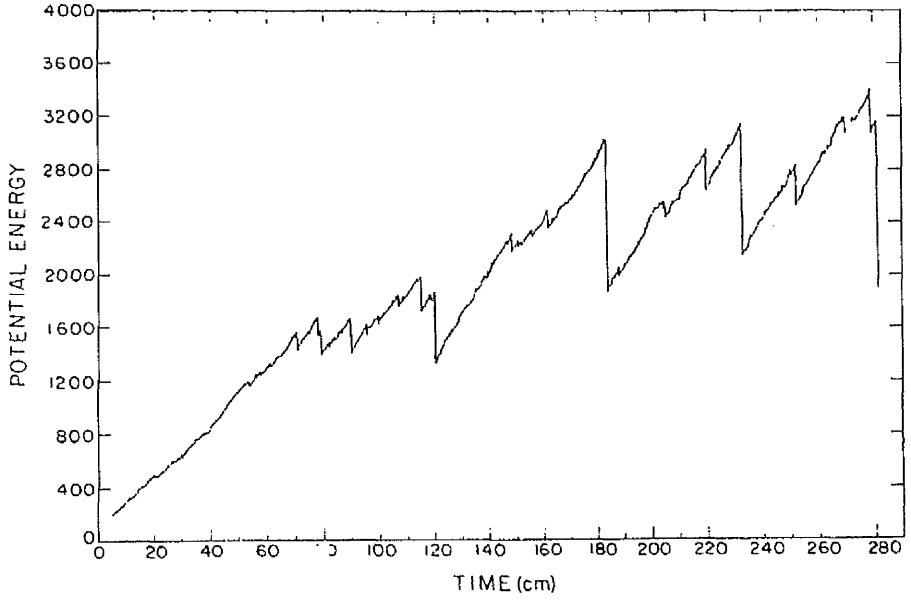

(Figure 8.5)

As we can see from the above diagram, the potential energy of the system is quite variable. Changes in the potential energy are due to the movement of the blocks. When the P.E. drops rapidly, we say that this is equivalent to an earthquake; the larger the drop, the larger the earthquake. The changes in the potential energy mirror that of real earthquakes, where we assume that the stress (energy) builds up slowly over time, and then the energy is released, in the form of an earthquake, before the strain (energy) is built up again. From the diagram, we can see that small events happen quite often, whereas the larger shocks are rarer, and quasi-periodic in nature. There also appears to be a maximum value that the potential energy can take before a large event "resets" the system. This may be due to the homogeneity of the system.

As outlined in chapter 7, there are a variety of relations between the "size" of an earthquake and the number of events of that "size". These relations can be formulated in terms of the number of events with a certain magnitude, area of rupture or energy released (see chapter 7, equations 7.2 - 7.8 for more details).

The energy-frequency distributions for this model were monitored, and the results of this analysis can be seen in figure 8.6, below.

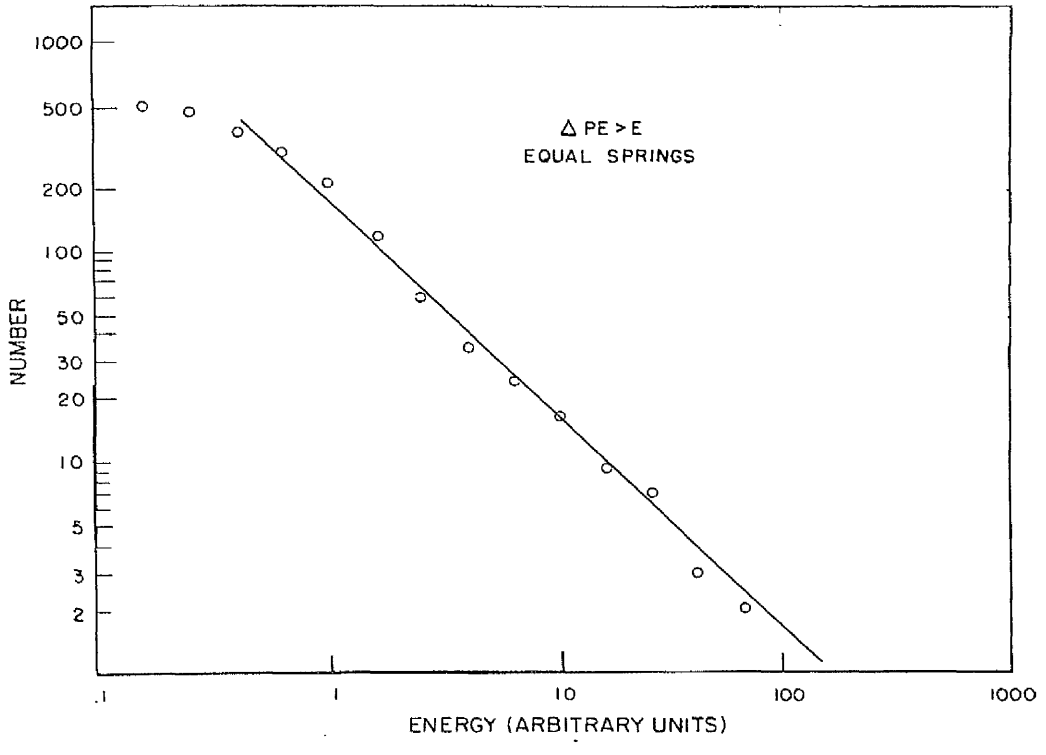

(Figure 8.6)

We can see that the relationship gives a straight line of gradient of -1, over a wide range of energies. As we know, this gives us a b-value of 1, which is the expected b-value for many regions of the Earth, i.e. the model reproduces the GR Law.

The experiments were also carried out using unequal lengths for the springs. These experiments yielded a similar set of results, only the results were far less regular than before. Figure 8.7, below, shows the graph of potential energy against time for these unequal springs.

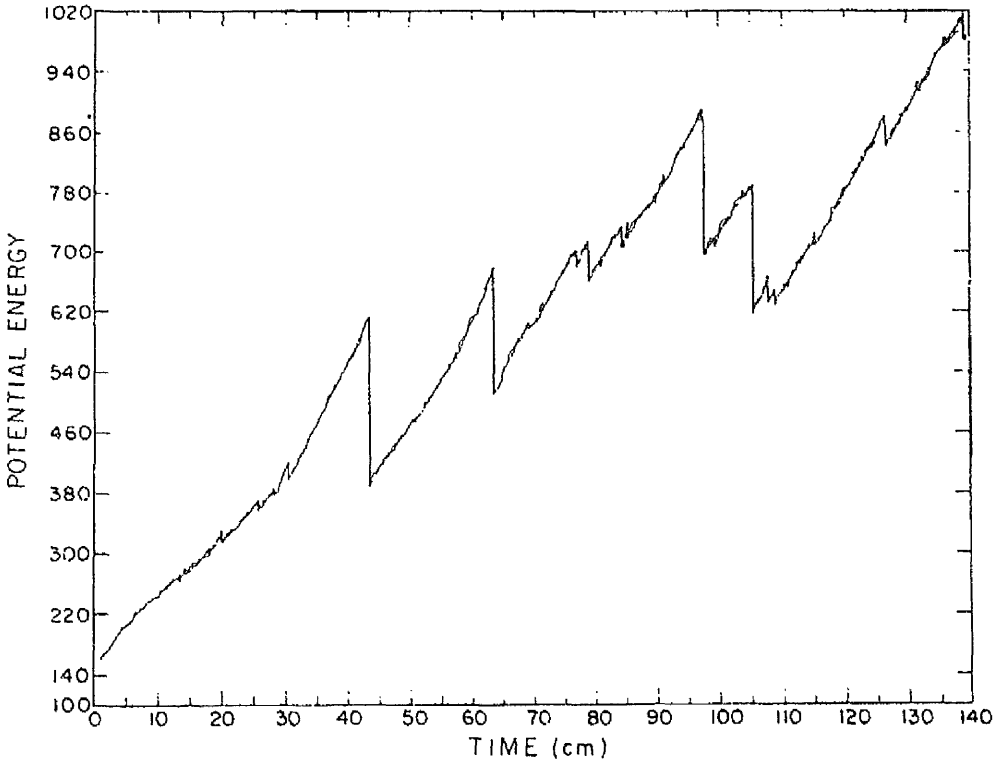

(Figure 8.7)

Once again, we can see that we have events of all sizes; large events where the entire system moves, and small events in which only one block moves. Note that this graph is not as regular as that of the equal springs scenario.

8.7 Analysis

As we have seen from the previous section, the results of the trials obtained using these models are very interesting. We can see that the relationships we obtain have certain similarities with those of real earthquakes. One of the main strengths of the BK model is that it naturally produces events of all sizes. It is therefore possible to examine correlations between small and large events.

If we compare figures 8.5 and 8.7, for the equal and unequal spring configurations, then we can see that figure 8.5 is far more regular than 8.7. In an earlier chapter we discussed characteristic earthquakes, and how they occurred at the same place on a periodic basis. Figure 8.5 resembles this situation; we have a period where the stress builds up and then we have our large, characteristic earthquake. The large synthetic events appear to occur on a regular basis, much like real characteristic earthquakes. For real earthquakes, the amount of available data for a characteristic event on a single fault is insufficient to accurately determine any mean repeat time. If this model does simulate these characteristic events, then we could analyse a large amount of synthetic data to see what we can learn.

8.8 Extensions

Variations of the BK model have been proposed by a number of parties, see *Carlson & Langer*[1989a,b], *Carlson*[1991] and *Brown et al.*[1991]. Most of the models are very similar to the original, with only minor alterations. Many extensions have tended to involve the use of a two dimensional lattice with a "driving plate", which pulls all of the blocks simultaneously. This is different from our model, where we only pulled the first block and its movement "triggered" larger earthquakes. The figure below, figure 8.8, represents this "driving plate" model.

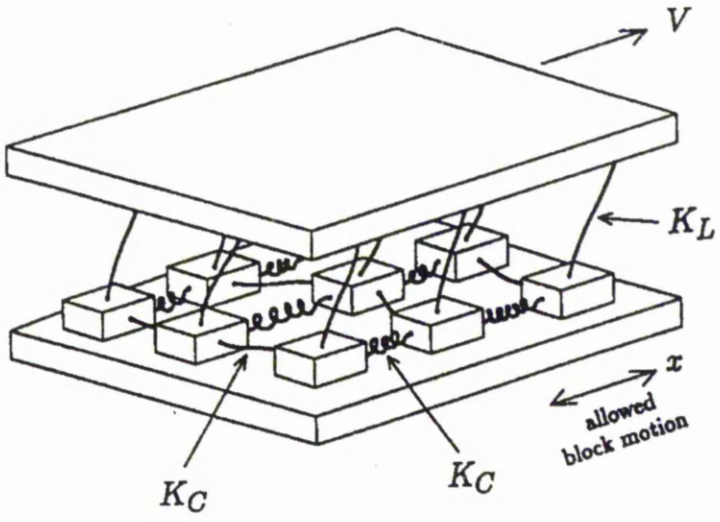

(Figure 8.8)

These models are usually "long and thin". That is we have a very large number of blocks in the x-direction, and a very small number in the y-direction. The authors also found that the ratio $\frac{K_L}{K_C}$ was an important one for the models. They found that by changing the value for $\frac{K_L}{K_C}$ they could change the seismicity patterns, as if they were changing from one type of fault to another.

We can see the connection between the cellular automata models outlined in chapter 7 and these physical models. Each block in the physical model above is represented by one square in the CA model. Obviously, the CA model is simpler as we have discrete values, whereas the slider-block models are analogue in nature.

8.9 Predictions

What does all this tell us about our ability to predict earthquakes? Work by *Brown et al.*[1989] showed that the model has the ability to improve long-term prediction of large events. They found that the recurrence time of large events had a weak temporal pattern; larger recurrence times are often followed by shorter recurrence times, and vice versa. They suggested that by training a neural network to recognise these patterns, the long-term prediction of large events could be improved. This discovery is useful, but ideally we are looking for improvements in *short-term* prediction methods.

In a very interesting paper by *Pepke & Carlson*[1994], an algorithm which measures the seismic "activity" in a certain space/time window is used to predict earthquakes. They define a space/time window as

$$R \equiv (\Delta x, \Delta t),$$

where Δx is a large circle, and Δt s some time frame. They measure the "activity", A, in this window, and use it as a measure of how likely a large event is likely to be. They define the activity as

$$A = \sum_{events\ in\ R} \Theta(M_i - M_0).$$

(Equation 8.7)

In equation 8.7, M_i is the magnitude of event i, M_0 is the lower magnitude cut-off of the events we wish to predict, and $\Theta(x)$ is the Heaviside unit step function. Basically, they count the number of events above a certain magnitude in a space/time window. When the value for the activity is either very high or very low, compared with the normal average value for this window, then they declare a *time of increased probability* (TIP) of a large event occurring. Using this they produce a *success curve* which plots the fraction of events predicted as a fraction of the total space/time occupied by the TIP alarms. As a null test they also plot the success curve for a set of random TIP alarms.

As well as the activity, *Pepke & Carlson* also define the *Active Zone Size*, AZS, which is a measure of the number of blocks which have slipped in some event contained within our current space time window. They define the AZS as

$$AZS = \sum_{sites\ k \in \Delta x} \delta(k - k') \qquad k' \text{ some event } M_i \text{ in } R.$$

(Equation 8.8)

Figure 8.9, below, shows the success curves for the activity and the AZS.

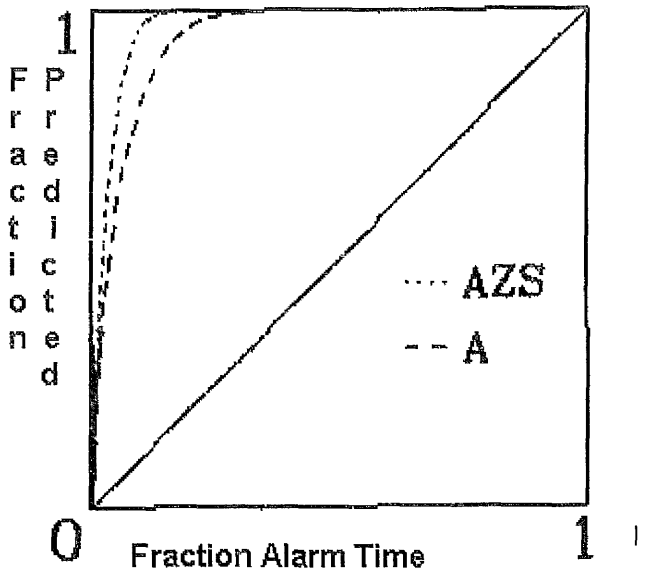

(Figure 8.9)

Their results for the BK slider block model showed success rates of over 90%. It would be interesting to see how these "precursors" worked with real seismic data. Much further work is required in this area.

8.10 Conclusions

Obviously, the model is far too simple to be an accurate representation of the earthquake mechanism, but it is a useful first approximation. With this model we have achieved a number of goals. Our simple model yields the same magnitude frequency relations and the same characteristic earthquakes as real seismic data. It also exhibits the same space/time clustering as real earthquakes. Experiments should be carried out using a larger version of this model, to see if any seismic precursors, such as quiescence or increased small shocks appear before large events. A number of the proposed extensions should also be implemented.

The advantage of these models is that we can run them for a long time to obtain large amounts of data, which is impossible in the real world. Unlike the cellular automata model that we discussed in the chapter 7, in which we randomly introduced strain, the BK model is a purely deterministic dynamical model.

The results highlighted in the last section are also promising, but once again, more research needs to be performed before we can claim any successes.

Chapter 9

Hurst Analysis and the Hurst Effect

9.1 Background

H.E. Hurst (1880 - 1978) was an English hydrologist, who spent much of his life in Egypt, studying the Nile. It is reported that he was nicknamed "Abu Nil" or "the Father of the Nile" by some of the locals, because he studied the river religiously and to such a great extent. Hurst was very interested in the designing and building of dams and reservoirs, and was involved in the planning of the great Aswan Dam. He was concerned about the storage capacity of the reservoir, in order to maximise irrigation from the Nile. In his own words:-

"The broad plan involves the storage of water from good years for use in bad ones and necessitates reservoirs of sufficient capacity to meet the shortages that might occur during a century." H.E. Hurs[1950].

Hurst spent years studying the extensive records that the Egyptians had made of the Nile's overflows. The Egyptians had recorded all the Nile's overflows since 622 AD, to produce a record stretching to 1469, a span of over 800 years. What Hurst found was that the record did not appear to be random! If there was a period with overflows which were larger than the "average", then the chances were that the preceding overflows would also be larger than average. The same applied to periods where there were smaller overflows, i.e. small overflows were followed by more small overflows. The change between large and small overflows also seemed to be rather abrupt. Hurst's work was concerned with the Nile, which was also the setting for the Biblical story of Joseph, and his interpretation of the Pharaoh's dreams. Joseph interpreted the dreams thus:-

"Seven years of great abundance are coming throughout the land of Egypt, but seven years of famine will follow them. Then all the abundance of Egypt will be forgotten, and famine will ravage the land" Genesis, 41:29-30.

This phenomenon, which Mandelbrot termed the *"Joseph effect"*, is an example of the tendency of wet and dry years to cluster into wet periods and droughts. This was demonstrated by Hurst's observations, which clearly showed that extreme periods of precipitation, whether high or low, can be lengthy. Basically, there appeared to be some sort of pattern, or some cyclic properties to the data, but with their length being nonperiodic. By using the standard statistical techniques of the time, no significant correlation could be discerned, so Hurst developed his own technique.

9.2 Brownian Motion

Since it was discovered in the early 1800s, the erratic movement of pollen grains (or smoke particles) when viewed under a microscope has been well documented. It has also been demonstrated to almost every schoolboy in the land. Robert Brown, a Scottish biologist, was the first to realise that this motion had a physical basis, and, in his honour, it is now known as Brownian Motion. Brownian Motion, or the movement of a random particle, is composed of steps, whose length seems to have some characteristic value, and whose direction is apparently random. As a result, Brownian Motion is often termed a "Random Walk" process. Albert Einstein showed that the distance that a particle travels increases with the square root of the time elapsed.

$$D = k\sqrt{T}$$

(Equation 9.1)

where D = Distance Travelled

T = Time Elapsed.

Hurst felt that, by using something similar to this, he could test for randomness in the Nile River's overflow data.

9.3 Hurst Analysis

Let $\{e_i\}$ be a time series, representing n consecutive values, of whatever quantity we are measuring. It is not important which time scale we actually use. We may use hourly data, yearly data, or whichever time scale we deem to be most appropriate for the measurements being made. When Hurst initially performed the analysis, he used annual data for the discharge from the Nile, see *Hurst*[1952]. The procedure Hurst used in his analysis was a relatively simple one, and his method is outlined below.

Hurst's technique involved the averaging of the data series to obtain the mean. He would then calculate the *accumulated* departure of the time series from the mean, using a very simple formula. The largest value for this accumulated departure is noted, as is the smallest. The Range is defined to be the difference between these two values. Finally, the sample standard deviation for the time series is calculated, and the value obtained used in the calculation of the *Rescaled Range*.

The value for the mean of the series is :-

$$\langle e \rangle = \frac{(e_1 + \ldots + e_n)}{n}$$

(Equation 9.2)

and the standard deviation of the series is :-

$$S = \left(\frac{1}{n} \sum_{t=1}^{n} \{ e_t - \langle e \rangle \}^2 \right)^{1/2}$$

(Equation 9.3)

Let X(t, n) be the accumulated departure of the time series from the mean.

$$X(t,n) = \sum_{i=1}^{t} \{e_i - \langle e \rangle\}$$

(Equation 9.4)

The greatest difference between the maximum and minimum values for the accumulated departure from the mean is called the range R.

$$R(n) = \max_{1 \le t \le n} X(t,n) - \min_{1 \le t \le n} X(t,n)$$

(Equation 9.5)

Note : The value for $\max_{1 \le t \le n} X(t,n)$ will always be greater than zero , and that of $\min_{1 \le t \le n} X(t,n)$ will always be less than zero. This occurs because we have adjusted the time series to a mean of zero. This is a consequence of equation 9.4, where at each stage we subtract the mean, before summing.

Hurst found that the rescaled range, given by R/S, was well described by the following empirical relationship:

$$\frac{R}{S} = k \left(\frac{n}{2}\right)^H$$

(Equation 9.6)

where k is a constant.

He showed that this relationship worked for a number of different types of data. There are many examples from the natural world, where we have obtained measurements of certain quantities in nature, and recorded them as a long time series, i.e. we have a series of measurements, of one particular variable, made regularly over a long period of time. For example, Hurst made use of data from a wide variety of different fields, such as Tree Growth Rings, Temperature & Pressure, Sunspot Numbers, Rainfall etc.. In fact, the exponent which we labelled H in equation 9.6, Hurst actually called K. Mandelbrot renamed it H, the Hurst Exponent, in honour of Hurst. Hurst showed that, for many natural data series, the Hurst exponent took a

Hurst. Hurst showed that, for many natural data series, the Hurst exponent took a value of approximately 0.72. This result is absolutely staggering, for if the values for our time series were independent we would expect a Hurst Exponent, H=0.5. Hurst had shown that there was some sort of correlation, and that the processes could not be assumed to be random and independent.

9.4 Why ?

An important question that needs to be addressed is :- "Why do natural phenomena show Hurst Statistics?". The generally accepted view can be expressed succinctly as "what happens now depends on what happened yesterday, and all the days before". That is, the data does not reflect a Markov process. For example, in the data Hurst originally used on river discharges, the amount of discharge from our river depends not only on the recent rainfall, but on earlier rainfall. The drainage area for a massive river, like the Nile, is obviously large. The level and amount of discharge from the river are, clearly, going to depend upon the amount of water stored in this area. For example, if we have a spell with low rainfall, we would expect the discharge level of the river to drop to a level below the average. We would also assume that the amount of water stored in the drainage area would decrease. Thus, when the rains eventually do come, the level of discharge from the river would remain lower than average, as the drainage area would absorb a proportion of the rainfall.

On the other hand, if we have a long period with high rainfall, we would expect that the quantity of water stored would increase, and that during drier spells, this excess water would be "used up", as it was released from storage in the drainage area to add to the discharges in drier years. These so called "memory" effects, or persistence, explain the appearance of the Hurst exponent, as it implies that our time series are not independent, since they depend upon earlier events.

9.5 Random Processes

To show that if we had a truly random process, we should expect the Hurst exponent to exist and take a value of 0.5, we will perform a similar experiment to the one originally performed by Hurst. There are a number of ways in which this can be achieved, Hurst himself used the tossing of coins, as well as the use of a so called "probability pack". He must have been very dedicated to his subject, as he performed thousands of repetitions of the coin experiment, as well as thousands of trials using his probability cards. We will prove mathematically, that a random process should produce a Hurst exponent of 0.5, as well as producing an empirical experiment which demonstrates this. We will use Hurst's probability pack as well as simple coin tossing to perform these experiments, but we will perform the experiments using computer simulations.

9.5.1 Preliminary Results

First we must prove a number of preliminary results. Throughout this section, we will use the following notation:

$$C_{m,n} = \binom{m+n}{n} = \frac{(m+n)!}{m!\,n!}$$

(Equation 9.7)

We also define H to be the number of heads, and T to be the number of tails as we proceed through a sequence of throws. See *Feller*[1951,1968] and *Whitworth*[1886].

Proposition 9.1

Given that we have m heads and n tails, $C_{m,n}$ is the number of sequences with m heads in $m+n$ throws. Define $J_{m,n}$ to be the number of sequences for which the condition $H \geq T$ is true at every stage. Then

$$J_{0,0}\, C_{m,n-1} + J_{1,1}\, C_{m-1,n-2} + \ldots\ldots + J_{n-1,n-1}\, C_{m-n+1,0} = C_{m,n} - J_{m,n}$$

(Equation 9.8)

Proof

Consider the diagram below (figure 9.1), in which a step to right is equivalent to a head, and a step up is a tail. The sequence of heads and tails can be thought of as a path from O to P. The line OV marks the points where H and T are equal. Note that point A is defined to be (r, r), while B = (r, r+1).

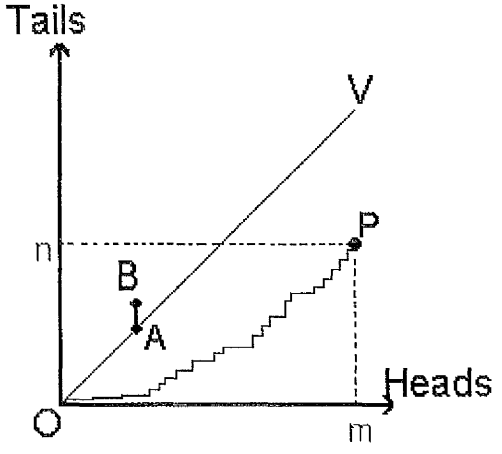

(Figure 9.1 - Sequence of Heads and Tails)

The condition will be fulfilled by *all* paths which do not cross the diagonal line OV. The paths *may* touch, the line but not cross it!

The total number of paths from O to P is $C_{m,n}$, and the number of routes which do not cross the line is $J_{m,n}$. Therefore, the number of paths which *fail* to fulfil the condition is $C_{m,n} - J_{m,n}$.

We classify these routes by the point at which they *first* cross OV. Consider the routes which first cross at the point A (r, r). At that stage we have r heads

We classify these routes by the point at which they *first* cross OV. Consider the routes which first cross at the point A (r, r). At that stage we have r heads (horizontal steps), and r tails (vertical steps). We may split the path OABP into 3 sections, OA, AB and BP.

The path OA may be made in $J_{r,r}$ ways (definition of $J_{r,r}$), while the path AB can only be made in one way. BP may be made in $C_{m-r,\, n-r-1}$ ways, as we do not care whether the path crosses the line OV again, after the point B. Therefore, OABP can be constructed in $J_{r,r} \times 1 \times C_{m-r,\, n-r-1}$ ways. Thus, the total number of paths which fail to fulfil the condition that $H \geq T$ at each stage is $\sum_{r=0}^{n-1} J_{r,r}\, C_{m-r,\, n-r-1}$, but we know that this is equal to $C_{m,n} - J_{m,n}$. Hence, equation 9.8 holds, i.e.

$$J_{0,0}\, C_{m,\, n-1} + J_{1,1}\, C_{m-1,\, n-2} + \ldots\ldots + J_{n-1,\, n-1}\, C_{m-n+1,0} = C_{m,\, n} - J_{m,\, n}$$

as required.

Using the above result, it can be shown by simple induction, that

$$J_{n,\, n} = \frac{1}{n+1}\, C_{n,\, n}$$

(Equation 9.9)

We need this result to prove proposition 9.2, below.

Proposition 9.2

Given that we have m heads and n tails, the total number of sequences in which, *at some stage*, the number of tails, T, exceeds the number of heads, H, is $\frac{n}{m+1} C_{m,n}$.

Proof

From Proposition 9.1, we have that the number of ways in which the condition (T > H) is satisfied is $C_{m,n} - J_{m,n}$, and that

$$J_{0,0}\, C_{m,n-1} + J_{1,1}\, C_{m-1,n-2} + \ldots\ldots + J_{n-1,n-1}\, C_{m-n+1,0} = C_{m,n} - J_{m,n}.$$

Substituting in the above equation for $J_{i,i}$, using equation 9.9, we have that :

$$C_{m,n-1} + \frac{1}{2} C_{1,1}\, C_{m-1,n-2} + \frac{1}{3} C_{2,2}\, C_{m-2,n-3} + \ldots\ldots + \frac{1}{n} C_{n-1,n-1}\, C_{m-n+1,0} = C_{m,n} - J_{m,n}$$

(Equation 9.10)

By using the following property of the binomial coefficient

$$C_{0,0}\, C_{m,n} + \frac{1}{2} C_{1,1}\, C_{m-1,n-1} + \frac{1}{3} C_{2,2}\, C_{m-2,n-2} + \ldots\ldots + \frac{1}{n+1} C_{n-1,n-1}\, C_{m-n,0} = C_{m+1,n}$$

(Equation 9.11)

but writing *n-1* in place of n, we may simplify equation 9.10 to obtain

$$C_{m+1,n-1} = C_{m,n} - J_{m,n}$$

(Equation 9.12).

We know, however that

$$C_{m+1,\,n-1} = \binom{m+n}{n-1} = \frac{(m+n)!}{(m+1)!\,(n-1)!} = \frac{(m+n)!}{m!\,n!}\,\frac{n}{m+1} = \frac{n}{m+1}\,C_{m,n}$$

(Equation 9.13)

Therefore,

$$\frac{n}{m+1}\,C_{m,n} = C_{m,n} - J_{m,n}$$

(Equation 9.14)

i.e. the number of ways in which T > H at some stage is $\frac{n}{m+1}\,C_{m,n}$.

Corollary 9.3

From proposition 9.2, and by rearranging equation 9.14 we get

$$J_{m,n} = C_{m,n} - \frac{n}{m+1}\,C_{m,n}$$

$$\text{i.e. } J_{m,n} = \frac{m-n+1}{m+1}\,C_{m,n}$$

(Equation 9.15)

i.e. the number of sequences in which the number of heads is always greater than or equal to the number of tails is $\frac{m-n+1}{m+1}\,C_{m,n}$.

Another useful property of the binomial coefficient is the following :

$$\frac{C_{n+h,\,n-h}}{h} = \frac{C_{h-1,0}\,C_{n,\,n-h}}{h} + \frac{C_{h,1}\,C_{n-1,\,n-h-1}}{h+1} + \ldots\ldots + \frac{C_{n-1,n-h}\,C_{h,0}}{n}$$

$$\text{i.e. } \frac{C_{n+h,\,n-h}}{h} = \sum_{r=0}^{n-h} \frac{1}{r+h}\,C_{r+h-1,\,r}\;C_{n-r,\,n-r-h}$$

(Equation 9.16).

Theorem 9.4

Given that we have n heads and n tails, then this occurs in $C_{n,n}$ ways. Of these, there are $C_{n+h,n-h}$ in which the number of tails will, at some point in the sequence, be *at least h* in excess of the number of heads.

Proof

Consider the diagram below (figure 9.2), in which a horizontal step is equivalent to the throwing of a head, and a vertical step equivalent to a tail. The line OV is the diagonal line in which the number of heads and tails are equal. The line GR is the line parallel to OV, but with a vertical offset of h, i.e. at a point on this line the number of tails is h greater than the number of heads.

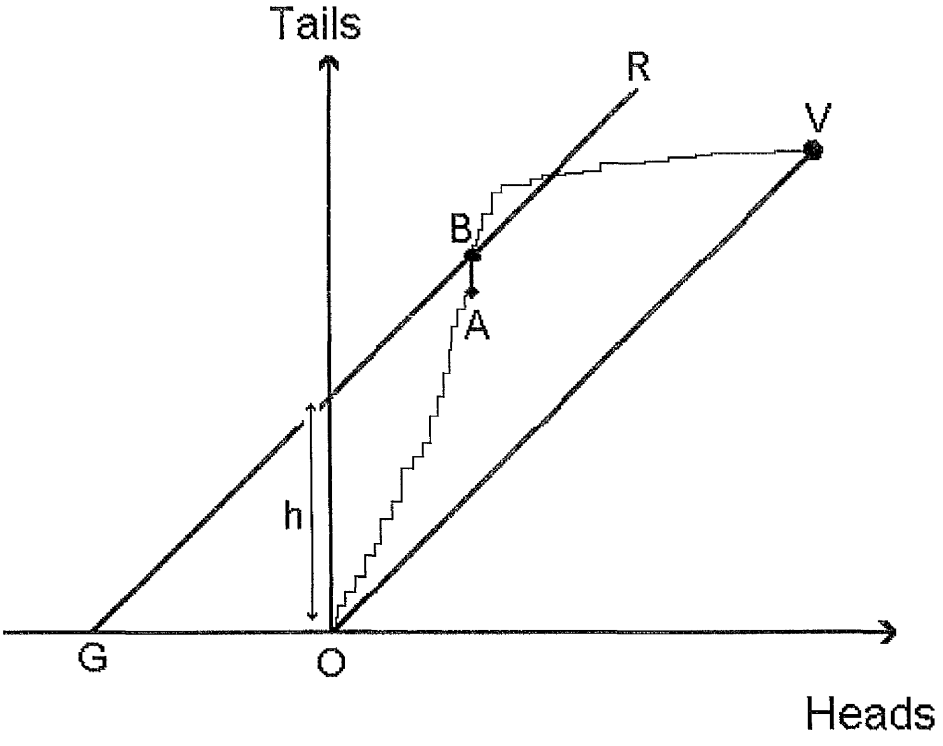

(Figure 9.2 - Representing the Sequence of heads and tails as a Path)

The point A denotes the point with r heads and $r+h-1$ tails, i.e. A = (r, r+h-1). The point B is the point with r heads and $r+h$ tails. Clearly, B lies on the line GR.

Using the above diagram, we are interested in the paths from O to V which touch or cross the diagonal line GR. We classify the paths according to the point at which they first touch the line GR.

Let OABV be any route which first reaches the line GR at a point B, a distance r steps horizontally and $r+h$ steps vertically.

Note

The point A is required because we can only get to B from 2 directions, see figure 9.3.

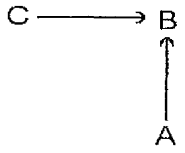

(Figure 9.3)

If we travel from C to B then we would *already* have crossed the line GR before. Therefore, we must approach B from A.

We can divide the path OABV into 3 components, namely OA, AB and BV. As before, AB can only happen in one way and BV can happen in $C_{n-r,\, n-r-h}$ ways, as we do not care how many times the path crosses the line GR after this first point; we must only ensure that we have the correct number of heads and tails.

Consider the diagram below, figure 9.4, and the path from O to A. This diagram is a simplification of figure 9.2. The line FS is parallel to GR, but is one step down, i.e. the vertical gap between FS and GR is always one unit.

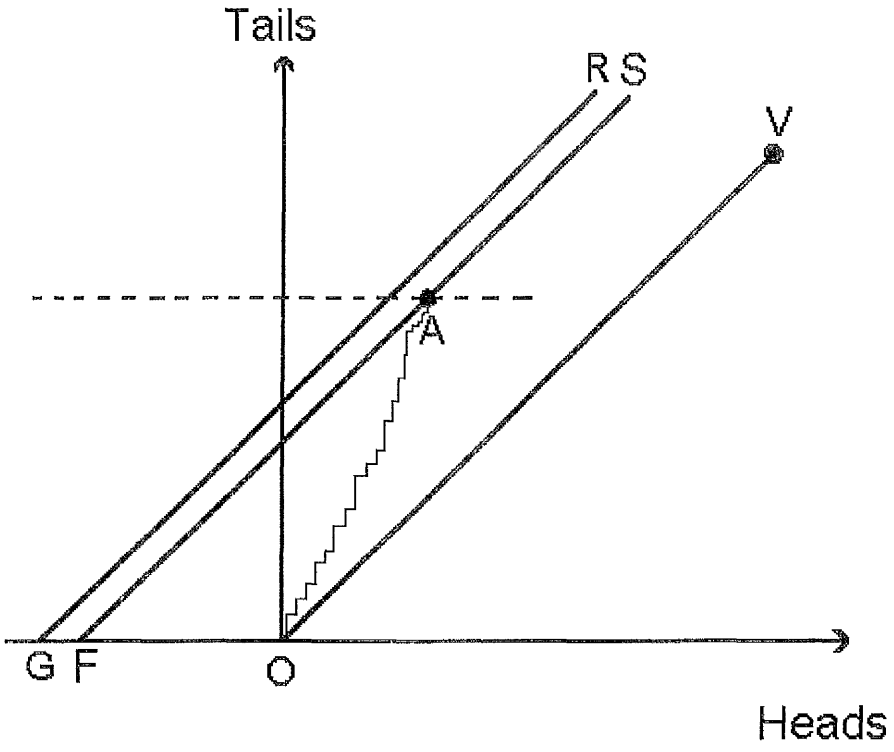

(Figure 9.4)

The path OA is the path from (0, 0) to (r, r+h-1). If, instead of the path OA, we consider the path going from A to O, such that we do not cross the line FS, we can easily calculate the number of ways of achieving this, and by using a symmetry argument, this will be the same as the total number of ways of travelling form O to A, without touching the line GR. Consider the path AO, such that we never cross the line FS. The path may *touch* the line FS, but it may not *cross* it. By symmetry, i.e. the interchangeability of heads and tails, and by a simple application of Corollary 9.3, the number of paths which fulfil this condition is:

$\frac{m-n+1}{m+1} C_{m,n}$. In this case, $m = r+h-1$ and $n = r$, which implies that the number of possible paths is $\frac{r+h-1-r+1}{r+h-1+1} C_{r+h-1,r} = \frac{h}{r+h} C_{r+h-1,r}$

Again, by using a symmetry argument, this is equal to the number of ways of travelling from O to A without touching the line GR, i.e. OA can be formed in $\frac{h}{r+h} C_{r+h-1,r}$ different ways.

Hence, the total number of paths OABV is $\frac{h}{r+h} C_{r+h-1,r} \times 1 \times C_{n-r,\, n-r-h}$.

Therefore, the total number of paths from O to V which touch or cross the line GR is

$$h\sum_{r=0}^{n-h} \frac{1}{r+h} C_{r+h-1,r}\, C_{n-r,n-r-h}.$$

From the property of binomial coefficients outlined previously (Equation 9.16), this simplifies to $C_{n+h,\, n-h}$, as required.

9.5.2 Hurst Exponent for Random Processes

We will now show that, for a random process, the expected value of the Hurst exponent is exactly 0.5. The following proof is similar to the one given by Hurst.

Consider tossing a set of $2m$ coins N times, denoting the appearance of a head by a "+1" and a tail by "-1". Note that we use $2m$ coins to make the calculation simpler. The important statistic that we wish to measure is the difference between the number of heads obtained and the number of tails obtained in our $2m$ tosses. We will denote this difference for each trial, i.e. each collection of $2m$ tosses by :-

$$e_i = \#\,heads - \#\,tails$$

(Equation 9.17)

We calculate the average for this time sequence using Equation 9.2. We then proceed to calculate the accumulated deviation from the mean, and hence calculate the range between the maximum and minimum values for the accumulated deviation. This calculation is outlined above, in equations 9.3 - 9.5.

The total number of coin tosses we have is $2mN$, and we should have the same number of heads and tails equal after all the trials are complete, namely mN heads and mN tails. This is the reason why we originally chose $2m$ coins. Henceforth, we shall denote mN by n, to simplify the notation. The total number of ways of arranging n heads and n tails is obviously :

$$\binom{2n}{n} = \frac{(2n)!}{n!\,n!}$$

(Equation 9.18)

where we are just using the standard definition for choosing n objects from a selection of $2n$. From theorem 9.4, we can see that among these orders there are

$\binom{2n}{n+h}$ occurrences of the number of tails exceeding the number of heads by h or more, at some stage of the proceedings. To calculate the mean range we need to calculate the number of arrangements where the difference between heads and tails take certain values, so that we may calculate each possible arrangement's contribution to the total. This will then allow us to calculate the mean value, by division by the total number of arrangements. For example, there are $\binom{2n}{n+1}$ arrangements where the number of heads minus the number of tails is greater than or equal to 1, and there are $\binom{2n}{n+2}$ in which heads exceeds tails by 9 or more. Therefore, the number of arrangements where, at some point in the process, the number of heads exceeds the number of tails by exactly 1, with this being the maximum "lead" the heads have over the tails, is $\binom{2n}{n+1} - \binom{2n}{n+2}$. The contribution this makes to the total is given by $1 \times \left\{\binom{2n}{n+1} - \binom{2n}{n+2}\right\}$. The multiplying factor is one, because the maximum value for the difference between heads and tails is 1. We can easily calculate the number of arrangements in which the number of heads minus the number of tails is exactly equal to k, for some k. (See Table 9.1.)

Table 9.1

Heads minus Tails	No. of Arrangements	Contribution
1	$\binom{2n}{n+1}-\binom{2n}{n+2}$	$1\left\{\binom{2n}{n+1}-\binom{2n}{n+2}\right\}$
2	$\binom{2n}{n+2}-\binom{2n}{n+3}$	$2\left\{\binom{2n}{n+2}-\binom{2n}{n+3}\right\}$
3	$\binom{2n}{n+3}-\binom{2n}{n+4}$	$3\left\{\binom{2n}{n+3}-\binom{2n}{n+4}\right\}$
.....	.....	.....
n-1	$\binom{2n}{2n-1}-\binom{2n}{2n}$	$(n-1)\left\{\binom{2n}{2n-1}-\binom{2n}{2n}\right\}$
n	$\binom{2n}{2n}$	$n\binom{2n}{2n}$
Sum	$\binom{2n}{n+1}$	$\binom{2n}{n+1}+\binom{2n}{n+2}+\ldots..+\binom{2n}{2n}$

We also know from the binomial distribution that:-

$$2^{2n}=1+\binom{2n}{1}+\binom{2n}{2}+\ldots...+\binom{2n}{n-1}+\binom{2n}{n}+\binom{2n}{n+1}+\ldots..+\binom{2n}{2n}$$

(Equation 9.19)

Hence, using the symmetrical property of the binomial coefficients, we get the sum of the products to be :

$$Sum=\frac{1}{2}\left(2^{2n}-\binom{2n}{n}\right)$$

(Equation 9.20)

Therefore, the mean maximum value of heads minus tails is

$$\frac{2^{2n-1}-\frac{1}{2}\binom{2n}{n}}{\binom{2n}{n}}$$

but this is also the mean maximum value of tails minus heads, and equals — mean min value of (heads – tails). Therefore, the mean range is:

$$Mean\ Range = R = \frac{2^{2n}}{\binom{2n}{n}} - 1$$

(Equation 9.21)

Now, as we want to be dealing with a large number of trials, n will be very large, hence we can use Stirling's Approximation for $n!$. i.e.

$$n! = \sqrt{2n\pi}\left(\frac{n}{e}\right)^n$$

(Equation 9.22)

Using this, we can calculate an approximation for $\binom{2n}{n}$.

$$\binom{2n}{n} = \frac{(2n)!}{n!\,n!} = \frac{\sqrt{4n\pi}\left({}^{2n}/_{e}\right)^{2n}}{\left(\sqrt{2n\pi}\left({}^{n}/_{e}\right)^{n}\right)^2} = \frac{2^{2n}}{\sqrt{n\pi}}$$

(Equation 9.23)

and thus, we have asymptotically :-

$$R \sim \sqrt{n\pi} = \sqrt{mN\pi}$$

(Equation 9.24)

The standard deviation of the binomial distribution produced by tossing $2m$ coins is :

$$\sigma = \sqrt{2m \times \frac{1}{2} \times \frac{1}{2}} = \sqrt{\frac{m}{2}}$$

(Equation 9.25)

This is the standard deviation for the number of heads, equally of the number of tails. The standard deviation for the number of heads minus the number of tails is twice σ.

$$S = 2\ \sigma = \sqrt{2m}$$

(Equation 9.26)

The proof of equation 9.26 is quite straight forward. Let H denote the number of heads in the series, and T the number of tails. Once again, the number of coins tossed is $2m$. Then,

$$(H-T) = H-(2m-H) = 2H-2m$$

(Equation 9.27)

The variance of H is simply the standard deviation squared, i.e.

$$V(H) = \sigma^2$$

(Equation 9.28)

The variance of (H-T) can then be calculated.

$$V(H-T) = 2^2 V(H)$$

(Equation 9.29)

Thus, the standard deviation of (H-T) is given by :

$$S(H-T) = 2\sigma = \sqrt{2m}$$

(Equation 9.30)

Therefore, as stated at the start of this section, for a random process, we get the relationship :

$$\frac{R}{S} = \frac{\sqrt{mN\pi}}{\sqrt{2m}} = \sqrt{\frac{N\pi}{2}} = \sqrt{\frac{\pi}{2}}\, N^{\frac{1}{2}}$$

(Equation 9.31)

9.6 Experiments with Random Processes

To produce data on random processes, Hurst performed experiments involving the tossing of sixpences, the cutting of cards and the numbers of odd and even digits appearing in premium bonds. These experiments are what we would now call the Monte Carlo method. We will perform two different experiments, one simulating Hurst's coin tossing and the other his card cutting procedure.

9.6.1 Coin Tossing

Hurst tossed 10 sixpences over a thousand times, in order to obtain a large amount of data with which to test his theory. We performed a similar experiment using a computer program, which generated up to 14000 different trials of 10 coin tosses. The computer does this in under a minute, even using a BASIC program, whereas Hurst would have taken over 6 hours to do only one thousand trials. The program is available in Appendix C. It must have taken a lot of dedication to have performed these trials so many times. We toss the 10 coins and, as outlined above, count a head as a "+1" and a tail as a "-1", the important quantity we measure is the *difference* between the number of heads and the number of tails in each trial. We then followed the procedure described previously, to obtain the range and the standard deviation. The data obtained can be seen in Table 9.2 and Graph 9.1. The results obtained from the computer simulation, for the Rescaled Range $\frac{R}{S}$ against time lag tau(τ), were recorded and the graph of $Ln\left(\frac{R}{S}\right)$ against $Ln\left(\frac{\tau}{2}\right)$ plotted. The graph appeared to be a straight line, as we would expect from the theory, and the gradient for the line of best fit is 0.503. This is clearly very close to the theoretical value of 0.5.

Data for Tossing Coins (Unbiased Random Process)

Table 9.2 Coin Tossing

Tau	Average R/S	ln (tau/2)	ln (R/S)
500	3.92	5.5214609	1.3660917
1000	5.25	6.2146081	1.6582281
2000	7.49	6.9077553	2.0135688
4000	10.8	7.6009025	2.3795461
8000	15.5	8.2940496	2.74084
12000	18.9	8.6995147	2.9391619

Gradient of Line of Best fit 0.503

Graph 9.1 Ln(R/S) against Ln (tau/2) for Coin Tossing

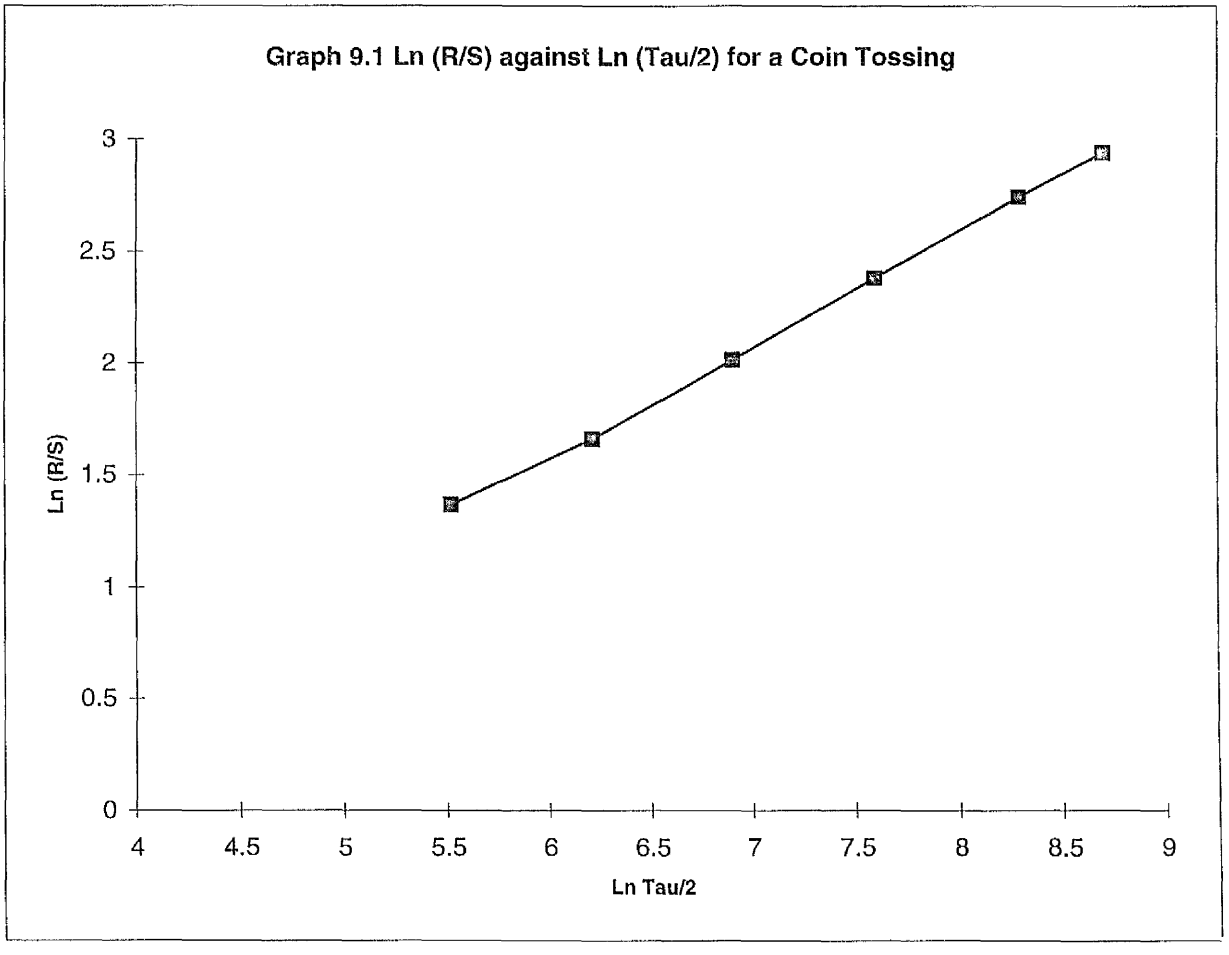

9.6.2 Probability Pack Experiments

Hurst also performed a series of experiments based upon what he called a "Probability Pack". Taking a pack of 52 cards, we label 13 of them with a "+1", and 13 with a "-1", 8 each of "+3" and "-3", 4 are labelled with "+5, and 4 with "-5", and finally we label 1 each with a "+7" and "-7". (See table 9.3)

Table 9.3 Probability Pack Distribution

Label	Distribution
-7	1
-5	4
-3	8
-1	13
1	13
3	8
5	4
7	1

We can see that the total number of cards is 52, and by examining the graph below we can see that it has the general appearance of the Normal Distribution with mean zero and standard deviation 3, i.e. N(0,3).

Graph 9.2 Distribution of Probability Pack

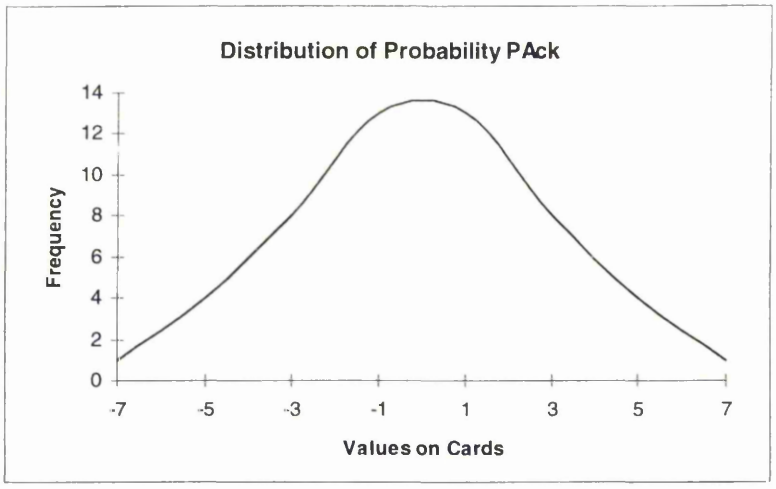

The procedure we used to perform the experiments is as follows:-

1) Shuffle the pack thoroughly.

2) Cut the pack and record the value on the exposed card.

3) Repeat the above process.

The sequence of cards cut, and values recorded, has a frequency distribution which is equal to that of the Normal Distribution. We would expect this, as the distribution of our cards is approximately Normal. This process could be performed manually, but it is easily simulated using a computer program. As before, a program was written in BASIC. This language was used as the procedure is relatively simple, and does not require a large amount of computer power. This program is available in Appendix C. The data obtained can again be seen in Table 9.4 and Graph 9.3. When we plot the graph of $Ln\left(\frac{R}{S}\right)$ against $Ln\left(\frac{\tau}{2}\right)$,we can see clearly that we obtain a straight line, as expected, and that the gradient of the line is 0.504. This is again very close to the theoretical value of 0.5.

Data for an Unbiased Random Process using Probability Cards

Table 9.4 Probability Pack Experiment Data

Tau	R/S	ln (Tau/2)	ln (R/S)
1000	35.65	6.21	3.57
2000	49.89	6.91	3.91
3000	60.34	7.31	4.10
4000	68.23	7.60	4.22
5000	75.56	7.82	4.32
6000	83.25	8.01	4.42
8000	97.56	8.29	4.58
10000	113.27	8.52	4.73
14000	137.51	8.85	4.92

Gradient of Line of Best Fit 0.504

Graph 9.3 Ln (R/S) against Ln(tau/2) for a Probability Pack

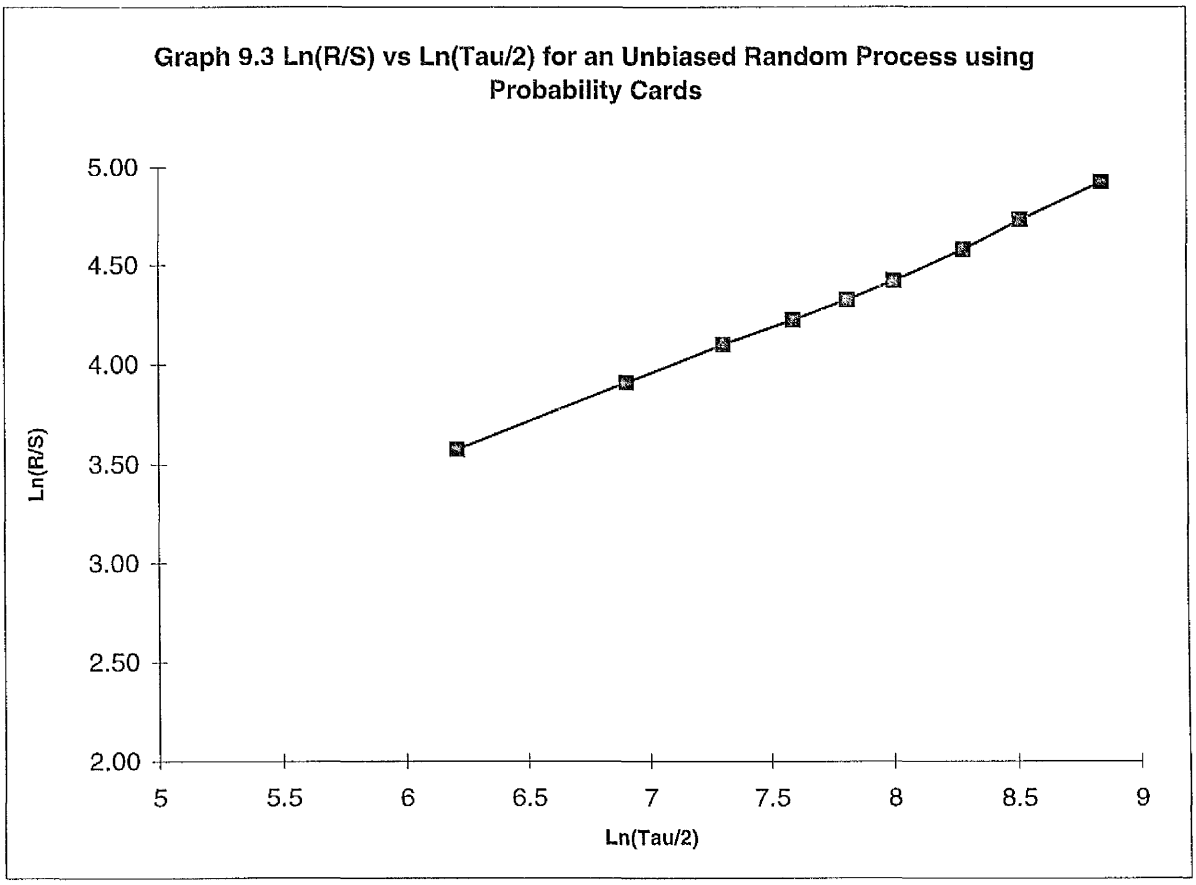

9.7 Biased Random Processes

Hurst extended his work on the Probability Pack to introduce some sort of biasing factor. He wanted to see if this biasing affected the value of the exponent obtained after using his new analysing technique, the rescaled range analysis. The procedure he followed, used the same pack of cards as before, but the deck was subtly biased using an ingenious technique.

9.7.1 Biasing the Probability Pack

Hurst biased the pack by transferring high cards (or low cards) from the first hand to the second hand, while simultaneously taking the lowest (or highest) cards in the second hand and transferring them to the first hand. The procedure used is as follows :-

1) Shuffle the pack thoroughly.

2) Cut the pack and note the value on the exposed card.

3) Deal two separate hands (each will have 26 members).

4) If the card exposed in part (2) was "+5", then the five highest cards in hand 1 are transferred to hand 2, and the five lowest in hand 2 removed and transferred to the first hand.

Note. It does not matter whether we now use the first or second hand, as long as we are consistent in our method throughout the trial. The hand we use will now be biased, with either a "positive" or "negative" bias. Over a large number of trials, and as a result of the symmetry of our distribution, we should obtain the same number of "positive" and "negative" biased hands.

5) Place a "joker" in the first hand. (or the second, see note above.)

6) Shuffle the first hand, again, to ensure that well mixed.

7) Cut the pack, and note the value on the exposed card.

This will be used to build up our biased sequence.

8) Repeat steps 6 & 7 until a "joker" is cut.

9) When a "joker" is cut go back to step 1.

We can repeat this process indefinitely, building up a long random sequence, but this time we have introduced a definite bias. Hurst performed this experiment a number of times with up to one thousand cuts. He obtained a value for the Hurst exponent of 0.714, which was very close to the value he obtained for natural series.

9.7.2 Experiments on Biased Packs

We generated a random sequence using the method described above. Again, the procedure was performed with the aid of a BASIC program, which is available in Appendix C. We analysed the data obtained, by plotting the graph of $Ln\left(\frac{R}{S}\right)$ against $Ln\left(\frac{\tau}{2}\right)$. It can be clearly seen from Table 9.5 and Graph 9.4, that we do have a straight line, but we do not have a gradient of 0.5, which we obtained with the unbiased processes. The gradient of the line of the best fit obtained from our computer simulation is 0.62. This strange change in the gradient is entirely due to the introduction of the "joker" and the biasing of the hands. Each hands biasing, and the subsequent memory of the deck, results in this change. Therefore, it is reasonable to assume that, for natural processes which display a Hurst exponent of greater than 0.5, there is some long term dependence or "memory", and that the events cannot be assumed to be random or independent. In the next section we will demonstrate that for Earthquake Data from the North California Earthquake Data Centre, one of the regions discussed earlier, that *earthquakes cannot be regarded as random or independent.*

Data for R/S and Tau using a biased Hurst hand

Table 9.5 Biased Probability Pack Experiments

Tau	R/S	ln tau/2	ln R/S
500	63.2	5.52	4.15
1000	89.76	6.21	4.50
2000	140.65	6.91	4.95
3000	172.23	7.31	5.15
4000	202.11	7.60	5.31
5000	232.21	7.82	5.45
6000	268.35	8.01	5.59
8000	325.14	8.29	5.78
10000	410.91	8.52	6.02
14000	498.36	8.85	6.21

Gradient of Line of best fit
0.621

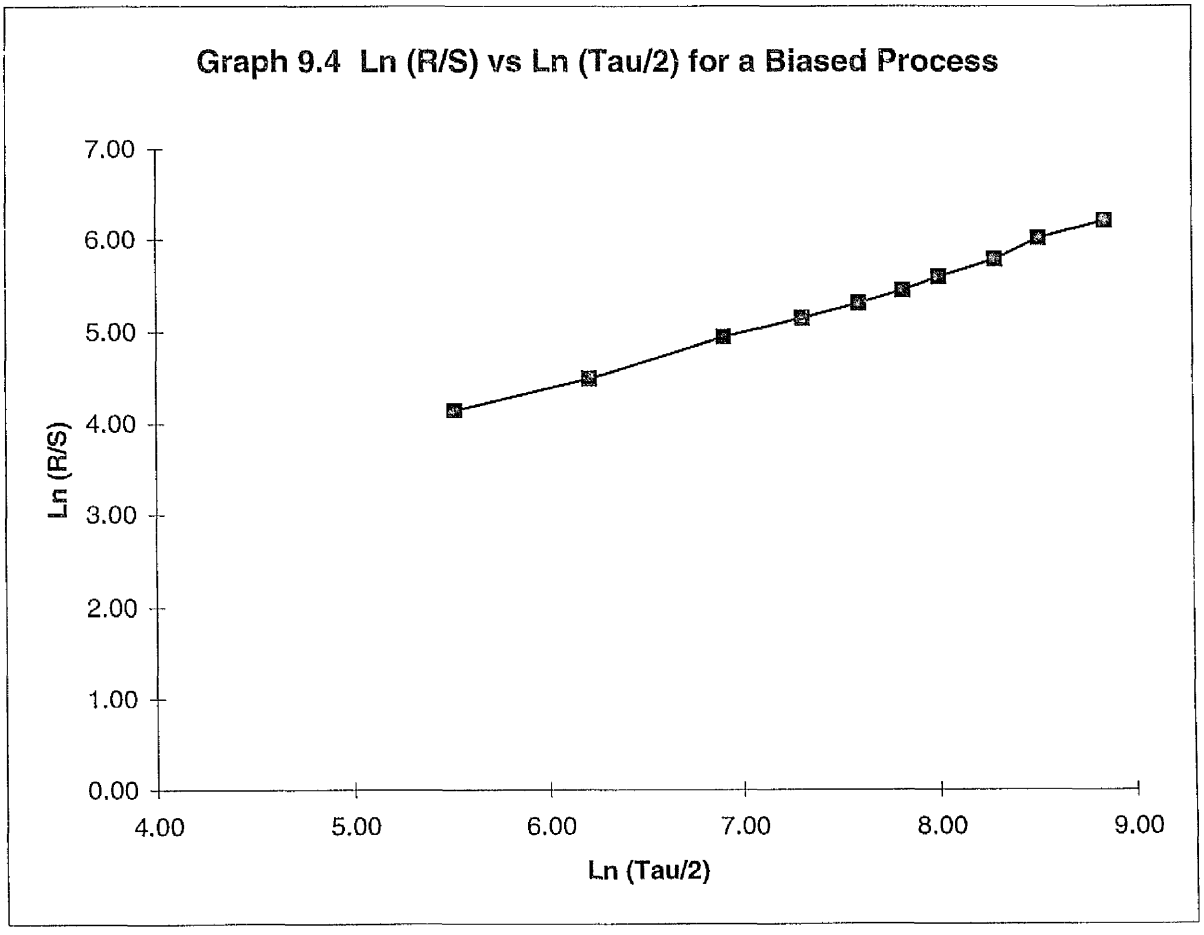

9.8 Interpreting the Hurst Exponent

We have shown, both mathematically and experimentally, that for an independent process, the Hurst exponent is expected to exist, and take a value of 0.5. In the previous section, it was shown that, by biasing the pack, and ensuring that the process was not independent, but had a "memory", that the value for the Hurst exponent increased to a value greater than 0.5. What does this increase actually imply?

In the case of $H > 0.5$, the important result is that the series is *persistent*. Persistent time series are characterised by long term memory effects. In theory, these memory effects are infinite; what happens today has an effect forever. These long memory effects occur, no matter what time scale we are using. As a result, there is no characteristic time scale. In Hurst's case, for annual river discharges, the Hurst exponent of 0.72 suggests that the time series is persistent, and that all future annual discharges are correlated. This property can be interpreted in another way. We can think of our time series as fractional brownian motion, and if the Hurst exponent is greater than 0.5, then our walk will cover more distance than a random walk.

We can also have a Hurst exponent less than 0.5. This result leads to an *antipersistent* time series. An antipersistent series tends to reverse its direction more frequently than a random one, and constantly turns back to the point form which it came. In our random walk analogy, this implies that the time series covers less ground than a random one.

As we have seen from Hurst's results, persistent time series are the most common found in nature.

9.9 Hurst Analysis of Earthquake Catalogues

In the previous sections, we discussed Hurst Analysis, and the application of this technique in relation to random or independent events, showing that for random events a Hurst exponent of 0.5 is expected. We also demonstrated that, for processes with long-term correlations or so called "memory" effects, the Hurst exponent increased to a value greater than 0.5. In this section, we will calculate the energy released by a series of earthquakes in the North California region. The energy values calculated will then be used as the basis of our Hurst Analysis. As discussed earlier, the energy of an earthquake, can be estimated empirically using the relation :-

$$Log_{10} E = 11.8 + 1.5 M_s$$

(Equation 9.32)

where the energy E is in ergs. This equation can be easily modified to enable us to calculate the energy explicitly from the magnitude of the earthquakes considered. We shall perform the Hurst analysis technique on this data set.

9.9.1 Which Earthquakes?

Thanks to the recent improvements in seismometers and the increased number of seismic stations, measuring techniques have developed significantly, with data more accurate, and more reliable than ever before. This has enabled seismic stations to record very small earthquakes, known as microquakes. These small events are frequent, and result in huge numbers of earthquakes being detected, and recorded, by the seismic monitoring networks. To ensure that the number of events which we handled would not be excessive, we placed certain limits on the size of the earthquakes used. Fortunately, the energy of the earthquakes is calculated using a logarithmic scale (see equation 9.32), and this is of considerable use to us. This

property means that an increase of only 1 in the magnitude of the earthquake results in an energy increase by a factor of over 30, and a magnitude increase of 2 implies an energy increase by a factor of 1000. As we can see from Table 9.6, a large event , such as a magnitude 6.0 quake, releases 1 *million* times more energy than an event with magnitude 2.

Table 9.6

Earthquake Magnitude	Energy Released (ergs)
2.0	6.31×10^{14}
3.0	2.00×10^{16}
5.0	2.00×10^{19}
6.0	6.31×10^{20}
8.0	6.31×10^{23}

Thus, a very large earthquake, or even a moderately large one, will completely dominate all the smaller quakes in energy terms, even allowing for the increased frequency of smaller events. It was felt that this property could be used to eliminate the smaller quakes, to make calculation easier. As a result, it was decided that only earthquakes with a magnitude in excess of 2.5 would be considered. In the region under investigation there were well over a hundred earthquakes with magnitude between 4 and 5, as well as more than twenty quakes with a magnitude greater than 5. In the catalogue considered, these events are enough to dominate the large number of small quakes. The employment of this selection procedure still resulted in over five thousand events for the period under consideration.

9.9.2 Procedure

We calculated the energy for each of the earthquakes remaining in our catalogue, using the formula given earlier (see equation 9.32). In the first analysis, we wanted to investigate the rescaled range for a time scale of the order of weeks. Thus, the energies for each individual earthquake were summed, to give a total value for each week's seismic energy release. This value was then used as the data for the time series, $\{ e_i \}$. We performed the analysis, outlined earlier, using this time series. We calculated the mean, the accumulated deviation from the mean and the maximum and minimum values of this deviation. This enabled us to calculate the range, and hence the rescaled range by division by the sample standard deviation.

The next step was to change the time scale, and then repeat the analysis. The time scale was changed to monthly, and the total energy released per month calculated for the data. The Hurst analysis was then performed on this time series, as above.

9.9.3 Results

Once the calculation of all the appropriate energies was complete, it was possible to work out the value for the rescaled range (R/S) for various time lags (τ). As before, the data were then plotted in the form of a graph of $Ln\left(\frac{R}{S}\right)$ against $Ln\left(\frac{\tau}{2}\right)$.

The results for the weekly time scale can be seen in Table 9.7 and Graph 9.5, while the results for the monthly time frame can be seen in Table 9.8 and Graph 9.6.

Hurst Analysis for Weekly Earthquake Energy Data
(North California)

Table 9.7 Hurst Analysis for Weekly Data

Tau (Weeks)	R/S	Ln (tau/2)	Ln (R/S)
10	2.85	1.61	1.05
15	3.62	2.01	1.29
20	4.25	2.30	1.45
25	4.80	2.53	1.57
30	5.30	2.71	1.67
35	5.75	2.86	1.75
40	6.17	3.00	1.82
45	6.56	3.11	1.88

Gradient of Line of Best Fit

0.552

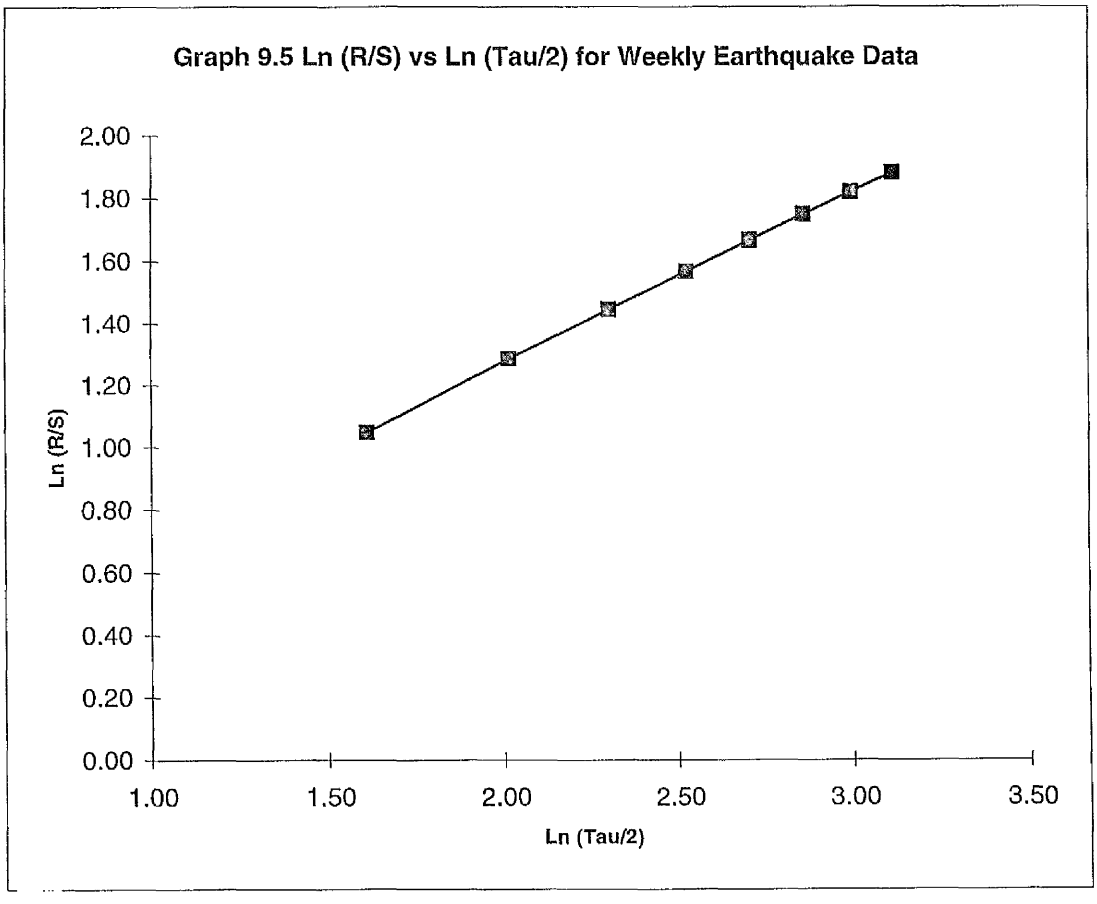

Hurst Analysis on Earthquake Catalogues for Monthly Data

(North California)

Table 9.8 Hurst Analysis for Monthly Data

Tau (Months)	R/S	ln tau/2	ln R/S
10	2.39	1.61	0.87
15	3.09	2.01	1.13
20	3.64	2.30	1.29
25	4.30	2.53	1.46
30	5.16	2.71	1.64
35	5.93	2.86	1.78
40	6.36	2.92	1.85

Gradient of Line of best fit

0.743

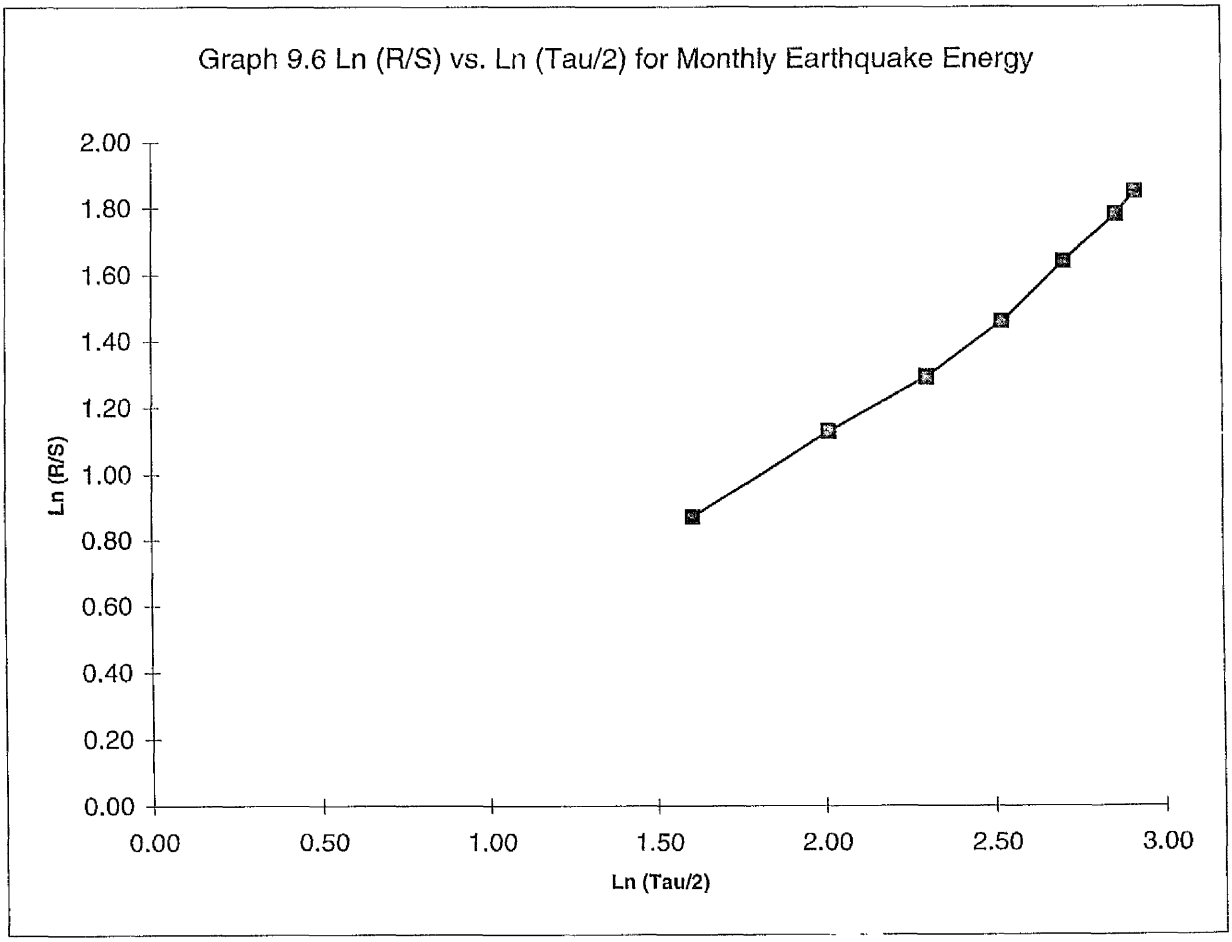

9.9.4 Analysis of Results

From the data in Table 9.7 and Graph 9.5, we can see that, in the case of the weekly time scale, the graph obtained is an excellent straight line. The gradient of the line of best fit is 0.55. From theory, (see equation 9.6) this is the value for the Hurst exponent. This value for the Hurst exponent, i.e. $H > 0.5$, tells us, as before, that there is a persistent time series, and that some sort of long term correlation, or memory effect, is involved. The value of 0.55 is lower than the 0.72 obtained by Hurst for many of his natural time series; whether there is something significant in this is difficult to ascertain. Another consideration must be that the value for the Hurst exponent is close to the theoretical value for an independent process, i.e. $H = 0.5$. Perhaps, this small increase could have been caused by our selection procedure or by experimental error. If this is the case then, we have shown that over a short time scale, the data are independent. Therefore, for short time spans in this region, it is difficult to make any firm conclusions as to the nature of the processes involved.

For the monthly case (see Table 9.8 and Graph 9.6), we can clearly see that the line of best fit obtained is not as good a fit as before, but that the line calculated is still valid. It is still a straight line, but the correlation is not as good as in the weekly case. The gradient of the line of best fit yields a gradient of 0.74. Again, this is the value for the Hurst exponent, i.e. $H = 0.74$. Clearly, this implies that over a monthly time frame, there is undoubtedly some long term correlation. In this case, experimental error could not be used as an explanation for the difference between this value and the theoretical value for a random process. Therefore, we must assume that over this time scale, there are definitely some "memory" effects in operation, and that the processes are not independent. Also, the value obtained for H is also very close to those achieved by Hurst for other natural data series.

9.10 Yearly Time Scales and Hurst Analysis

After analysis of the results from the previous section, where we have shown for a monthly time frame, that there is a correlation involved, it was felt that the analysis should be expanded to a longer catalogue and a longer time frame. For this second case, a catalogue from the same source, i.e. the North California Earthquake Data Centre, was downloaded, but this time the catalogue ran from 1967 until the present day. As discussed earlier, the number of events recorded is prohibitive, and so to make calculation easier, selection procedures were again employed. To this end, only large earthquakes were retained, resulting in a catalogue consisting of only earthquakes of magnitude > 5. Once again, the reasoning employed earlier forms the basis of the logic behind this decision. The same procedure discussed previously, and utilised in the previous section, was employed once more. The data obtained from this analysis are shown in Table 9.9 and Graph 9.7.

Hurst Analysis for Yearly Earthquake Energy Data
(North California 1969-1997)

Table 9.9 Hurst Analysis for Yearly Data

Tau	R/S	ln (tau/2)	ln (R/S)
5	1.74	0.92	0.55
7	2.18	1.25	0.78
10	2.83	1.61	1.04
13	3.31	1.87	1.20
16	3.78	2.08	1.33
20	4.29	2.30	1.46
28	5.49	2.64	1.70

Gradient of Line of Best Fit
0.660

Graph 9.7 Ln (R/S) against Ln (tau/2) for Yearly Data

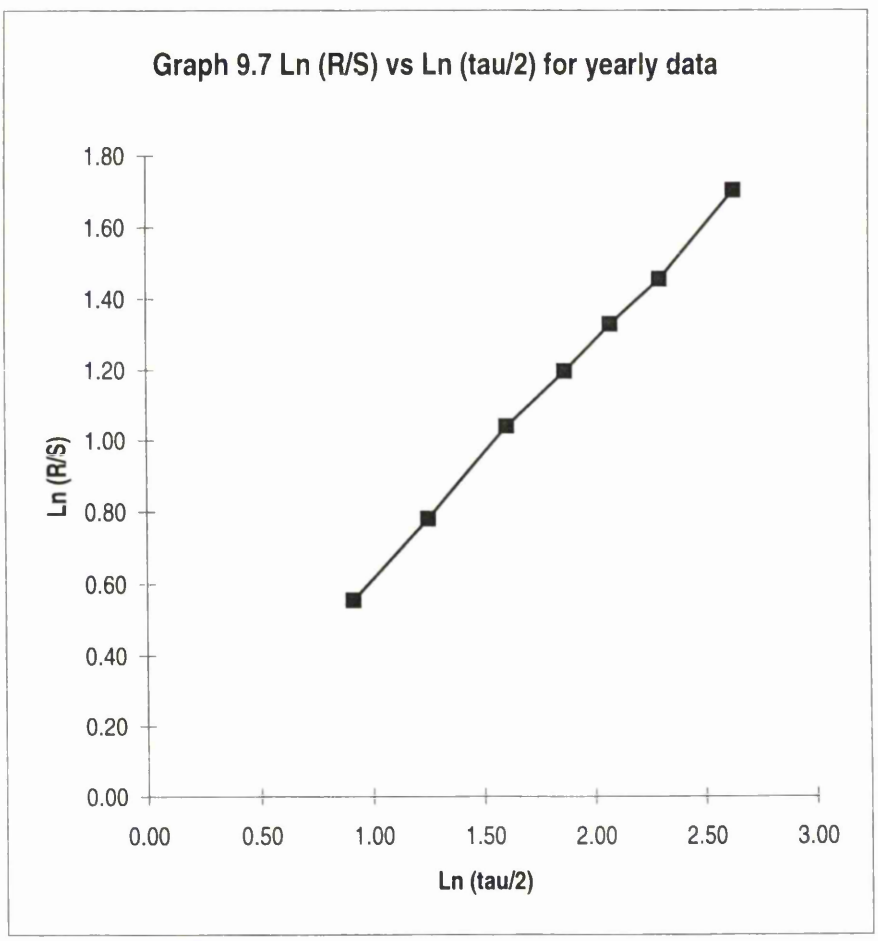

9.10.1 Results and Analysis

The analysis was performed on the earthquake energy data, using the method outlined earlier. We can clearly see form the results obtained, that for a time scale of the order of years, the graph of $Ln\left(\frac{R}{S}\right)$ *against* $Ln\left(\frac{\tau}{2}\right)$ is a straight line. Again, the correlation is excellent, and the line of best fit is a very good one. This implies that the Hurst exponent does exist. From the table, we can see that the gradient of the line of best fit is 0.66. Once again, this is the value of the Hurst Exponent, i.e. H = 0.66. Since the value for H is greater than 0.5, this shows us that there is a long term correlation between the energies of the earthquakes on a yearly scale. As before, we must make allowances for the selection procedure employed, and its possible effect on the results. However, the value for H is significantly greater than that for an independent process, and therefore it is reasonable to conclude that there is some memory effect at work in the earthquake process.

9.11 Conclusion

Hurst Analysis is a very interesting topic, with much research still needed. From the results we have obtained for the North California region, it is fair to conclude that over longer time scales, such as months or years, there is undoubtedly a long term correlation between the energies of the earthquakes. Hence, using equation 9.32, there is some memory effect involved in the magnitude of the earthquakes. We must however consider the simplifications made in the earthquake catalogue. These omissions were made in the interests of simplicity and ease of calculation, and only very small events which, although numerous, do not contribute significantly to the energy released, were omitted. Overall, it is felt that the inclusion of these small events would not affect the underlying results.

9.12 Extensions

A number of possible extensions to this work have been considered. In the previous experiments, severe limitations were placed on us by the length of the available earthquake catalogues. As a consequence, it would be interesting to experiment with longer catalogues, to see if the same results were obtained. Also, although in our yearly example only large earthquakes were used, another extension could be to remove any aftershocks or foreshocks from the catalogue, and perform the analysis on the remaining main shocks, to discover if any correlation exists. This procedure would be difficult, as selection criteria would need to be decided upon to distinguish between foreshocks, main shocks and aftershocks. Another extension could be in the use of the Hurst statistic to pick out cycles, and periodic fluctuations (see reference 3). This extension is however beyond the scope of this thesis.

Chapter 10

Fractals & Dimensions

In this chapter we will lay the foundations for some of the mathematics we will use in the next chapter. We explain more thoroughly the idea of fractals and dimensions, and highlight the methods used for the numerical calculation of a fractional.

10.1 Introduction

In chapter 7 we mentioned briefly the idea of a fractal. Many people have a preconceived notion of what constitutes a fractal. Usually this consists of a "multicoloured swirly pattern", normally the Mandelbrot set, which they have seen on the back of a T-shirt. Although some of these are fractals, and are very pretty, there are other fractals which we do not even recognise as such, e.g. clouds, ferns and snowflakes. Figure 10.1 below, is an example of a fractal. We can see that if we take the whole shape and reduce it, then it exactly mirrors a smaller section of the picture. This is one of the main properties of fractals. Also, if we zoom in on a particular section, we continue to see more detail at a smaller scale. This is another property of fractals, see *Falconer*[1990] and *Feder*[1988].

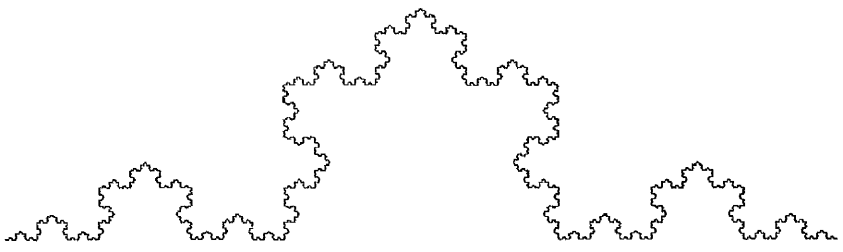

(Figure 10.1 The Koch Curve)

Fractals, as we think of them today, were "discovered" by *Benoit Mandelbrot*[1982]. Mandelbrot's book, "The Fractal Geometry of Nature", is one of the seminal works of the 20th Century, and is a fascinating study by a unique individual. It is also an interesting read! Quoting from "The Fractal Geometry of Nature", Mandelbrot says:

"I conceived and developed a new geometry of nature....It describes many of the irregular patterns around us, and leads to a number of fully fledged theories, by identifying a family of shapes I call fractals. *The most useful fractals involve* chance *and both their regularities and their irregularities are statistical. Also, the shapes here tend to be* scaling, *implying that the degree of their irregularity....is identical at all scales. The concept of fractal dimension plays a central role in this work."*

10.2 Classic Fractals

The prototypical example of a fractal is a rocky coastline. Figure 10.1 could be thought of as a coastline, but one which is very regular. We can measure the length of a coastline by counting the number of steps, N(ε), of a divider of length ε. The length of the coastline, L(ε), is then found to be given by the following *empirical* equation :

$$L(\varepsilon) = N(\varepsilon) \times \varepsilon .$$

(Equation 10.1)

This relationship is an empirical fact, and was discovered by Richardson in 1961. Obviously, N(ε) will change as we vary ε. The shorter we make ε, the more steps we will need to measure the length of the coast. We would also expect that the measurement would "settle down", or tend to, some well defined value called the *true length*. For coastlines, this does not happen, and what we get is that N(ε) is related to ε by a power law, i.e.

$$N(\varepsilon) = \frac{C}{\varepsilon^D}.$$

(Equation 10.2)

Therefore, the length of the coastline becomes

$$L(\varepsilon) = \frac{C}{\varepsilon^D} \times \varepsilon$$
$$= C\,\varepsilon^{1-D}$$

(Equation 10.3)

If D > 1 then, as the size of the dividers *decreases*, the length *increases*. In most cases L(ε) increases *without limit*. This happens because a "bay" noticed at large scale will have "sub-bays" contained within it at a smaller scale, and each of these smaller features adds to the total length. D is called the *fractal dimension*, and for real coastlines is approximately in the range 1.15 to 1.25.

Another classical fractal is the Sierpinski gasket, this is given below, in figure 10.2. The Sierpinski gasket has a fractal dimension $D = \frac{\log 3}{\log 2} = 1.58...$

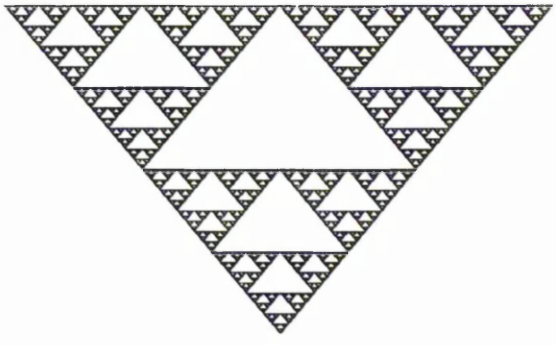

(Figure 10.2 The Sierpinski Gasket)

10.3 Dimensions

There are many different definitions of "dimension" in mathematics, and we must be very careful about which one we are using. The reasoning behind this multitude of different dimensions is that in some cases different definitions give

different answers. Also, some methods are easier to evaluate than others. Mandelbrot[1982] originally defined a fractal as:

"A fractal is by definition a set for which the Hausdorff-Besicovitch dimension strictly exceeds the topological dimension."

In this short statement we have already used two different definitions of dimension!!

10.4 Topological Dimensions

The subject of Topology is often referred to as "Rubber Sheet Geometry". We say that two objects are the same (topologically) if one can be pulled and stretched into the same shape as the other. Topology is a complicated subject, and has many facets. As a result, we do not go into any detail, but simply use an obvious result.

The idea of the topological dimension, D_T, that we use is the natural one. It relies on the number of parameters required to describe the position. A single point is said to have a topological dimension of zero; a curve has a topological dimension of 1; a plane has $D_T = 2$, and so on. We can see that this is the intuitive way of defining dimension. Figure 10.3, below, illustrates this idea. See *Hoggar*[1992] for further details.

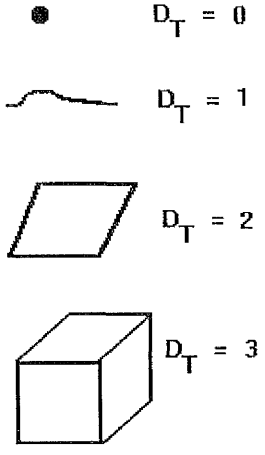

(Figure 10.3)

Note that topological dimension, D_T, is defined to have an *integer* value.

10.5 Hausdorff Dimension

Before discussing the Hausdorff Dimension, we must talk about the Hausdorff measure. Consider $V \subseteq R^n$, such that $V \neq \varphi$. Then the *diameter* of V is defined as

$$|V| = \sup \{|x-y| : x, y \in V\}$$

(Equation 10.4)

where $|x-y|$ is the normal Euclidean distance between x and y.

Let $F \subseteq R^n$. Then a δ *-cover of* F is a countable collection of sets $\{W_i\}$, with $0 < |W_i| \leq \delta$, which cover F, i.e. $F \subseteq \bigcup_{i=1}^{\infty} W_i$.

Using this, and for $F \subseteq R^n$, $s \geq 0$ and $\delta > 0$, we define the following quantity:

$$H^s_\delta(F) = \inf \left\{ \sum_{i=1}^{\infty} |W_i|^s : \{W_i\} \text{ is a } \delta - \text{cover of F} \right\}.$$

(Equation 10.5)

We try to minimise this quantity over all δ. As δ tends to zero, the number of possible coverings reduces, and $H^s_\delta(F)$ approaches a limit. (Note that this limiting value may be infinite). We define the s-dimensional Hausdorff measure as follows:

$$H^s(F) = \lim_{\delta \to 0} H^s_\delta(F) \quad .$$

(Equation 10.6)

Also, for any δ-cover, $\{W_i\}$, if $t > s \geq 0$ and $0 < \delta < 1$ then we have

$$\sum_i |W_i|^t = \sum_i |W_i|^{t-s} |W_i|^s \leq \sum_i \delta^{t-s} |W_i|^s .$$

(Equation 10.7)

Thus, by taking the infima we get that

$$H^t_\delta(F) \leq \delta^{t-s} H^s_\delta(F).$$

(Equation 10.8)

Letting $\delta \to 0$ we see that if $H^s(F) < \infty$ then $H^t(F) = 0$ for t > s. The graph of $H^s(F)$ against s is given below, in figure 10.4. There is a critical value of s at which $H^s(F)$ "jumps" from ∞ to 0. We call this critical value the *Hausdorff dimension* of F, $\dim_H F$.

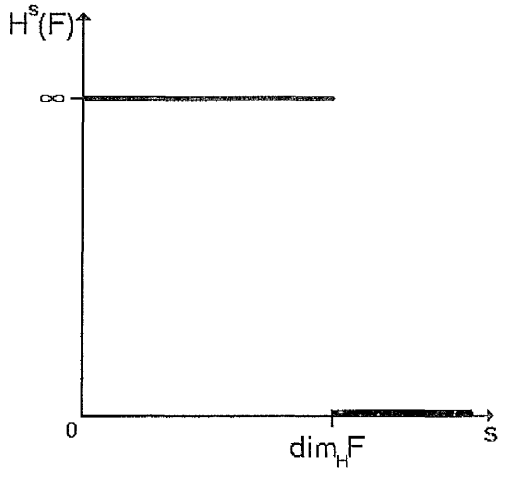

(Figure 10.4)

We can formally define it as:

$$\dim_H F = \inf\{s : H^s(F) = 0\} = \sup\{s : H^s(F) = \infty\}.$$

(Equation 10.9)

Unfortunately, the Hausdorff (or Hausdorff-Besicovitch) dimension is quite difficult to evaluate in experimental situations. Hence, we must find ways of calculating the dimension more easily.

10.6 Evaluating Dimensions

Measurement at scale ε is crucial to most definitions of dimension. In section 10.2, we discussed measuring the length of a coastline, F, using dividers of length ε. This method means that we ignore all the irregularities of size less than ε. When we measure the object, the dimension of F is determined by the power law relationship (if

there is one) between the number of objects (the number of steps of the divider) N(ε) and ε, the size, see equation 10.2. Taking logarithms of both sides of equation 10.2 yields:

$$Log\ N(\varepsilon) = Log\ c - D\ Log\ \varepsilon$$

(Equation 10.10)

and

$$D = \lim_{\varepsilon \to 0} \frac{Log\ N(\varepsilon)}{-Log\ \varepsilon}.$$

(Equation 10.11)

In practice, D is constant over a range of scales. This means that we can plot the log-log graph of N(ε) against ε and we will obtain a fixed straight line over a large section of the graph. We can use the above formula experimentally, as we can estimate D from the gradient of the log-log graph of N(ε) against ε.

10.7 Box Counting

Box-counting is probably the most popular method for estimating fractal dimensions. This is due to the ease with which calculations can be performed. It is based on the same idea as outlined in the last section. Our method involves placing a *regular* grid of *boxes* over the fractal set, and observing how many boxes contain some part of the set. Let N(ε) be the *smallest* number of these regular boxes of side ε which cover F, then the *box-counting dimension* is defined to be

$$D = \lim_{\varepsilon \to 0} \frac{Log\ N(\varepsilon)}{-Log\ \varepsilon}.$$

Note that this is the same as equation 10.11 above. We note how the number of boxes, N(ε), varies as ε changes. The gradient of the log-log graph of N(ε) against ε is then used as an estimate of D, just as in Richardson's coastline analysis.

10.8 Correlation Dimension

If we calculate the box-counting dimension, D, we can see that it is a purely geometric measure. The value for D relies on the number of boxes containing part of the set, and is independent of the "amount" contained within each box. For example, consider a box which has only one point of our set contained within it, and another box which contains a thousand points. The box-counting (and Hausdorff) dimension consider both boxes equal. This is like counting the number of coins in your pocket without considering the denomination. The correlation dimension is different, and takes this into account, see proposition 10.1 and the subsequent discussion.

Hentchel & Procaccia[1983] exhibits an *infinite* sequence of generalised dimensions. Their sequence includes the fractal dimension and the correlation dimension, but excludes the topological dimension. We will restrict our discussion to the correlation dimension, as this will be the main method we use to calculate dimensions throughout the rest of this thesis.

Let $\{X_i\}_{i=1}^{N}$ be the points of a time series, with N a large number. We define the *correlation integral*, C(r) as:

$$C(r) = \frac{1}{N^2} \sum_{i,j=1}^{N} \Theta\left(r - \left|X_i - X_j\right|\right),$$

(Equation 10.12)

where Θ is the Heaviside step function, defined by

$$\Theta(x - a) = \begin{cases} 0 & x < a \\ 1 & x \geq a \end{cases}$$

(Equation 10.13)

with x variable and a constant. It is found that C(r) obeys a power law over a range of scales. That is, for some constant k, we get that

$$C(r) = k\ r^{\nu}\ .$$

(Equation 10.14)

Hence, the *correlation dimension,* ν ,of the time series is defined as

$$\nu = \lim_{r \to 0} \frac{\log C(r)}{\log r}.$$

(Equation 10.15)

To calculate ν experimentally, we plot a graph of *log C(r)* against *log r*, and the gradient of the line of best fit is taken as the correlation dimension. Note that in the following chapter we only obtain straight lines in a so called "scaling region". This is because, with real data, the time scales involved mean that only very rarely do we have large gaps between earthquakes. This affects the results at larger time intervals, and results in a deterioration of the straight line.

We can actually show that the correlation dimension ν is a *lower bound* for the box-counting (fractal) dimension, D. Once again, consider our time series, $\{X_i\}_{i=1}^{N}$. If we cover the time line by intervals of length r, then the probability, p_i, that one of the points of our time series falls into interval *i* is given by

$$p_i = \frac{1}{N} \mu_i$$

(Equation 10.16)

where μ_i is the number of points of the time series which fall into interval *i*. Let the number of *intervals* required to cover the line be M(r). The *expectation*, or average value for the probability of landing in an interval is then

$$\langle p_i \rangle = \frac{1}{M(r)}.$$

(Equation 10.17)

From the definition of the correlation integral, C(r), given in equation 10.12 we get

$$C(r) = \frac{1}{N^2} \sum_{i=1}^{M(r)} \mu_i^2 = \sum_{i=1}^{M(r)} p_i^2 = M(r) \times \langle p_i^2 \rangle$$

(Equation 10.18)

Here we have replaced the number of pairs with distance less than r by the number of pairs which fall into an interval of length r.

Proposition 10.1

Consider a probability distribution $\{p_i\}$. For this distribution $\langle p_i^2 \rangle \geq \langle p_i \rangle^2$.

Proof

Let $\vec{p} = (p_1, p_2, ..., p_N)$. Then

$$\vec{p}.\vec{1} = (p_1, p_2, ..., p_N).(1,1,.....,1) = p_1 + p_2 + ... + p_N = \sum_i p_i = 1$$

(Equation 10.19)

Using Schwarz's Lemma, we get that

$$\left|\vec{p}.\vec{1}\right| \leq \left|\vec{p}\right|^2 \left|\vec{1}\right|^2,$$

(Equation 10.20)

and using equation 10.19, above, we obtain the following

$$1^2 \leq \left|\vec{p}\right|^2 \times N.$$

(Equation 10.21)

Therefore, by expanding and rearranging equation 10.21 we obtain the following:

$$\frac{1}{N} \leq \sum_i p_i^2 .$$

(Equation 10.22)

We have now shown that

$$\frac{\sum_i p_i^2}{N} \geq \frac{1}{N^2}.$$

(Equation 10.23)

The left hand side on equation 10.23 is just $\langle p_i^2 \rangle$, and we already know that $\langle p_i \rangle = \frac{1}{N}$, which tells us that the right hand side is simply $\langle p_i \rangle^2$. We have therefore proved the proposition, i.e. $\langle p_i^2 \rangle \geq \langle p_i \rangle^2$.

Returning to equation 10.18, we can see that

$$C(r) = M(r) \langle p_i^2 \rangle \geq M(r) \langle p_i \rangle^2 = M(r) \cdot \left(\frac{1}{M(r)} \right)^2 = \frac{1}{M(r)}$$

(Equation 10.24)

Now, we have seen earlier, from equation 10.2, that *M(r)* varies as $\frac{1}{r^D}$. Thus, for some *l*, equation 10.24 becomes

$$C(r) \geq l\, r^D \ .$$

(Equation 10.25)

But we already know from equation 10.14 that $C(r) = k\, r^\nu$, hence

$$r^{\nu - D} \geq \frac{l}{k} \qquad \text{(a positive constant)} .$$

(Equation 10.26)

If $\nu > D$ then letting $r \rightarrow 0$ we get a contradiction. Therefore,

$$\nu \leq D \ .$$

(Equation 10.27)

Grassberger & Procaccia[1983] claim that in cases where $\nu \neq D$, ν is more relevant. They claim that the neighbourhoods of certain points have higher "seniority", in that they are visited more often than others. The fractal dimension is ignorant of seniority, being a purely geometric concept. The correlation integral (and dimension) weights intervals according to their seniority. It is this property that we are most interested in and which we will make use of in the next chapter, where we calculate fractal dimensions for earthquake series.

Chapter 11

A New Prediction Method

In the last chapter we discussed fractal dimensions, and in particular the correlation dimension. We now use these definitions to propose our own method for predicting earthquakes.

11.1 Introduction

We have already looked at the Hurst exponent and the Hurst analysis of a time series. This was discussed in chapter 9, where it was shown that earthquakes were *not* independent events. The Hurst exponent, H, was found to be greater than 0.5, which suggested a *persistent* time series, with long term correlations, i.e. earthquakes are dependent upon the past as well as the present. The correlation dimension is also a measure of how points are related, and we wanted to see how the correlation dimension varied as the earthquakes under consideration changed. The main aim of monitoring changes in the value for the correlation dimension was to discover whether any *precursory* changes could be identified, especially changes which could lead to some sort of earthquake prediction method.

In this chapter we discuss the method used for calculating the correlation dimension, i.e. the computer algorithm and program used, as well as the procedure followed. We then go on to consider the results of some preliminary studies.

11.2 The Computer Program

The program used to calculate the correlation dimension throughout the rest of this chapter is given in appendix D. The program was developed over a period of a few months, and although the basic structure was in place fairly quickly, many refinements and improvements were gradually added. The program was originally written in BASIC, as this is the language with which we are most familiar. Unfortunately, because of the huge number of data points under consideration, this was found to be impractical, as the length of time taken to compute the correlation dimension was excessive. Also, the number of data points that could be handled easily was too small to be useful. The original BASIC programs are not given as they were never used in any experiments.

To improve the performance it was necessary to change the programming language to one which would facilitate faster calculation. Hence, the final program was written in C++, as this language fulfilled all the necessary criteria. Thankfully, the increase in speed of operation allows the rapid calculation of the correlation dimension. In most cases, one complete calculation took around 45 seconds. However, as we make over 1000 calculations at a time, the total length of time involved was still significant.

The program uses the *Grassberger & Procaccia* algorithm to calculate the correlation integral. This can be found in their paper, *Grassberger & Procaccia*[1983]. The equation used was given in the last chapter, in equation 10.12.

We now explain the main sections of the code, and the functions they perform. Firstly, the program sets up all the variables required; it then reads in the time series data to be analysed from the appropriate data file. The number of pieces of data read in at each step can be entered at the start of the program. Obviously, the smaller the size of the jump, the longer it will take to process a complete data set.

The program now calculates the "distance" between *all* possible pairs of points in the data set under consideration. At this stage we are considering approximately

33000 pieces of data! It was found that by sorting the resulting data into numerical order, the speed of calculation could be increased dramatically. Hence, the next part of the program sorts the data into *ascending* numerical order.

We now calculate the correlation integral using the sorted data we have just obtained. The formula used is given below, where we repeat equation 10.12 for convenience.

$$C(r) = \frac{1}{N^2} \sum_{i,j=1}^{N} \Theta(r - |X_i - X_j|).$$

(Equation 11.1)

The program goes through the sorted data and *counts* how many points there are up to the current value of r. This counting is equivalent to the action of the Heaviside step function. We can then calculate the correlation integral. The process is then repeated as we change r.

To calculate the correlation dimension, D, we need to calculate the gradient of the graph of *Log C(r)* against *Log r*. We must first ensure that we do indeed have a straight line. To check this, the data is output to a data file from which the graph can be plotted using the computer application MATLAB. It was found that, in many cases, the graph followed a straight line up to a certain point, and then deviated from this line by tailing off slightly. This occurs because of the small number of large time intervals between earthquakes. The region in which we have a linear relationship is termed the *scaling region*. Throughout the rest of this chapter, all the gradients we calculate are for lines of best fit in the scaling region. Examples of these graphs, illustrating the scaling region and the deviation are given in appendix E.

The program then calculates the line of best fit in the scaling region, and the value for the gradient is output to a data file. It is this quantity that we are interested in; this is the correlation dimension, D, of our data. This process is repeated as we go through the data, and provides an illustration of how D is changing.

11.3 Method

The method of calculation uses the data obtained from earthquake data sites on the world wide web. In the preliminary study, data from Alaska were used. For subsequent studies, the region under consideration was changed, as obtaining the necessary data became more difficult. Hence, as in chapter 9, data from the North California Earthquake Data Centre was used. All the earthquakes of magnitude ≥ 2.5 were included in the catalogue. Note that this gives us a huge amount of data to analyse, almost 5000 events in Northern California.

We cannot, however, use the data as it currently stands, i.e. as a set of dates and times. We must first calculate the *inter-arrival times*, i.e. the length of time *between* earthquakes in minutes. This technique is a fairly standard one from the field of statistics. We calculate the inter-arrival times using a large spreadsheet, and then export the appropriate values to a data file for use with the computer program. We can now perform the analysis on this data set.

We run the program, and using MATLAB, check to see if we get a linear relationship. As stated before, examples of these plots are given in appendix E; we can clearly see the "tailing off" of the graphs at larger values of r. The program calculates the line of best fit, and its gradient, in the appropriate scaling region.

The gradient, as mentioned before, is the correlation dimension. We monitor how the correlation dimension changes as we move through the data set.

11.4 Preliminary Study

After testing the program and ensuring its reliability, the first serious experiment was performed on data from Alaska. We calculated the inter-arrival times for all the earthquakes with magnitude ≥ 2.5 for the years 1992 to 1996. This encompassed approximately 600 events. We then ran the program, and calculated the correlation dimension for the data series. Using MATLAB, a graph of the correlation dimension against current position in the data series was plotted. Note that in this case the number of data points read in at each step was only 1. The graph obtained can be seen below, in figure 11.1.

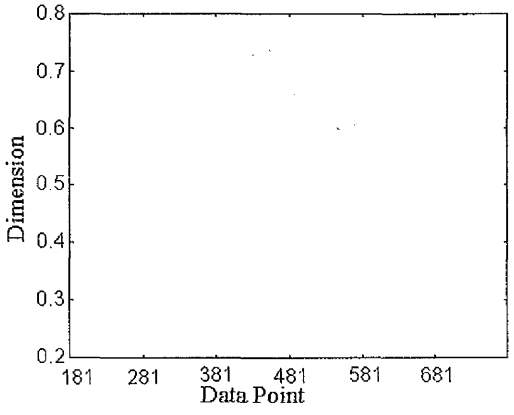

(Figure 11.1 Correlation Dimension Vs Position for Alaska 1992-1996)

As we can see from the above graph, the correlation dimension changes quite significantly. It peaks at a value of 0.75, and has a minimum value of about 0.25. This preliminary study looks quite promising, that is there are distinct variations in the value for the correlation dimension. It was hoped that these variations could be used as a prediction method. For example, if a peak (or a trough) occurred before a large earthquake in the past, then we might expect the same pattern to repeat itself, and this could be used as a precursor. Hence, we decided to do a more detailed study.

We extended the data to include a far bigger sample, this time the data for Alaska incorporated all earthquakes in the region for the period 1985 to 1996. This gave us a large number of events to process, well over 1500. In this example, we read

in the data in chunks of 5 points in an attempt to speed up processing. This enables us to analyse the data more quickly, and within a reasonable time frame. Figure 11.2, below, shows the MATLAB output. Note that the x-axis on the graph starts at 181, this is because the program uses the first 181 points of data before it will return a value for the correlation dimension.

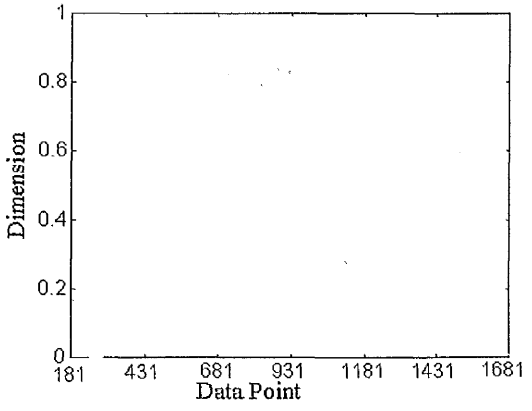

(Figure 11.2 Correlation Dimension Vs Position for Alaska 1985-1996)

By comparing figures 11.2 and 11.1, we can see that there are a number of points of interest. The correlation dimension takes values in the range 0 to 0.9, and is quite variable. Obviously, as we are using an extended set of data in figure 11.2 there will be more peaks and troughs. The last section of figure 11.2, from about position 931 on, is the same as figure 11.1, this is because we are using the same data, i.e. this is the 1992 to 1996 section of the data.

Figure 11.2 has a number of similarities with the build up of stress in the Earth's crust and the elastic rebound theory which was outlined in chapter 2. It appears that the correlation dimension gets "built up" over time, and then something happens, like a large earthquake, which causes the correlation dimension to drop rapidly. It is then "built up" again over a period of time. This is very like the elastic rebound theory.

The next step was to identify the largest earthquakes in the data set. All the earthquakes above magnitude 4.9 were found, and their position in the data series

noted from the spreadsheet. These data were tabulated, and the results are presented in table 11.1 below.

Table 11.1 Major Earthquakes and their Positions

Position in Series	Magnitude
649	4.9
926	5.6
953	5.9
967	6.0
1278	5.0

If we examine the actual numerical data produced by the program, as well as the data from figure 11.2, then we can calculate exactly the positions on the figure where there is a significant drop in the correlation dimension. We obtain a rough estimate of the position from the graph, and we can then check the exact point by reviewing the data file. Figure 11.3, below, shows the points on the graph where the correlation dimension "peaks" before dropping rapidly. The numbers given refer to the *exact* positions in the data series.

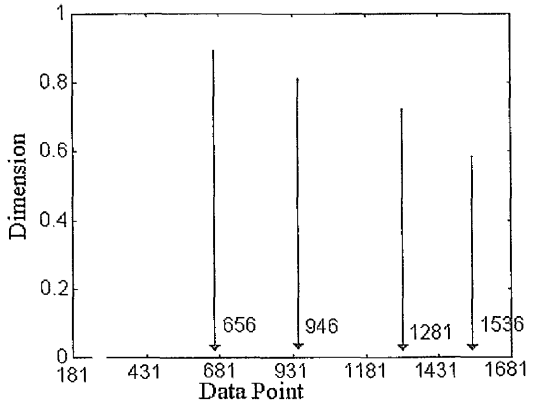

(Figure 11.3 Alaskan Data with "peaks" illustrated)

As we can see from the values given in figure 11.3, the peaks we have identified are very close to the positions of the large earthquakes given in table 11.1. For example, the first peak/dip occurred at data point 656, while the first major earthquake occurred at position 649. There are 3 major earthquakes relatively close to each other in the data series, e.g. positions 926, 953 and 967. Our second peak/dip, at position 946, appears to be in the middle of these 3 large events. The third drop we have identified occurs at position 1281, while a large event occurred at position 1278. The last peak that we have illustrated, position 1536, is not a valid peak. This peak/dip is achieved because the data series has ended, i.e. the computer runs out of data points to consider, and the correlation dimension drops to zero. Hence, we do not consider this in our analysis.

At first sight it appears that these peaks/dips in the correlation dimension occur at, or very near the time of major earthquakes. It was hoped that by monitoring the correlation dimension, and any variations that might occur, some prediction method could be produced. This could only be done if the correlation dimension could be monitored regularly. Unfortunately, there are just not enough large earthquakes for us to consider in the Alaskan region. From 1985 to 1996 there were only 5 "large" events in our time series, see table 11.1. This is not really enough to allow us to test any theories, as we would have to wait a very long time for the next reasonably large event. Hence, it was necessary to change the region under consideration. In the following section we consider Northern California, and the earthquakes in this region.

11.5 Probability beyond Chance

Before we go on to consider anything further with our prediction method, we must consider the chances of "guessing" randomly and still making a correct prediction. First we must consider the *size* of the earthquakes we are going to try and predict. Note that the size of an earthquake was discussed in chapter 2.

Earthquake prediction is usually performed in attempt to save human life. Therefore, we are only interested in trying to predict the occurrence of large, destructive events. Hence, it was decided that we would only try to predict events with magnitude greater than 5. Another factor which influenced this decision is the fact that events with a magnitude of between 4 and 5 are fairly common. If we had decided to try to predict smaller events, then we would have encountered serious difficulties as a result of the larger number of events. The high frequency of smaller events makes the task of deciding whether we are actually *predicting* them almost impossible; the probability of being successful while making random guesses is too high. Obviously, the chances of just guessing the time of a "large" earthquake are much higher if there are more earthquakes for us to claim as successes. For example, consider the following hypothetical prediction scheme:

1) We state that a large earthquake is going to occur on a certain date. This date is the start of our alarm period.

2) If within one week of the start of our alarm an earthquake of magnitude 4 or above occurs, then we deem this to be a successful prediction.

If we choose the start dates at random, what are the chances of getting a "successful prediction"?

At this stage, let us consider the earthquakes to be distributed randomly in time, i.e. their inter-arrival times are represented by a Poisson distribution. We will use the data for Northern California which we employ in the next section. The period under consideration runs from February 1994 to May 1997; a period of approximately

166 weeks. In total, there are about 5000 events of magnitude 2.5 or greater, yet there are only 165 "large" events, i.e. earthquakes with magnitude 4.0 or above. This implies that the mean number of "large" earthquakes per week is :

$$\lambda = \frac{165}{166} \approx 0.994 \quad \text{to 3 decimal places},$$

(Equation 11.2)

where the symbol $\approx$ means "approximately equal to". The Poisson distribution is given by :

$$P(x) = e^{-\lambda} \frac{\lambda^x}{x!},$$

(Equation 11.3)

where $P(x)$ denotes the probability of x events occurring in one week. Hence, assuming this distribution, the probability that simply by choosing a start date randomly we could get a "successful prediction" is given by:

$$P(x \geq 1 \text{ event per week}) = 1 - P(0) \approx 1 - e^{-0.994} \frac{0.994^0}{0!} \approx 0.630 \text{ to 3 dp}.$$

(Equation 11.4)

So simply by guessing we could get 63% of our predictions to be successful! This is clearly not acceptable.

If we change the criteria of what constitutes a successful prediction, and insist that only earthquakes larger than magnitude 5 are counted, then the probability of guessing and obtaining a successful prediction is significantly reduced. There are 8 events of magnitude 5.0 or greater, in our 166 week time frame. This means that the average number of "large" events per week is given by

$$\lambda = \frac{8}{166} \approx 0.048 \text{ to 3 decimal places}.$$

(Equation 11.5)

Once again, assuming the Poisson distribution, and that we choose the start of the alarm randomly, we get that the probability of a successful prediction is given by the following

$$P(x \geq 1 \text{ event per week}) = 1 - P(0) \approx 1 - e^{-0.048}\frac{0.048^0}{0!} \approx 0.047 \text{ to 3 dp.}$$

(Equation 11.6)

So the chances of guessing the start date, and an earthquake of magnitude 5.0 occurring within one week of that start date is only 5%. This is a far more acceptable figure than the 63% obtained for magnitude 4.0 earthquakes. Hence, it was decided that all predictions would only involve the prediction of earthquakes of over magnitude 5.0.

11.6 Northern California

After the preliminary study in Alaska, the focus of our study was changed to Northern California. This region was chosen because of the ease with which large amounts of data could be obtained, and the fact that computerised seismic records are available for long periods. This computerisation made the processing of vast quantities of data much less tedious. Another factor was the *quantity* of earthquakes occurring in this region, as it appeared that the level of seismic activity was far higher in this region than in Alaska. We downloaded the earthquake catalogue for the years February 1994 to May 1997. This included all earthquakes with a magnitude of over 2.5. As a result, almost 5000 events were considered. As before, the data was imported to a spreadsheet, and the inter-arrival times calculated. This data was then exported to our C++ program, and analysed. The graph of the correlation dimension against position in the data series is given below, in graph 11.1.

Graph 11.1 Correlation Dimension against Position for North California 1994 - 1997

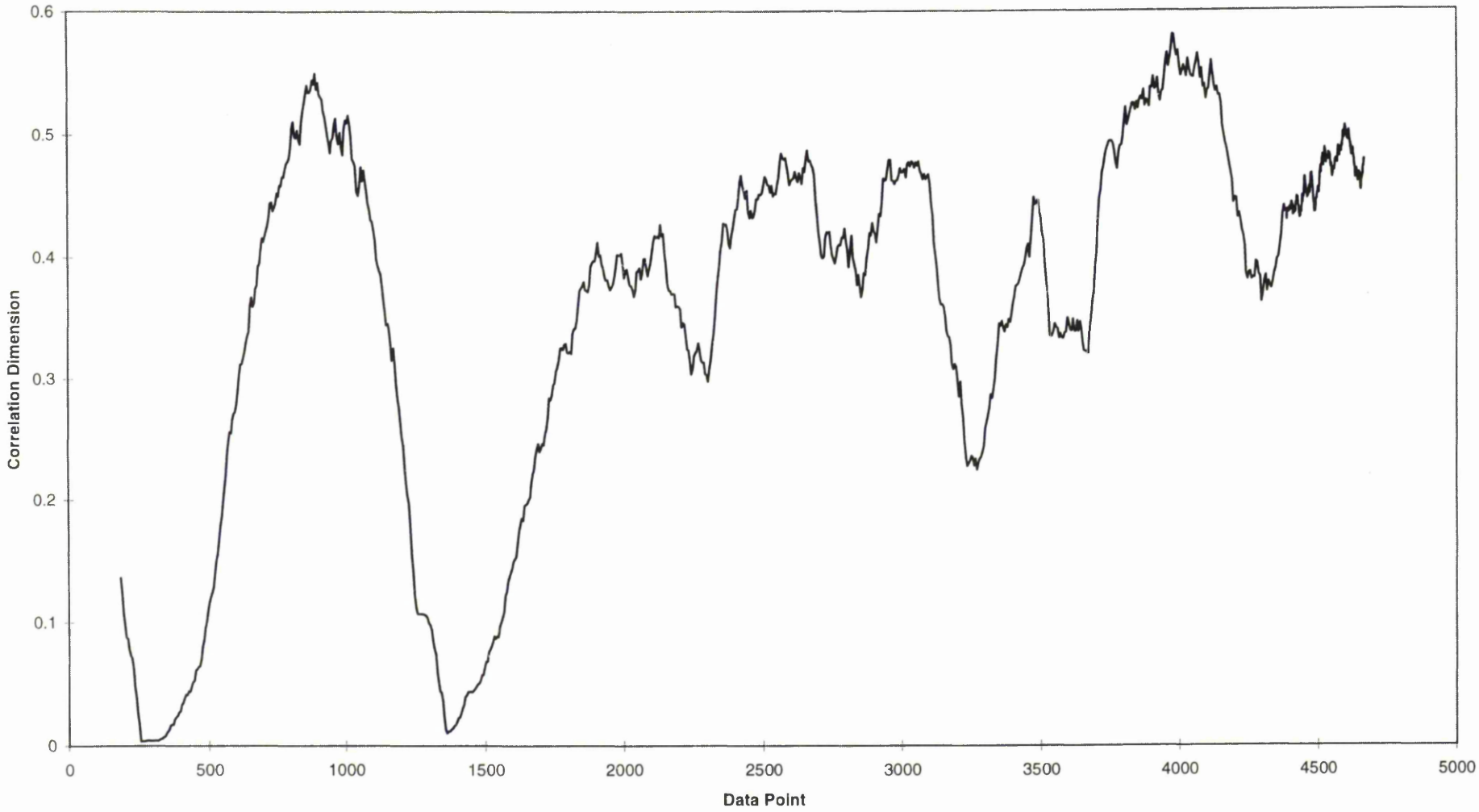

As we can see from the graph above, graph 11.1, there are a number of peaks and troughs in the value for the correlation dimension. We identify the points where we have a high value for the correlation dimension, followed by a sharp drop in that value. We begin, as we did in the last section by examining the graph to obtain a rough estimate of the position, and then finding the exact position by checking the actual numerical data. In all, 7 peaks/drops were identified in the graph. These are given below, in figure 11.4. The final, exact, positions in the data series are also given in the diagram.

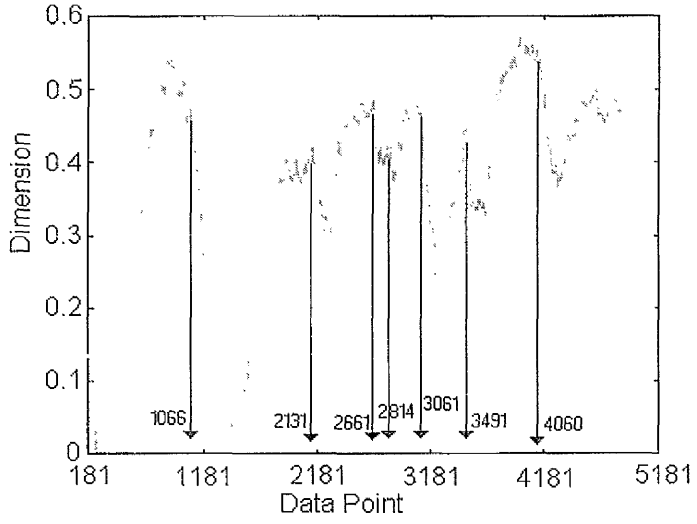

(Figure 11.4)

The "large" earthquakes in our time frame, i.e. earthquakes with a magnitude of 5 or above, were also identified, as were their positions in the data series. In total, there are only 8 events of magnitude 5.0 or above in our data series. These earthquakes and their positions in the data series are given below, in table 11.2.

Table 11.2 Large Earthquakes in Northern California January 1994 to March 1997

Position	Magnitude
1073	6.8
1176	5.5
1942	5.0
2131	6.1
2682	5.3
2820	5.4
3508	5.62
3847	5.0

From figure 11.4, and the above table, we can see that the peaks we identified tie in very closely with the large earthquakes identified above, in table 11.2. The peaks/drops occur slightly before the large earthquake strikes. For example, the first drop we identified was at event number 1066. This was followed by a large, magnitude 6.8 earthquake, which occurred at position 1073 in our data series. A magnitude 6.1 earthquake occurred at data point 2131, and we also identified a peak/drop at this point. This pattern is reproduced throughout the rest of the data.

Unfortunately, we do not have a perfect record, as some of the large earthquakes which occur do not have a related peak/dip. Also, two of the peaks which we claim should be followed by a large earthquake are not. We must also count these wrongly identified periods as failures in any analysis of the success of our prediction method. Table 11.3, below, summarises these results. Note that, once again, the positions refer to the position in the data series.

Table 11.3 Summary of Results

Peak Position	Actual Earthquake Position	Earthquake Magnitude	Result
1066	1073	6.8	Identified
---	1176	5.5	Missed
---	1942	5.0	Missed
2131	2131	6.1	Identified
2661	2682	5.3	Identified
2814	2820	5.4	Identified
3061	---	---	No Earthquake
3491	3508	5.62	Identified
---	3847	5.0	Missed
4060	---	---	No Earthquake

Overall, our record does not appear to be too bad. We made 7 claims of large earthquake occurrence, and in 5 of these cases our claims appear to be justified. These are the five "identified" results in table 11.3. We also *miss* 3 large events, where a large event occurs, and we do not have a corresponding peak. In addition, two of our peaks are not followed by large events. In summary, we appear to have "predicted" five out of the eight earthquakes, with two "false alarms".

In defence of the "missing" of two of the earthquakes, we put forward the following argument. From graph 11.1, we can see that the value for the correlation dimension drops to almost zero after the first large earthquake (data point 1073). The two large events which we miss, occur just after this first large earthquake, at data points 1176 and 1942. At this stage, the dimension has not recovered its value, and perhaps it is too early for it drop again. We can see from the graph that the correlation dimension only drops significantly when it takes a value above 0.4, and at the time of the second missed event, the correlation dimension is only 0.35. Another possibility

could be that the two events we miss are *aftershocks* of the very large, magnitude 6.8, first event.

What are the chances of achieving this sort of success rate randomly? From section 11.5, we showed that the probability of making a prediction of a magnitude 5.0, or above, event occurring within one week of our alarm starting was approximately 5%. If we assume that each of our 7 random "predictions" are independent, then the probability of getting 5 "successes" out of 7 predictions is given by the binomial distribution.

$$P(5 \text{ out of } 7) = {}^{7}C_{5}\ (0.05)^{5}(0.95)^{2} \approx 6\times10^{-6}$$

(Equation 11.6)

Hence, it is fair to assume that we are not just "lucky".

11.7 Prediction

Unfortunately, the process we have used to date is more a form of *post-diction* than it is *pre-diction*. We have already mentioned the problem of post-diction, and some of the pitfalls of post-dictive claims of a possible earthquake prediction method. These discussions took place in chapter 5, where we discussed the VAN prediction method. We must rectify this problem, and convert this "backwards in time" method of identifying large earthquakes, to one which can look forward in time, i.e. we must spot the earthquakes before they happen.

This has proved to be a very difficult problem to solve. It is all very well picking out the peaks and sudden drops from the graph once they have happened, but it is altogether more tricky to see where they are going to occur beforehand. In the following sections, we highlight two of the techniques used.

11.8 A First Attempt

From graph 11.1, figure 11.4 and our previous analysis, we can see that large earthquakes only occur when the correlation dimension is high. It has been shown that D takes a high value before dropping away rapidly. The large earthquakes only occur when the correlation dimension takes a value above 0.4. Would it be possible to announce an alarm, or a time of increased probability whenever the correlation dimension takes a value over 0.4?

Unfortunately, this would not be practical. Analysis of the data has shown that the correlation dimension takes a value above 0.4 just over half of the total time. This would mean that the alarm time would be too high. Any evacuations or action taken on the basis of this prediction method would probably be more expensive than the results of the actual earthquake. We need to narrow the limits of the time of increased probability to make the method more viable.

11.9 Prediction Method 1

The first method we applied to the data was an idea based on the appearance of "plateaux" in the graph of correlation dimension against position. For example, if we examine graph 11.1 more closely, it appears that the correlation dimension rises sharply, reaches a certain height, before the rate of increase drops, and the graph very nearly levels out. A rough schematic of the situation is given in figure 11.5, below, while the actual situation, with the "plateaux" marked on is given in figure 11.6. Note that in figure 11.5, figures (a) and (b) represent two of the situations.

The idea behind this conjecture was that in many cases the lengths of these relatively flat sections appeared to be very similar. On first inspection it appeared that the correlation dimension rose steeply, levelled out for a period of time, and then dropped sharply just before a large earthquake. It was hoped that by looking at the lengths of these flat sections we could predict when the next dip would be.

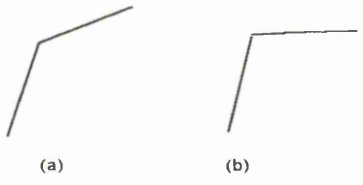

(Figure 11.5)

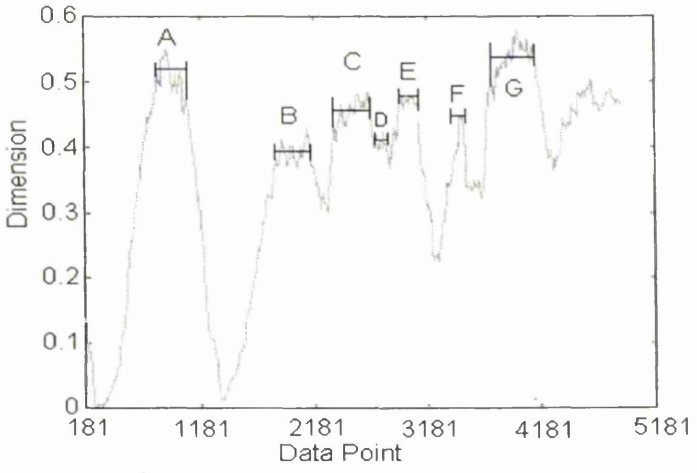

(Figure 11.6)

In figure 11.6, we have marked in the seven plateaux that we have identified. These are denoted by the letters A - G. Note that these tie in with the earthquake identifications discussed in the preceding sections. Plateau F is less of a plateau than the others; it almost appears to be just a "spike", but we will consider it as a very thin plateau for this analysis.

We define the start of the plateau to be the point where the dimension stops climbing rapidly. Thankfully, in all of the plateaux, the correlation dimension appears to rise very sharply, then drop very slightly before levelling out, or just rising. This allows us to calculate the exact point of the start of our plateau, by taking this "mini-peak" as the start of the plateau. We use the actual numerical data to calculate these points, after obtaining rough estimates from the graph. We then calculate the width of each plateau, by defining the end of the plateau to be the point at which the graph drops sharply; these were obtained in the previous section.

Table 11.4, below, summarises the data obtained for this plateau analysis. Note that, once again, the start and finish column denotes the position in the data series.

Table 11.4 Start, Finish and Length of Plateaux

Plateau	Start	Finish	Length
A	811	1069	258
B	1856	2131	275
C	2356	2661	305
D	2716	2814	98
E	2886	3061	185
F	3351	3491	140
G	3806	4060	254

As we can see, the lengths of the plateaux are fairly variable; they range from less than 100 data points to over 300. Perhaps by using these maximum and minimum values for the plateau lengths, a time of increased probability (TIP) of a

large earthquake occurring could be declared. The TIP is started after our plateau length passes the minimum value obtained for a plateau length, i.e. 98 events.

It was found that the average number of events per week in this region was approximately 30. Thus, if we declare a time of increased probability after the minimum plateau length, i.e. 98 events, then we could have an alarm time of 7 weeks, and this would extend beyond the maximum length of plateau so far recorded. This method would mean that we would *predict* the occurrence of large earthquakes with the same success rate as before.

We know that earthquakes are not distributed according to the Poisson distribution, but by using it we can calculate an *approximate* probability for the prediction of earthquakes. Thus, the probability of getting one of the earthquakes to occur in our 7 week time window at random is 28%, i.e.

$$P(x \geq 1 \text{ event in 7 week window}) = 1 - P(0) \approx 1 - e^{-0.333}\frac{0.333^0}{0!} \approx 0.283 \text{ to 3 dp.}$$

(Equation 11.6)

Thus, the chances of getting five out of the seven events correct is given by

$$P(5 \text{ out of } 7) \approx {}^7C_5\ (0.283)^5\,(0.717)^2 \approx 0.019\,,$$

(Equation 11.7)

i.e. the chances of obtaining this success by chance is less than 2%.

We now consider predicting the *next* large earthquake. From figure 11.7, below, we show the start of the next plateau is at data point 4383.

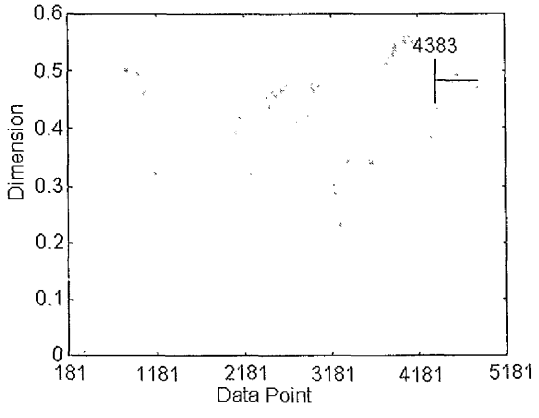

(Figure 11.7)

Thus, our time of increased probability starts at 4481; 98 data points from the start of our plateau. The maximum length of plateau we have obtained so far was 305 data points, thus our plateau should end before this, i.e. we should have a large earthquake, of magnitude greater than 5.0, by the time we reach data point 4688. This is our prediction:

Somewhere between data point 4481 and 4688 a magnitude 5.0 or above earthquake will occur.

Based on our past record, the probability of us being correct in our prediction is 0.714. In this case, we are definitely projecting forward in time, and there can be no claims of post-diction. We use data from the past to allow us to determine the parameters for our prediction, but our prediction is made entirely forward in time.

Unfortunately, no large earthquake occurred in the time period specified! In fact, no earthquake larger than magnitude 5.0 occurred in a much longer time window, and to date, no such earthquake has occurred in this region. We are now at position 4900 in the data series, and no such earthquake has occurred, although there have been a number of earthquakes over magnitude 4.5.

The correlation dimension remains high, and as yet has not dropped. This is, however, not much use to us as it is very difficult to predict when it will drop, and this is what we need to identify. This does not mean that the method is a failure, it could just be that it needs more "training". If we had more events to establish our parameters, then perhaps we could improve the success rate. Unfortunately, the length of time needed to analyse a larger data set goes beyond that available here.

11.9 Method 2

The second method of *predicting* the position of a large earthquake is based on the value of the correlation dimension, and the "amount of drop" after each large earthquake. As we have already pointed out, just before a large earthquake the correlation dimension drops. If we examine graph 11.1 and figure 11.4 closely, we can see that after each peak, the graph dips significantly, but that the amount of drop is different in each case. Also, the distance between the peaks is different. What we are interested in is the possibility of any relationship between the amount of drop, and the time to "recover" the value, before dropping again.

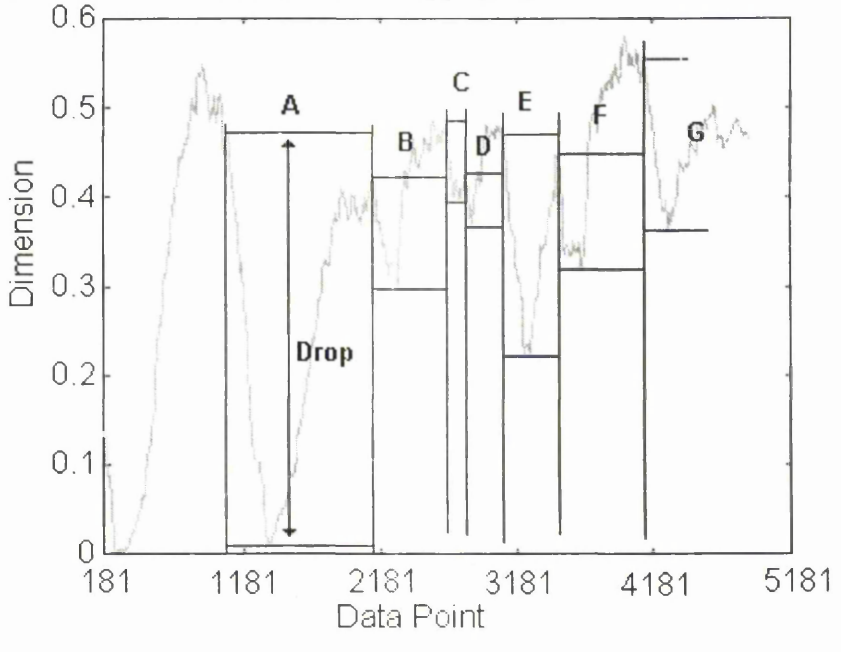

(Figure 11.8)

We use the numerical data to find the value for the correlation dimension, at the peak, just before the drop. We then use the same data to obtain the lowest value in each section. The difference is the amount the correlation dimension has dropped. The data represented by figure 11.8 is given by, in table 11.5. This shows the length of each drop, and the distance before the next peak.

Table 11.5 Size of Drop and Distance to next peak

Section	Size of Drop	Distance to Next Peak
A	0.457	1065
B	0.123	530
C	0.088	153
D	0.050	248
E	0.211	429
F	0.174	575
G	0.201	?

The graph of the size of drop was plotted against the distance to the next peak, and the line of best fit calculated. This can be seen below, in graph 11.2.

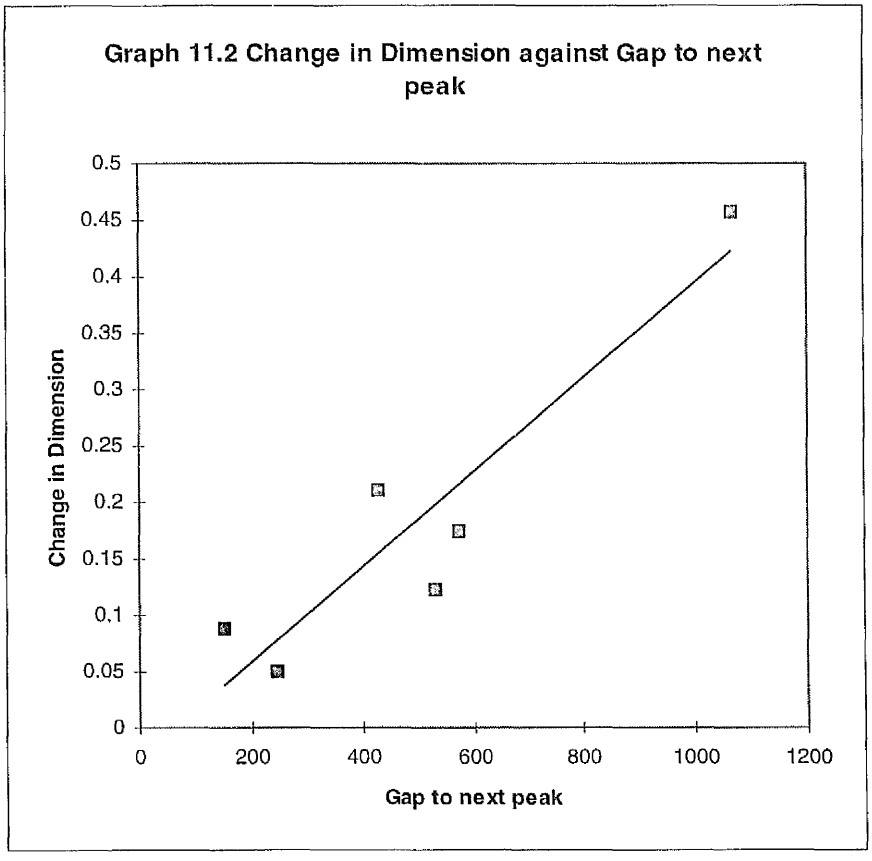

Obviously, the graph of 11.2 is not perfect, it is extremely dependent on the outlying point for section A. More data is essential before we can see that there is a straight line dependence. However, it is felt that there is enough of a trend to justify the tentative estimate of a line of best fit. Clearly, there will be a large uncertainty due to the scarceness of data points. The proposition is that using the data for the size of drop G, we can estimate the distance to the next peak. This is done using the line of best fit from graph 11.2. Using the value 0.201 for the size of the drop we can estimate the distance to the next peak. This resulted in us obtaining a value for the gap to be 540 data points. The error in this estimate can be measured from the graph. The error was found to be approximately 30 data points, i.e. our estimate for the distance to the next peak is 540 ± 30 data points. This means that we predict the next peak, and hence the next large earthquake, to be at position 4606 ± 30. This is very similar to the answer given by the last method, only with a slightly smaller range. The probability of success is once again 71%.

Unfortunately, as with method 1, no large earthquake occurred in this period. In fact, as stated before, no large earthquake has occurred up to data point 4900, which is quite a distance from our projected next earthquake. Once again, this does not mean that our method is a complete failure, but that an extended trial needs to be performed. As stated previously, there is not enough time to perform a large trial because of the time scale involved.

11.10 Conclusions

What can we conclude from this chapter? The correlation dimension does change, in some cases quite significantly, especially just before large earthquakes. We showed that the probability of this happening randomly, assuming earthquakes are distributed in time according to a Poisson process was negligible, and that there is almost certainly a link between the correlation dimension and the large earthquakes. Unfortunately, we have the problem of identifying when these changes are going to take place. It is easy to spot where these changes take place after they have happened, but it is not as easy to look forward in time!

One major worry is the problem of post-diction, which has been discussed a number of times. Are we only identifying these earthquakes after they have occurred? If so, the method will be no use as a predicting tool. We proposed two methods of altering the method to produce a forward looking prediction rule. Unfortunately, neither of the two methods appeared successful in this instance. It would, however, be nice to try an extended trial, where we wait for the results of a large number of events, but this could take years, and there is not enough time available. This very long time scale is one of the main problems in earthquake prediction work.

This work on the correlation dimension does look quite hopeful, and there may be some prospects for a more successful rule later on. As yet, however, a lot of work still needs to be done.

Chapter 12

Summary & Conclusions

In this thesis, we have introduced the theory of earthquake production, and some of the measurements that can be made regarding earthquakes. For example, we discussed in detail the definition of the *size* of an earthquake, and the distinction between magnitude, intensity and energy released. We also discussed the Gutenberg Richter Law.

In chapter 3, we reviewed the history of earthquake prediction. This review was a light hearted look at some of the crazy ideas which have been proposed past as possible earthquake precursors. While the review was light hearted, it should be remembered that earthquake prediction is a serious business, and should not be taken lightly, as millions of dollars and thousands of lives are at stake. A number of more serious precursors were reviewed in chapter 4. Many of these precursors provided a great deal of excitement for scientists in the 1970's; most of them, however, appear to have been nothing more than "noise", with the phenomena being unreproducable in other areas. We did suggest that were still a number of active fields of research. We also pointed out one of the main problems of earthquake prediction, namely the appearance of phenomena in one instance, followed by their non-appearance the next time. This variability results in the failure of many prediction schemes. It is almost as if the Earth gives us a "taster" to get our hopes up, before dashing them.

One of the most controversial, and interesting, modern prediction methods was outlined in chapter 5. The VAN method, proposed by Professor Varotsos and his group at the University of Athens, is a marvellous example of the pitfalls surrounding modern earthquake predictors. The VAN controversy highlights another problem, that as yet, no method of *testing* an earthquake prediction program has been unanimously agreed upon. Different scientists from all over the world have debated

the VAN method, and there has even been a number of journals which have devoted an entire issue to the discussion of the VAN method. There has been a lot of disagreement about the success, or not, of Varotsos' method. We have tried to present a balanced case for the VAN method, neither totally sceptical, nor totally pro-VAN.

In chapter 7, we presented the idea of self organised criticality, which was first postulated by *Bak, Tang & Weisenfeld.* We performed our own experiments, suggested our own model, and simulated our model using a computer program. The results of this analysis did not auger well for the prospects of earthquake prediction. It was felt that, if the Earth's crust is in a state of self-organised criticality, then the small scale properties of the distribution of the strain will affect strongly the size of the earthquake. Hence, to allow us to predict the size of an earthquake we would need to know the strain distribution very accurately.

In chapter 8, we discussed the possibility of using a mechanical model to simulate the occurrence of earthquakes, and we showed that the results were similar to those obtained in chapter 7.

Chapter 9, on Hurst Analysis, was a bit of a digression, but nonetheless is an important chapter. We showed that earthquakes were definitely *not* random events, and that their arrival times were correlated in some way. This was all due to the value obtained for the Hurst exponent. A value of 0.5 indicated a random series, while a value of over 0.5 implied the appearance of a persistent time series with long term correlations. We obtained values well in excess of 0.5, thus suggesting correlations between the earthquakes. This is an important chapter; in the past some people have tried to claim that large earthquakes could be thought of as random events. Chapter 9 shatters this proposal, as we also showed for large events that the Hurst exponent was greater than 0.5.

We then went on to discuss some of the mathematics behind fractal dimensions, before utilising this information to propose our own prediction method. This method was based on variations in the correlation dimension. We showed that

the correlation dimension dropped at around the time of large earthquakes. We were, however, concerned about the possible post-dictive nature of the method, and attempted to convert it to a predictive technique. Although our resulting methods were unsuccessful, it was felt that with further work and a much longer time scale, some more promising results could have been obtained.

One of the main problems with earthquake prediction is the time scale involved in large earthquakes. As already mentioned before, in some areas, the repeat time of large earthquakes can be almost 200 years. We have only been keeping accurate records for 100 years, at most, and in some cases a lot less than that. Thus, the lack of long term data is a major problem.

In conclusion, the problem of earthquake prediction while not easy has provided us with some hope of solution. It will not be easy, and a lot of hard work and further research is needed before a reasonable method can be accepted. This author, does not subscribe to the view that just because we haven't solved the problem in a hundred years we should give up. We feel that there is always hope for a more predictable future!

Appendices

Appendix A - The Modified Mercalli Scale

Intensity	Description
I.	Not felt except by a very few under especially favourable circumstances.
II.	Felt only by a few persons at rest, especially on upper floors of buildings. Delicately suspended objects may swing.
III.	Felt quite noticeably indoors, especially on upper floors of buildings, but many people do not recognise it as an earthquake. Standing automobiles may rock slightly. Vibration like passing of truck.
IV.	During the day felt indoors by many, outdoors by few. At night some awakened. Dishes, windows, doors disturbed; walls make creaking sound. Sensation like heavy truck striking building. Standing automobiles rocked noticeably.
V.	Felt by nearly everyone, many awakened. Some dishes, windows and so on broken; cracked plaster in a few places; unstable objects overturned. Disturbances of trees, poles, and other tall objects sometimes noticed. Pendulum clocks may stop.
VI.	Felt by all, many frightened and run outdoors. Some heavy furniture moved; a few instances of fallen plaster and damaged chimneys. Damage slight.
VII.	Everybody runs outdoors. Damage negligible in buildings of good design and construction; slight to moderate in well-built ordinary structures; considerable in poorly built or badly designed structures; some chimneys broken. Noticed by persons driving cars.
VIII.	Damage slight in specially designed structures; considerable in ordinary substantial buildings with partial collapse; great in poorly built structures. Panel walls thrown out of frame structures. Fall of chimneys, factory stacks, columns, monuments, walls. Heavy furniture overturned. Sand and mud ejected in small amounts. Changes in well water. Persons driving cars disturbed.
IX.	Damage considerable in specially designed structures; well-designed frame structures thrown out of plumb; great in substantial buildings, with partial collapse. Building shifted off foundations. Ground cracked conspicuously. Underground pipes broken.
X.	Some well-built wooden structures destroyed; most masonry and frame structures destroyed with foundations; ground badly cracked. Rails bent. Landslides considerable from river banks and steep slopes. Shifted sand and mud. Water splashed, slopped over banks.
XI.	Few, if any, masonry structures remain standing. Bridges destroyed. Broad fissures in ground. Underground pipelines completely out of service. Earth slumps and land slips in soft ground. Rails bent greatly.
XII.	Damage total. Waves seen on ground. Lines of sight and level distorted. Objects thrown into the air.

Appendix B

BASIC Programs for Chapter 7

Cellular Automata

1. Sand Box Program to Calculate Earthquake Sizes

```
REM Sand Box Program to Calculate Earthqauke Sizes
REM By Euan Fraser July 1997


REM This sets up the size of the arrays, and the arrays etc.
REM They are here so that we can change evrything by altering
REM one number.  The arrays are bigger than necessary so we can
REM see what happens at the boundary, if required.
CLS : size = 50: howmany = 10000: RANDOMIZE TIMER
DIM x(size + 2, size + 2): DIM magn(howmany + 1)
DIM critx(10000): DIM crity(10000)

REM This resets all the entries in the cellular automata.
FOR i = 1 TO size: FOR j = 1 TO size: x(i, j) = 0: NEXT j: NEXT i

REM We initially add lots of sand randomly, to ensure that we reach
REM a statistically stationary state.
total = 4 * size * size: PRINT total
FOR l = 1 TO total
addx = INT(size * RND) + 1
addy = INT(size * RND) + 1
x(addx, addy) = x(addx, addy) + 1
NEXT l

PRINT "Finished adding"
PRINT


REM We now redistribute sand from all the unstable blocks.
FOR i = 1 TO size
FOR j = 1 TO size
IF x(i, j) >= 4 THEN
x(i, j) = x(i, j) - 4
x(i, j - 1) = x(i, j - 1) + 1
x(i, j + 1) = x(i, j + 1) + 1
x(i + 1, j) = x(i + 1, j) + 1
x(i - 1, j) = x(i - 1, j) + 1
END IF
NEXT j
NEXT i

REM This is a special routine which speeds up the redistribution of
REM the strain by "remembering" the unstable blocks.
checkit:
s = 0
FOR i = 1 TO size
FOR j = 1 TO size
IF x(i, j) >= 4 THEN
s = s + 1
critx(s) = i
crity(s) = j
END IF
NEXT j
NEXT i

PRINT s

IF s > 0 THEN
FOR i = 1 TO s
```

```
x(critx(i), crity(i)) = x(critx(i), crity(i)) - 4
x(critx(i) - 1, crity(i)) = x(critx(i) - 1, crity(i)) + 1
x(critx(i) + 1, crity(i)) = x(critx(i) + 1, crity(i)) + 1
x(critx(i), crity(i) - 1) = x(critx(i), crity(i) - 1) + 1
x(critx(i), crity(i) + 1) = x(critx(i), crity(i) + 1) + 1
NEXT i
GOTO checkit
END IF

PRINT "Finished Setup"

REM We now print out the array, just for interests sake
REM This also helped with development, when ensuring that no blocks
REM had slipped through.
FOR i = 1 TO size: FOR j = 1 TO size: PRINT x(i, j); : NEXT j: NEXT i
PRINT
PRINT



REM We now add strain one unit at a time and redistribute, again using
REM our optimised routine.  We also count the number of blocks that
REM are involved in each earthquake.
counter = 1

DO
addx = INT(size * RND) + 1
addy = INT(size * RND) + 1
x(addx, addy) = x(addx, addy) + 1

IF x(addx, addy) >= 4 THEN
x(addx, addy) = x(addx, addy) - 4
x(addx - 1, addy) = x(addx - 1, addy) + 1
x(addx + 1, addy) = x(addx + 1, addy) + 1
x(addx - 1, addy) = x(addx - 1, addy) + 1
x(addx + 1, addy) = x(addx + 1, addy) + 1

magn(counter) = 1

checkit2:
s = 0
FOR i = 1 TO size
FOR j = 1 TO size
IF x(i, j) >= 4 THEN
s = s + 1
critx(s) = i
crity(s) = j
END IF
NEXT j
NEXT i

magn(counter) = magn(counter) + s

IF s > 0 THEN
FOR i = 1 TO s
x(critx(i), crity(i)) = x(critx(i), crity(i)) - 4
x(critx(i) - 1, crity(i)) = x(critx(i) - 1, crity(i)) + 1
x(critx(i) + 1, crity(i)) = x(critx(i) + 1, crity(i)) + 1
x(critx(i), crity(i) - 1) = x(critx(i), crity(i) - 1) + 1
```

```
x(critx(i), crity(i) + 1) = x(critx(i), crity(i) + 1) + 1
NEXT i
GOTO checkit2
END IF


END IF
PRINT counter;

counter = counter + 1
LOOP UNTIL counter > howmany


REM We now write the earthquakes to a data file for analysis
OPEN "c:\projects\phd\writeup\cells\magnit.dat" FOR OUTPUT AS #1
FOR i = 1 TO howmany
IF magn(i) > 0 THEN WRITE #1, magn(i)
NEXT i
```

Appendix C

BASIC Programs for Chapter 9

Hurst Anlaysis

1. Hurst Analysis of Coin Tossing

2. Probability Pack Cutting Experiment

3. Hurst Analysis of Biased Probability Pack

```
REM Hurst Analysis of Coin Tossing by Euan M. Fraser

REM This Program calculates the Rescaled Range for
REM a sequence of coin tossings
REM We set up the Arrays needed to store the numbers
CLS : DIM e(14000): DIM X(14000): RANDOMIZE TIMER

REM We calculate the difference between the number
REM of heads and tails for 10 tossses.
REM We repeat this 14000 times to produce our random sequence

FOR i = 1 TO 14000
FOR j = 1 TO 10
RANDOMIZE RND
RANDOMIZE RND
y = INT(RND * 2)
IF y = 0 THEN e(i) = e(i) - 1
IF y = 1 THEN e(i) = e(i) + 1
NEXT j
NEXT i

REM We start the analysis here. This allows us to vary the
REM time lag for the same sequence

LOOPY:
PRINT "What value do you want for tau?"
INPUT tau
newrs = 0

FOR k = 1 TO 10
sum = 0: start = INT(RND * (14000 - tau)) + 1: stp = start + tau

REM This calculates the average.

FOR i = start TO stp
sum = sum + e(i)
NEXT i
average = sum / tau


REM This calculates the accumulated deviation form the mean
REM as well as the sample standard deviation

oldX = 0
FOR t = start TO stp
X(t) = oldX + e(t) - average
oldX = X(t)
stdsum = stdsum + (e(t) - average) ^ 2
NEXT t

REM This section finds the maximum and minimum values for
REM X, the accumulated deviation from the mean

max = X(start)
FOR j = start TO stp - 1
IF X(j + 1) > X(j) THEN newmax = X(j + 1)
IF newmax > max THEN max = newmax
NEXT j
```

```
min = X(start)
FOR j = start TO stp - 1
IF X(j + 1) < X(j) THEN newmin = X(j + 1)
IF newmin < min THEN min = newmin
NEXT j

REM This calculates the range, standard deviation and finally,
REM the rescaled range.

range = max - min
stdev = ((1 / tau) * stdsum) ^ (.5)
RS = range / stdev
newrs = newrs + RS

NEXT k

REM This section prints out the results obtained,
REM before asking if you'd like to start again.
PRINT "Average R/S= ", newrs / 10
PRINT "Tau/2= ", tau / 2

PRINT "log R/S = ", LOG(newrs / 10)
PRINT "log tau/2= ", LOG(tau / 2)

PRINT "Do you want to go again?"
INPUT X$
IF X$ = "y" THEN GOTO LOOPY
```

```
REM Probability Pack Card Cutting Experiment by Euan M. Fraser

REM This program performs Hurst Analysis on the Probability Pack,
REM based on the experiment by Hurst.

REM We set up the arrays required, and the random number generator
CLS : RANDOMIZE TIMER: DIM card(52): DIM y(14000): DIM X(14000)

REM This is the Probability Pack we will use.
REM It has 13 1's,  8 3's, 4 5's and 1 7
REM It also has the same distribution of -1, -3, -5, -7
card(1) = -1: card(2) = 1: card(3) = -3: card(4) = -1: card(5) = 1
card(6) = 3: card(7) = 3: card(8) = -3: card(9) = 5: card(10) = -5
card(11) = -7: card(12) = 7: card(13) = -5: card(14) = 1: card(15) = 5
card(16) = 5: card(17) = -5: card(18) = 5: card(19) = 3: card(20) = -3
card(21) = -3: card(22) = 1: card(23) = -1: card(24) = 1: card(25) = 1
card(26) = 1: card(27) = -3: card(28) = -1: card(29) = 3: card(30) = -1
card(31) = -1: card(32) = 1: card(33) = -1: card(34) = -1: card(35) = -3
card(36) = -1: card(37) = -3: card(38) = 3: card(39) = 3: card(40) = 1:
card(41) = -1: card(42) = 1: card(43) = 3: card(44) = 1: card(45) = -1
card(46) = -1: card(47) = -5: card(48) = 1: card(49) = 3: card(50) = -1
card(51) = -3: card(52) = 1

REM This gets a series of Random numbers between 1 and 52
REM These will be used to determine which cards are drawn.
FOR i = 1 TO 14000
RANDOMIZE RND: RANDOMIZE RND
y(i) = INT(52 * RND) + 1
NEXT i

REM This calculates the distribution of the cards cut.
FOR i = 1 TO 14000
IF card(y(i)) = -1 THEN neg1 = neg1 + 1
IF card(y(i)) = 1 THEN pos1 = pos1 + 1
IF card(y(i)) = -3 THEN neg3 = neg3 + 1
IF card(y(i)) = 3 THEN pos3 = pos3 + 1
IF card(y(i)) = -5 THEN neg5 = neg5 + 1
IF card(y(i)) = 5 THEN pos5 = pos5 + 1
IF card(y(i)) = -7 THEN neg7 = neg7 + 1
IF card(y(i)) = 7 THEN pos7 = pos7 + 1
NEXT i
PRINT neg7, neg5, neg3, neg1, pos1, pos3, pos5, pos7

REM This is the start of the Hurst Analysis

LOOPY:
REM Here we ask for the time lag required
PRINT "What value do you want for tau?"
INPUT tau

REM This calculates the average value for our sequence.
sum = 0
FOR i = 1 TO tau
sum = sum + card(y(i))
NEXT i
average = sum / tau

REM This calculates the accumulated deviation from the mean
REM and the standard deviation.
```

```
oldX = 0: stdsum = 0
FOR t = 1 TO tau
X(t) = oldX + card(y(t)) - average
oldX = X(t)
stdsum = stdsum + (card(y(t)) - average) ^ 2
NEXT t

REM This section finds the max and min for this deviation
max = X(1)
FOR j = 1 TO tau - 1
IF X(j + 1) > X(j) THEN newmax = X(j + 1)
IF newmax > max THEN max = newmax
NEXT j

min = X(1)
FOR j = 1 TO tau - 1
IF X(j + 1) < X(j) THEN newmin = X(j + 1)
IF newmin < min THEN min = newmin
NEXT j


REM This calculates the range and the rescaled range
range = max - min
stdev = (1 / tau * stdsum) ^ (.5)
RS = range / stdev

REM This prints the  results obtained
PRINT "Range= ", range
PRINT " Standard deviation= ", stdev
PRINT "R/S= ", RS
PRINT "Tau/2= ", tau / 2

PRINT "log R/S = ", LOG(RS)
PRINT "log tau/2= ", LOG(tau / 2)

PRINT "Do you want to go again?"
INPUT X$
IF X$ = "y" THEN GOTO LOOPY
```

```
REM Hurst Analysis of Biased Probability Pack by Euan M. Fraser

REM This is a program which calculates the rescaled range for a
REM sequence of biased hands

REM We set up the required arrays etc.
REM e denotes the values for each draw
REM X denotes the values for the accumulated deviation from the mean
REM i.e. the "hurst statistic"
CLS : RANDOMIZE TIMER: DIM card(52): DIM e(15000): DIM X(15000)

REM This is our Probability Pack
card(1) = -1: card(2) = 1: card(3) = -3: card(4) = -1: card(5) = 1
card(6) = 3: card(7) = 3: card(8) = -3: card(9) = 5: card(10) = -5
card(11) = -7: card(12) = 7: card(13) = -5: card(14) = 1: card(15) = 5
card(16) = 5: card(17) = -5: card(18) = 5: card(19) = 3: card(20) = -3
card(21) = -3: card(22) = 1: card(23) = -1: card(24) = 1: card(25) = 1
card(26) = 1: card(27) = -3: card(28) = -1: card(29) = 3: card(30) = -1
card(31) = -1: card(32) = 1: card(33) = -1: card(34) = -1: card(35) = -3
card(36) = -1: card(37) = -3: card(38) = 3: card(39) = 3: card(40) = 1
card(41) = -1: card(42) = 1: card(43) = 3: card(44) = 1: card(45) = -1
card(46) = -1: card(47) = -5: card(48) = 1: card(49) = 3 card(50) = -1
card(51) = -3: card(52) = 1

REM Need to "deal" 2 hands, h1= hand1 and h2=hand2, rd is the random numbers
DIM h1(26): DIM h2(26): DIM rd(52)

REM This sets all the values to zero
FOR i = 1 TO 52: rd(i) = 0: NEXT i

REM This chooses 52 different random numbers between 1 and 52
FOR i = 1 TO 52
check:
rd = INT(52 * RND) + 1
FOR j = 1 TO 52
IF rd = rd(j) THEN GOTO check
NEXT j
rd(i) = rd
NEXT i

REM This Deals the two hands, alternate cards going to different hands
FOR i = 1 TO 52 STEP 2:  h1((i + 1) / 2) = card(rd(i)): NEXT i
FOR i = 2 TO 52 STEP 2: h2(i / 2) = card(rd(i)): NEXT i

REM Need a sort routine, to sort the hands into order to
REM help to remove highest and lowest members
FOR j = 1 TO 25
n = j
DO
IF h1(n) < h1(n + 1) THEN
SWAP h1(n), h1(n + 1)
IF n > 1 THEN n = n - 1
END IF
LOOP UNTIL h1(n) >= h1(n + 1)
NEXT j

FOR j = 1 TO 25
n = j
DO
```

```
IF h2(n) < h2(n + 1) THEN
SWAP h2(n), h2(n + 1)
IF n > 1 THEN n = n - 1
END IF
LOOP UNTIL h2(n) >= h2(n + 1)
NEXT j

FOR i = 1 TO 26: PRINT h1(i); : NEXT i
FOR i = 1 TO 26: PRINT h2(i); : NEXT i

counter = 1
FOR k = 1 TO 500
REM first thing we do is get the sign of the value of card drawn
REM cut the pack and choose a card
y = INT(52 * RND) + 1
REM Note the value on the card chosen
value = card(y)
sign = SGN(value)

IF sign > 0 THEN GOSUB positive
IF sign < 0 THEN GOSUB negative

REM FOR i = 1 TO 26: PRINT h1(i); : NEXT i
REM FOR i = 1 TO 26: PRINT h2(i); : NEXT i

REM Need to include the jokers now
REM WE will just stick them in as h1(0) and h2(0)


DO
RANDOMIZE RND: RANDOMIZE RND
randy = INT(RND * 27)
e(counter) = h1(randy)
counter = counter + 1
LOOP UNTIL (randy = 0)
REM PRINT "Cut at "; counter;
NEXT k

REM This is the start of the Hurst Analysis
Loopy:
REM We ask for the required time lag
PRINT "What Value do you want for tau?": INPUT tau

totalrs = 0
FOR n = 1 TO 25
start = INT(RND * (14000 - tau)) + 1: stp = start + tau


REM This calculates the average
sum = 0
FOR i = start TO stp
sum = sum + e(i)
NEXT i
average = sum / tau

REM This calculates the accumulated deviation from the mean
REM and the standard deviation
X(0) = 0: stdsum = 0
FOR i = start TO stp
```

```
X(i) = X(i - 1) + e(i) - average
stdsum = stdsum + (e(i) - average) ^ 2
NEXT i

REM This finds the max and min values for this deviation
max = X(start)
FOR j = start TO stp - 1
IF X(j + 1) > X(j) THEN newmax = X(j + 1)
IF newmax > max THEN max = newmax
NEXT j

min = X(start)
FOR j = start TO stp - 1
IF X(j + 1) < X(j) THEN newmin = X(j + 1)
IF newmin < min THEN min = newmin
NEXT j

range = max - min
stdev = ((1 / tau) * stdsum) ^ (.5)
RS = range / stdev
halftau = tau / 2
totalrs = totalrs + RS

NEXT n

PRINT "Tau/2=", halftau
PRINT "Average RS= ", totalrs / 25
PRINT "Ln (halftau)=", LOG(halftau)
PRINT "Ln (RS)=", LOG(totalrs / 25)


PRINT "Do you want to go again?"
INPUT c$
IF c$ = "y" THEN GOTO Loopy

END

positive:
numb = ABS(value)
FOR i = 1 TO numb
temp = h1(i)
h1(i) = h2(27 - i)
h2(27 - i) = temp
NEXT i
RETURN

negative:
numb = ABS(value)
FOR i = 1 TO numb
temp = h1(27 - i)
h1(27 - i) = h2(i)
h2(i) = temp
NEXT i
RETURN
```

Appendix D

C++ Program for Chapter 11

A New Prediction Method

Correlation Dimension Calculation Programme

```
#include<iostream.h>
#include<math.h>
#include<stdio.h>

// M is the number of datapoints we use (181 is the maximum)
// high is how far we go in each correlation integral calculation
// howmany is the number of times we read in new data and do a calculation
const M=181; const high=4000;

// These are the 3 classes we use, we had to do this because
// we had problems incorporating more data points
class XDATA
{
public:
unsigned short int x;
};

class ZDATA
{
public:
unsigned short int z;
};

class CORDATA
{
public:
float cor;
};

main()
{
// jump is the number of data points we read in at each cycle
unsigned short int i,j,l=0,temp,r,cont=0,jump=1;
float factor,q=2,power;
unsigned short int tempstore, offset=0;
unsigned short int begin,max=M;
unsigned long int howmany;

// Print the factor we use in the correlation integral
factor=pow(181*180,-1);cout << "Factor is " << factor << "\n";

// We set up the large arrays required for each of the calculations
XDATA * xdata = new  XDATA[M];XDATA *pxdata;
ZDATA * zdata= new  ZDATA[M*M];ZDATA *pzdata;
CORDATA * cordata = new CORDATA[high];CORDATA *pcordata;

// Open the file with data on the hard disk i.e. data.m
FILE *stream;
stream=fopen("data.m", "r+");

// Read the first lot of data , first (181-jump) points
// This means that when we read in the next "jump" amount
// of points that we now use the first 181 points in our data set
// We want to find out where along the data we want to start calculating
cout << "Where do you want to start the data from?"  << endl;
cout << "Remember that we will take the NEXT 181 points from the one specified";
cout << endl;
cin >> begin;
cout << endl;
```

```
cout << "How many values do you wish to calculate?";
cin >> howmany;
cout << endl;
cout << "\nNow reading in the appropriate data\n";

for (j=1; j<begin; j++)
{
fscanf(stream, "%d", &tempstore);
}
for (i=0; i<M; i++)
{
fscanf(stream, "%d", &tempstore);
pxdata= new XDATA;
pxdata->x=tempstore;
xdata[i]=*pxdata;
delete pxdata;
}

// Read new points in to replace the first jump amount of points
newdata:
for (j=0; j<jump; j++)
{
fscanf(stream, "%d", &tempstore);
pxdata=new XDATA;
pxdata->x=tempstore;
xdata[offset]=*pxdata;
delete pxdata;
cout << xdata[offset].x << " ";
if (offset<(M-1))
offset++;
else
offset=0;
}
// Calculate the time difference data from the original data
for (i=0; i<=M-1; i++)
 {
        for (j=0; j<=M-1; j++)
        {
        pzdata= new ZDATA;
        pzdata->z=abs(xdata[i].x-xdata[j].x);
        zdata[l]=*pzdata;
        delete pzdata;
        l++;
        }
 }

// Sort the Data into numerical order
// This speeds up the calculation in the long term
for (i=0;i<M; i++)
{
                j=0;
                do
                {
                        if (zdata[j+i*M].z>zdata[j+1+i*M].z)
                                {
                                        temp=zdata[j+1+i*M].z;
                                        zdata[j+1+i*M].z=zdata[j+i*M].z;
                                        zdata[j+i*M].z=temp;
                                        if (j>1)
```

```
                                        j=j-1;
                                        else
                                        j=0;
                                }
                        else
                        j++;
                } while (j<M-1);
}
cout << "Finished sorting";
// Calculate the correlation integral using the correct formula
// This is based on the Grassberger/Procaccia Algorithm
unsigned int counter,p;
float add;


for (r=1; r<high; r++)
{
        add=0;
        for (i=0; i<M; i++)
                {
                        p=0;
                        if (r<=zdata[M-1+i*M].z)
                                {
                                        do
                                                {
                                                p=p+1;
                                                }  while (r>zdata[p+i*M].z);
                                counter=p-1;
                                }
                        else
                        counter=M-1;

                        if (counter>0)
                        add=add+counter;
                }

        pcordata= new CORDATA;
        pcordata->cor=factor*add;
        cordata[r]=*pcordata;
        delete pcordata;
}

// This section writes the data to an output file
// This was used to ensure that we actually have a stright line when
// we plotted the data of log correaltion integral vs log r
// We don't use it here because we had difficuty having more than one stream
// open at the one time
FILE *stream2;
stream2=fopen("getdata.m", "w+");
fprintf(stream2, "function x=getdata\n\n");

for (r=1; r<high; r++)
{
fprintf(stream2,"x(%d)= %f;\n", r , log10(cordata[r].cor));
}
fclose(stream2);

cout << "Finished Calculating and Outputting Data ";
```

```
// Least square regression calculation
 int start=50,stop=3000;
 float sumx2=0,sumx=0,sumxy=0,sumy=0,sumy2=0,sxx=0,sxy=0,error=0,syy=0;
 float gradient[100];

 for(r=start;r<=stop; r++)
 {
 sumx2=sumx2+pow(log(r),2);
 sumx=sumx+log(r);
 sumxy=sumxy+log(r)*log(cordata[r].cor);
 sumy=sumy+log(cordata[r].cor);
 sumy2=sumy2+pow(log(cordata[r].cor),2);
 }

 sxx=sumx2-pow(sumx,2)/(stop-start);
 sxy=sumxy-sumx*sumy/(stop-start);
 syy=sumy2-pow(sumy,2)/(stop-start);
 error=(sxx*syy-pow(sxy,2))/((stop-start-2)*pow(sxx,2));
 gradient[cont]=sxy/sxx;
 cout << jump*(cont+1)+M+begin << "  " << "Gradient is " << gradient[ cont] << endl;

 cont++;
 if (cont<howmany)
 goto newdata;
 fclose(stream);

// We open a new file and put gradient data in it
// The first file is for use in MATLAB, and we need to multiply by jump
// then add M to get the actual position in the data set.
FILE *stream3;
stream3=fopen("grad.m", "a+");
// fprintf(stream3, "function X=grad\n\n");
for (i=0; i<howmany; i++)
fprintf(stream3, "X(%d)= %f;\n", i+1+begin/5, gradient[i]);
fclose(stream3);

// This file is for use in EXCEL, and gives the actual position in the Dataset
FILE *stream4;
stream4=fopen("grad2.m", "a+");
for (i=0; i<howmany; i++)
fprintf(stream4, "%d   %f\n", jump*(i+1)+M+begin, gradient[i]);
fclose(stream4);
}
```

Appendix E

Scaling Regions from Chapter 11

A New Prediction Method

Scaling Region Diagrams From MATLAB

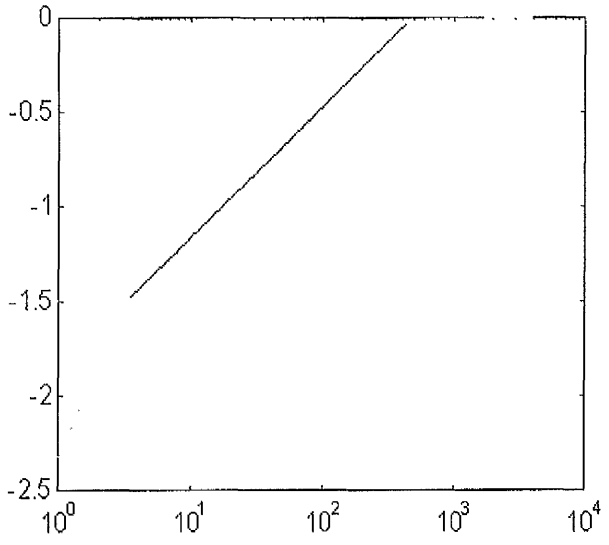
0
-0.5
-1
-1.5
-2
-2.5
10^0
10^1
10^2
10^3
10^4

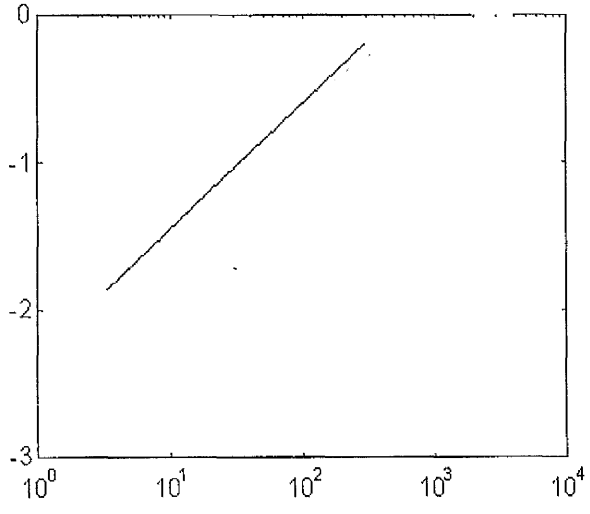
0
-1
-2
-3
10^0
10^1
10^2
10^3
10^4

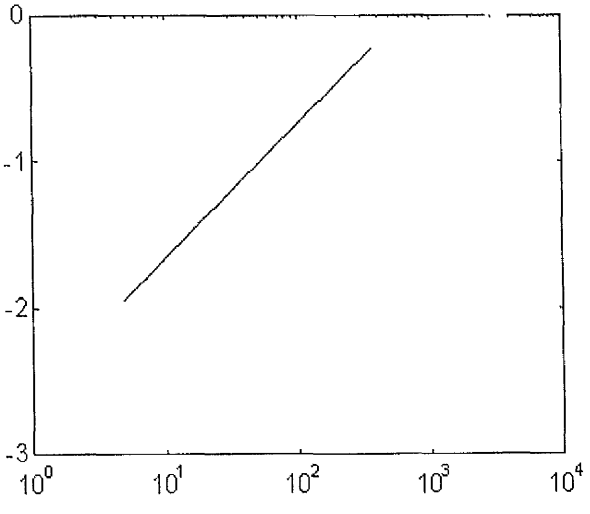
0
-1
-2
-3
10^0
10^1
10^2
10^3
10^4

Appendix F

Earthquake Catalogue Used in Hurst Analysis

catalog = NCSN
start time = 1967/01/01,00:00:00
end time = 1997/05/01,15:45:14
minimum magnitude = 5.0
maximum magnitude = 10
event_type = E

Date	Time	Lat	Lon	Depth	Mag	Magt	Nst	Gap	Clo	RMS	SRC	Event ID
1969/10/02	04:56:45.37	38.4882	-122.6770	0.03	5.60	ML	47	105	51	0.38	NCSN	
1969/10/02	06:19:56.12	38.4540	-122.7653	2.70	5.70	ML	57	138	58	0.27	NCSN	
1972/02/24	15:56:51.05	36.5947	-121.1965	...41	5.10	ML	7	125	5	0.15	NCSN	
1974/11/28	23:01:24.56	36.9203	-121.4657	6.06	5.05	MLm	51	61	4	0.14	NCSN	
1975/06/07	08:46:23.55	40.5453	-124.2710	23.07	5.30	ML	14	173	5	0.07	NCSN	
1975/08/01	20:20:05.19	39.4515	-121.5377	2.87	5.70	ML	4	158	12	0.00	NCSN	
1975/08/02	20:22:16.87	39.4638	-121.4737	0.60	5.10	ML	7	111	2	0.24	NCSN	
1975/08/02	20:58:56.27	39.4512	-121.4728	0.54	5.20	ML	7	93	1	0.18	NCSN	
1975/11/16	17:29:39.43	40.6305	-125.3728	3.66	5.00	ML	13	321	95	0.13	NCSN	
1976/11/26	11:19:32.41	41.0300	-124.9208	39.08	6.30	ML	13	317	71	0.08	NCSN	
1978/10/04	16:42:47.93	37.5350	-118.6982	22.88	5.40	coda	37	171	58	0.20	NCSN	
1978/10/04	17:39:02.41	37.5447	-118.6657	25.19	5.10	ML	170	89	56	0.32	NCSN	
1979/02/03	09:58:17.12	40.8667	-124.3130	23.14	5.20	ML	15	233	19	0.08	NCSN	
1979/02/22	15:57:28.63	39.9883	-120.1222	8.22	5.30	ML	47	75	20	0.22	NCSN	
1979/03/15	23:07:58.07	34.3293	-116.4367	1.88	5.20	coda	27	43	7	0.11	NCSN	
1979/04/07	06:18:48.28	41.3293	-125.5500	4.95	5.40	coda	10	332	134	0.10	NCSN	
1979/08/06	17:05:22.91	37.1035	-121.5118	8.89	5.60	MLm	80	97	6	0.07	NCSN	
1979/10/07	20:54:40.71	38.2550	-119.3303	5.00	5.00	ML	12	137	53	0.19	NCSN	
1980/01/24	19:00:08.72	37.8300	-121.7715	14.49	5.43	MLm	72	132	3	0.12	NCSN	
1980/01/24	19:01:01.55	37.8118	-121.7757	7.03	5.10	ML	10	149	2	0.22	NCSN	
1980/01/27	02:33:35.31	37.7488	-121.7037	14.70	5.08	MLm	75	103	8	0.11	NCSN	
1980/03/03	14:17:04.05	40.4228	-125.1103	12.15	5.10	ML	32	283	66	0.15	NCSN	
1980/05/25	16:33:43.93	37.5893	-118.8458	10.16	6.10	ML	12	163	2	0.27	NCSN	
1980/05/25	16:49:27.11	37.6747	-118.9152	8.86	6.00	ML	5	141	6	0.04	NCSN	
1980/05/25	19:44:49.45	37.4788	-118.8332	20.60	6.10	ML	7	299	12	0.13	NCSN	
1980/05/25	20:35:48.03	37.6258	-118.8407	8.15	5.70	ML	6	175	2	0.09	NCSN	
1980/05/25	20:59:22.38	37.6070	-118.8245	17.15	5.00	ML	4	143	2	0.00	NCSN	
1980/05/26	12:24:24.84	37.5582	-118.8765	7.86	5.10	ML	12	196	7	0.11	NCSN	
1980/05/26	18:57:55.49	37.5150	-118.8805	4.72	5.70	ML	15	215	10	0.13	NCSN	
1980/05/27	14:50:56.73	37.4927	-118.8132	16.06	6.20	ML	20	188	6	0.17	NCSN	
1980/06/29	07:46:13.27	38.0133	-118.6620	9.32	5.00	ML	20	78	11	0.14	NCSN	
1980/08/01	16:38:55.92	37.5643	-118.8742	6.21	5.40	ML	14	178	5	0.11	NCSN	
1980/09/07	01:30:42.02	38.0708	-118.5765	10.44	5.10	ML	8	97	17	0.08	NCSN	
1980/09/07	04:36:37.48	38.0647	-118.5905	10.95	5.50	ML	7	96	16	0.07	NCSN	
1980/09/07	06:48:09.91	38.0642	-118.5955	10.42	5.30	ML	12	110	16	0.06	NCSN	
1980/11/08	10:27:30.10	41.1488	-124.7535	2.24	6.90	coda	134	227	65	0.33	NCSN	
1980/11/28	18:21:12.99	39.2598	-120.4563	3.60	5.10	ML	132	82	38	0.29	NCSN	
1980/12/24	13:29:31.64	41.2948	-124.7577	3.51	5.00	ML	13	316	69	0.16	NCSN	
1980/12/28	22:58:08.77	38.1633	-118.3662	6.88	5.00	ML	12	135	16	0.11	NCSN	
1981/09/30	11:53:26.18	37.5852	-118.8665	5.65	5.94	MLm	14	109	4	0.10	NCSN	
1982/02/06	12:02:00.87	41.0907	-125.1617	0.84	5.19	MLm	56	295	91	0.20	NCSN	
1982/04/15	21:52:08.10	38.0898	-118.5397	26.21	5.05	MLm	55	75	51	0.28	NCSN	
1982/06/15	23:49:21.31	33.5472	-116.6753	11.61	5.10	coda	42	43	8	0.18	NCSN	
1982/09/24	07:40:24.04	37.8548	-118.1512	12.74	5.43	MLm	28	104	17	0.12	NCSN	
1982/10/15	10:58:42.66	32.9867	-125.6410	5.00	5.00	coda	395	277	505	0.40	NCSN	
1982/10/25	22:26:03.62	36.3198	-120.5093	12.14	5.36	MLm	66	87	12	0.14	NCSN	
1983/01/07	01:38:10.32	37.6380	-118.8988	9.75	5.32	MLm	7	140	18	0.05	NCSN	
1983/01/07	03:24:18.98	37.6295	-118.9350	5.82	5.37	MLm	11	109	3	0.07	NCSN	
1983/05/02	23:42:38.14	36.2267	-120.3175	9.84	6.48	MLm	36	212	3	0.07	NCSN	
1983/05/29	06:55:28.39	40.4470	-126.0770	5.17	5.47	MLm	21	299	147	0.18	NCSN	
1983/07/03	18:40:07.62	37.5598	-118.8445	11.52	5.26	MLm	20	112	4	0.08	NCSN	
1983/07/22	02:39:53.97	36.2358	-120.4117	7.98	5.20	Mamp	44	47	6	0.12	NCSN	
1983/07/25	22:31:39.48	36.2245	-120.4015	8.63	5.00	coda	43	41	6	0.09	NCSN	
1983/08/24	13:36:29.49	40.3818	-124.9120	16.77	5.58	MLm	42	257	50	0.19	NCSN	
1983/08/29	10:10:30.94	35.8383	-121.3393	5.89	5.35	MLm	50	181	9	0.07	NCSN	
1983/09/09	09:16:13.51	36.2195	-120.2790	7.01	5.40	coda	41	125	7	0.05	NCSN	
1983/12/20	10:41:00.81	40.4765	-125.9312	22.40	5.66	MLm	93	288	141	0.30	NCSN	
1984/02/16	11:14:57.59	39.9735	-117.8168	4.49	5.05	MLm	9	192	72	0.27	NCSN	
1984/04/24	21:15:18.75	37.3097	-121.6767	8.61	6.04	MLm	97	26	6	0.06	NCSN	
1984/09/10	03:14:01.95	40.6693	-127.7088	4.50	6.62	MLm	98	297	285	0.44	NCSN	
1984/11/23	18:08:25.33	37.4590	-118.6057	11.46	5.75	MLm	29	66	13	0.10	NCSN	
1984/11/23	19:12:34.77	37.4372	-118.6070	12.13	5.51	MLm	44	77	3	0.06	NCSN	
1984/11/26	16:21:40.85	37.4487	-118.6475	8.94	5.27	MLm	33	124	10	0.05	NCSN	
1985/03/25	16:05:12.78	37.4545	-118.6118	7.62	5.06	MLm	43	55	3	0.06	NCSN	
1985/08/04	12:01:55.88	36.1442	-120.1548	16.01	5.52	MLm	41	163	10	0.09	NCSN	
1986/01/26	19:20:50.92	36.8032	-121.2840	8.86	5.52	MLm	72	26	7	0.08	NCSN	
1986/03/31	11:55:39.81	37.4790	-121.6847	8.95	5.67	MLm	87	65	3	0.05	NCSN	
1986/07/08	09:20:44.59	34.0010	-116.6117	9.56	6.28	MLm	47	47	4	0.14	NCSN	
1986/07/13	13:47:30.12	34.0283	-119.2323	29.11	5.80	ML	103	291	68	0.49	NCSN	
1986/07/20	14:29:45.46	37.5668	-118.4380	6.67	5.81	MLm	39	54	9	0.05	NCSN	
1986/07/21	14:42:26.02	37.5388	-118.4425	10.48	6.21	MLm	41	56	10	0.06	NCSN	
1986/07/21	14:51:09.02	37.4928	-118.4280	11.78	5.61	MLm	30	243	14	0.05	NCSN	
1986/07/21	22:07:16.43	37.5940	-118.3768	6.10	5.46	MLm	16	316	33	0.16	NCSN	
1986/07/31	07:22:39.74	37.4732	-118.3653	8.10	5.68	MLm	43	83	6	0.07	NCSN	
1986/08/01	14:28:18.16	37.5158	-118.3962	9.00	5.13	MLm	27	54	8	0.08	NCSN	

1986/11/21 23:33:01.40 40.3550 -124.4272 17.64 5.11 MLm 5 258 15 0.01 NCSN
1986/11/21 23:34:19.09 40.3682 -124.3885 16.24 5.06 MLm 4 239 13 0.00 NCSN
1987/02/14 07:26:50.30 36.1732 -120.3407 15.46 5.25 MLm 43 50 8 0.09 NCSN
1987/07/31 23:56:57.79 40.4160 -124.3857 17.56 5.63 MLm 9 247 8 0.09 NCSN
1987/10/01 14:42:18.30 34.0263 -118.1198 9.08 5.92 MLm 57 197 68 0.40 NCSN
1987/10/04 10:59:34.98 33.9120 -118.1812 0.63 5.44 MLm 36 212 127 0.34 NCSN
1987/11/24 13:16:09.54 33.7365 -116.6948 4.77 5.50 coda 31 314 236 0.37 NCSN
1988/02/20 08:39:57.24 36.7947 -121.3108 9.69 5.08 MLm 68 25 3 0.08 NCSN
1988/06/10 23:06:42.53 34.9485 -118.7330 9.77 5.24 MLm 15 100 24 0.13 NCSN
1988/09/19 02:56:31.32 38.4562 -118.3393 6.62 5.35 MLm 55 65 16 0.11 NCSN
1988/12/03 11:38:25.05 34.1042 -118.1458 11.10 5.00 ML 42 284 101 0.24 NCSN
1988/12/16 05:53:08.11 34.1980 -116.8825 5.39 5.30 ML 19 302 168 0.09 NCSN
1989/01/19 06:53:24.90 33.7370 -118.6557 1.91 5.30 ML 102 279 90 0.35 NCSN
1989/03/03 07:03:58.44 35.7442 -124.5838 5.01 5.00 ML 30 332 259 0.27 NCSN
1989/08/08 08:13:27.37 37.1445 -121.9272 13.90 5.40 ML 89 51 3 0.09 NCSN
1989/10/18 00:04:15.26 37.0397 -121.8773 16.79 7.00 ML 84 70 1 0.08 NCSN
1989/10/18 00:41:23.76 37.1852 -122.0542 15.44 5.10 ML 52 60 4 0.15 NCSN
1990/01/16 20:08:20.33 40.2438 -124.3840 9.18 5.40 ML 211 249 76 0.42 NCSN
1990/02/28 23:43:44.77 34.3953 -118.2350 25.32 6.20 ML 114 275 79 0.44 NCSN
1990/04/18 13:53:51.28 36.9312 -121.6585 5.81 5.40 ML 95 47 0 0.15 NCSN
1990/04/18 15:46:03.43 36.9577 -121.6843 6.41 5.10 ML 88 34 1 0.13 NCSN
1990/10/24 06:15:17.77 38.1712 -119.1997 8.22 5.80 ML 25 316 53 0.06 NCSN
1991/06/28 14:43:56.07 34.3575 -118.1135 14.97 5.70 ML 91 264 79 0.29 NCSN
1991/07/13 02:50:14.37 42.0748 -125.8328 6.23 6.60 ML 115 305 181 0.38 NCSN
1991/08/16 22:26:11.23 41.7748 -126.1260 2.53 6.10 ML 167 299 186 0.28 NCSN
1991/08/17 19:29:40.62 40.2872 -124.2380 8.47 6.00 ML 10 185 12 0.09 NCSN
1991/08/17 22:17:08.55 41.7578 -126.0007 3.05 6.50 ML 101 298 176 0.22 NCSN
1991/09/17 21:10:28.95 35.8187 -121.3335 6.00 5.20 ML 52 174 11 0.08 NCSN
1992/03/08 03:43:04.45 40.2582 -124.2303 10.74 5.30 coda 15 191 9 0.15 NCSN
1992/04/23 04:50:23.44 33.9728 -116.4555 13.73 6.20 coda 62 212 104 0.36 NCSN
1992/04/25 18:06:05.18 40.3327 -124.2295 10.21 6.50 coda 9 116 12 0.06 NCSN
1992/04/26 07:41:39.76 40.4272 -124.5965 19.42 6.30 coda 17 253 23 0.15 NCSN
1992/04/26 11:18:25.66 40.3753 -124.5853 22.63 5.90 coda 12 263 24 0.07 NCSN
1992/05/04 16:19:49.84 33.9600 -116.2272 31.20 5.10 coda 40 164 83 0.32 NCSN
1992/05/18 15:44:18.70 33.9005 -116.3333 27.13 5.00 coda 67 154 85 0.37 NCSN
1992/06/28 11:57:33.72 34.2002 -116.4367 12.00 7.20 coda 239 164 115 1.16 NCSN
1992/06/28 14:43:28.54 34.5447 -117.4023 0.01 5.20 coda 25 287 160 0.44 NCSN
1992/06/28 15:05:29.04 34.2033 -116.8268 10.00 6.40 coda 345 297 267 1.58 NCSN
1992/06/29 10:14:20.91 36.6620 -116.1997 3.10 5.50 coda 86 271 151 0.23 NCSN
1992/06/29 16:01:53.10 34.2672 -116.8687 26.86 5.40 coda 45 288 109 0.29 NCSN
1992/07/05 21:18:39.07 34.9495 -117.2265 23.70 5.30 coda 167 275 80 0.33 NCSN
1992/07/09 01:44:01.42 34.4063 -117.1033 1.02 5.10 coda 49 287 141 0.29 NCSN
1992/07/11 18:14:15.85 35.2137 -118.0777 16.02 5.20 coda 19 139 22 0.10 NCSN
1992/07/24 18:14:44.28 34.2198 -116.7790 29.37 5.00 coda 39 291 84 0.26 NCSN
1992/09/15 08:47:18.94 34.3993 -116.8753 17.49 5.10 coda 51 275 78 0.28 NCSN
1992/11/27 16:01:09.40 34.7187 -117.6483 24.81 5.30 coda 96 274 98 0.42 NCSN
1992/12/04 02:09:08.30 34.7158 -117.5405 33.30 5.20 coda 71 276 107 0.31 NCSN
1993/03/25 13:34:37.14 45.1700 -123.4613 6.99 5.20 coda 253 324 319 0.97 NCSN
1993/05/17 23:20:49.00 37.1680 -117.7948 0.01 6.10 coda 177 211 48 0.24 NCSN
1993/05/28 04:47:39.82 35.1398 -119.1003 28.65 5.00 coda 23 80 19 0.16 NCSN
1993/09/21 03:28:55.31 42.2930 -122.0687 6.20 5.50 coda 134 240 75 0.46 NCSN
1993/09/21 05:45:35.15 42.3085 -122.1090 5.49 5.70 coda 143 238 76 0.49 NCSN
1993/12/04 22:15:19.59 42.2815 -122.0153 4.32 5.20 coda 5 117 8 0.02 NCSN 3
1994/01/17 12:30:54.46 34.1903 -118.5665 15.51 6.60 coda 64 196 45 0.24 NCSN
1994/01/17 23:33:29.77 34.2935 -118.7227 14.00 6.00 coda 114 184 31 0.38 NCSN
1994/01/18 00:43:07.89 34.3353 -118.7338 14.71 5.20 coda 99 154 26 0.38 NCSN
1994/01/19 21:09:27.41 34.3302 -118.7318 15.91 5.40 coda 99 154 26 0.35 NCSN
1994/01/29 11:20:35.64 34.2738 -118.5898 9.58 5.10 coda 63 185 36 0.27 NCSN
1994/03/20 21:20:11.17 34.1998 -118.5085 12.98 5.00 coda 72 162 42 0.26 NCSN
1994/09/01 15:15:42.30 40.4368 -126.8898 7.03 6.80 coda 344 286 217 0.50 NCSN
1994/09/12 12:23:43.20 38.8173 -119.6808 0.04 5.50 coda 344 161 87 0.52 NCSN
1994/12/26 14:10:29.14 40.7413 -124.3068 22.86 5.00 coda 31 196 30 0.11 NCSN
1995/02/19 04:03:11.95 40.5862 -126.0793 7.83 6.10 coda 294 274 148 0.56 NCSN
1995/08/17 22:39:58.48 35.7665 -117.6522 10.54 5.30 coda 17 140 11 0.10 NCSN
1995/09/20 23:27:35.90 35.7478 -117.6422 8.32 5.40 coda 16 141 13 0.12 NCSN
1996/03/30 15:22:23.76 37.6230 -118.8600 8.45 5.62 MLm 28 76 2 0.08 NCSN
1996/07/24 20:15:40.94 41.9358 -126.3233 5.00 5.00 coda 17 299 184 0.08 NCSN
1997/03/18 15:24:51.04 34.9800 -117.0640 17.18 5.00 coda 168 235 103 0.52 NCSN

Acknowledgements

I would like to thank my supervisor Dr. S.G. Hoggar for all his work and invaluable advice and suggestions regarding my project. I would also like to thank Dr. Ben Doody of the Geology Department for his help, and for allowing me to participate in some of his Geology classes. I must also thank Professor John Chapman of the Physics Department for answering a number of questions regarding mechanisms in solid state physics.

Finally, I would like to thank three fellow students for all their support and encouragement when things got tough. I would like to thank Mr. Paul Fotheringham, Mr. Graeme Morrison and last but not least Mr. Kenny McAlpine.

References

1. Aggarwal, Y.P., Sykes, L.R., Armbruster, J. and Sbar, M.L. [1973]. Premonitory Changes in Seismic Velocities and Prediction of earthquakes. *Nature*, **241,** pp101-104.

2. Bak, P. [1990]. Self-organised Criticality. *Physica A*, **163**, pp403-409.

3. Bak, P. & Paczuski, M. [1995]. Complexity, contingency, and criticality. *Proc. Natl. Acad. Sci. USA*, **92**, pp6689-6696.

4. Bak, P., Tang, C. & Weisenfeld, K. [1987]. Self Organised Criticality : An explanation of 1/f noise *Physical Review Letters*, **59,** pp381-384.

5. Bak, P., Tang, C. & Weisenfeld, K. [1988]. Self Organised Criticality. *Physical Review A*, **38**, p364.

6. Bak, P. & Tang, C. [1989]. Earthquakes as Self-organised Critical Phenomenon. *Journal of Geophysical Research*, **94**, B11, pp15635-15637.

7. Bakun, W.H., Steward, R.M., Tocher D. [1973]. Variations in Vp/Vs in Bear Valley in 1972. *Proceedings of the Conference on Tectonic Problems on the San Andreas Fault System*, Stanford University Publishing, edited by Kovach, R.L. and Nur, A.

8. Bakun, W.H. & Lindh, A.G. [1985]. The Parkfield, California Earthquake Prediction Experiment. *Science,* **229,** pp619-624.

9. Barriere, B. & Turcotte, D.L. [1994]. Seismicity and Self-Organized Criticality. *Physical Review E*, **49**, pp1151.

10. Bolt, B.A.[1993]. *Earthquakes* , W.H. Freeman and Company, New York.

11. Brown, S.R., Scholz, C.H. & Rundle, J.B. [1989]. A simplified spring-block model of earthquakes. *Geophysical Research Letters*, **18**, pp215-218.

12. Burridge, R. & Knopoff [1967]. Model and Theoretical Seismicity. *Bulletin of the Seismological Society of America*, **57**, pp341-371.

13. Carlson, J.M. & Langer, J.S. [1989a]. Mechanical Model of an earthquake fault. *Physical Review A*, **40**, pp 6470-6484.

14. Carlson, J.M. & Langer, J.S. [1989b]. Properties of Earthquakes generated by fault dynamics. *Physical Review Letters*, **62**, pp2632-2635.

15. Carlson, J.M. [1991]. Time intervals between characteristic earthquakes and correlations with smaller events : An analysis based on a mechanical model of a fault. *Journal of Geophysical Research*, **96 B3,** pp4255-4267.

16. Chen, K. & Bak, P. [1989]. Is the universe operating at a self-organised critical state? *Physics Letters A*, **140**, pp299-302.

17. Dologou, E., [1993]."A three year continuous sar[illegible] of officially documented predictions issued in Greece using the VAN method: 1987-1989," *Te[illegible]physics,* **224,** pp.189-202.

18. Doyle, H. [1995]. *Seismology*, John Wiley, Chichester.

19. Ellsworth, W.L., Lindh, A.G., Prescott, W.H., & Herd, D.G.[1981]. The 1906 San Fransisco earthquake and the seismic cycle. In *Earthquake prediction Maurice Ewing Series IV (Editors Simpson, D.W. and Richards, P.G.)* American Geophysical Union, Washington D.C..

20. Falconer, K. [1990]. *Fractal Geometry: Mathematical Foundations and Applications.* John Wiley & Sons, Chichester.

21. Feder, J. [1988]. *Fractals.* Plenum Press, New York.

22. Fedotov, S.A. [1965]. Regularities of the distribution of strong earthquakes in Kamchatka, the Kurile Islands and northeast Japan. *Tr. Inst. Fiz. Zemli, Akad. Nauk SSSR* , **36,** pp66-93.

23. Feller, W. [1951]. The Asymptotic Distribution of the Range of sums of independent random variables. *Annals of Mathematical Statistics,* **22,** pp427-432.

24. Feller, W. [1968]. *An Introduction to Probability Theory and its Applications,* Wiley, New York.

25. Geller, R.J. [1996]. Debate on evaluation of the VAN method : Editor's introduction. *Geophysical Research Letters*, **23**, pp1291-1294.

26. Gershenzon, N., Gokhberg, M., Karakin, A. Petviashvilli, N. & Rukunov, A. [1989]. Modelling the connection between earthquake preparation processes and crustal electromagnetic emission. *Physics of the Earth and Planetary Interiors,* **57**, pp129-138.

27. Gershenzon, N. & M. Gokhberg, [1993]. On the origin of electrotelluric disturbances prior to an earthquake in Kalamata, Greece. *Tectonophysics,* **224,** pp.169-174.

28. Godano, C. & Caruso, V. [1995]. Multifractal Analysis of earthquake catalogues. *Geophysical Journal International*, **121**, pp 385-392.

29. Grassberger, P. & Procaccia, I. [1983a]. Estimation of the Kolmogorov entropy from a chaotic signal, *Phsical Review A,* **28**, pp 2591-2593.

30. Grassberger, P. & Procaccia, I. [1983b]. Measuring the Strangeness of Strange Attractors, *Physica D*, **9**, pp 189-208.

31. Gutenberg, B. & Richter C.F.[1942]. Seismicity of the Earth. *Bulletin of the Geological Society of America*, **32**, pp163-191

32. Gutenberg, B. & Richter C.F.[1944]. Frequency of earthquakes in California. *Bulletin of the Seismological Society of America*, **34**, pp185-188

33. Gutenberg, B. & Richter, C.F. [1954]. *Seismicity of the Earth and Associated phenomena,* Princeton University Press, Princeton, New Jersey

34. Hadjioannou, D., F. Vallianatos, K. Eftaxias V. Hadjicontis and K. Nomikos, [1993]. Subtraction of the telluric inductive component from VAN measurements. *Tectonophysics,* **224,** pp.113-124.

35. Hamada, K. [1987]. Characteristics of successive occurrences of foreshock sequences preceding major earthquakes in the Kanto-Tokai Region of Japan. *Tectonophysics*, **138**, pp1-6

36. Hamada, K., [1993]."Statistical evaluation of the SES predictions issued in Greece: Alarm and success rates," *Tectonophysics,* **224,** pp.203-210.

37. Hentschel, H.G.E. & Procaccia, I. [1983]. The Infinite Number of Generalized Dimensions of fractals and strange attractors. *Physica D*, **8**, pp 435-444.

38. Hippel & McLeod [1978]. Preservation of the Rescaled Adjusted Range 1. A reassessment of the Hurst phenomenon. *Water Resources Research,* 14, pp

39. Hirabayashi, T., Ito, K. & Yoshii, T. [1992]. Multifractal Analysis of Earthquakes. *Pure and Applied Geophysics*, **138**, pp591-610

40. Hoggar, S.G. [1992]. *Mathematics for Computer Graphics*, University Press, Cambridge.

41. Honkura, Y. & Tanaka, N. [1996]. Probability of earthquake occurrence in Greece with special reference to the VAN predictions. *Geophysical Research Letters*, **23**, pp1417-1420.

42. Huang, J. & Turcotte, D.L. [1988]. Fractal Distributions of stress and strength and variations of b-value, *Earth and Planetary science letters,* **91**, pp 223-230.

43. Huang, J. & Turcotte, D.L. [1990]. Are earthquakes examples of deterministic chaos?, *Geophysical Research Letters*, **17**, pp 223-226.

44. Hurst, H.E. [1950]. Long Term Storage Capacity of Reservoirs. *Transactions of the American Society of Civil Engineers*, **116**, pp770-808

45. Hurst, H.E. [1952]. *The Nile* , London

46. Ito, K. & Matsuzaki, M. [1990]. Earthquakes as Self-organised critical phenomenon. *Journal of Geophysical Research,* **95**, B5, pp6853-6860

47. Ito, K. [1992]. Towards a new view of earthquake phenomena. *Pure and Applied Geophysics*, **138,** pp 531-548

48. Jackson, D.D[1996]. Earthquake prediction evaluation standards applied to the VAN method. *Geophysical Research Letters*, **23**, pp1363-1364.

49. Kadanoff, L.P. , Nagel, S.R.., Wu, R. & Zhou, S. [1989]. Scaling and universality in avalanches. *Physical Review A*, **39**, pp6524-6537

50. Kagan, Y.Y. & Jackson, D.D. [1991]. Seismic Gap Hypothesis : Ten Years After. *Journal of Geophysical Research,* **96,** pp 21419-21431

51. Kagan, Y.Y. [1996]. VAN earthquake predictions: An attempt at statistical evaluation. *Geophysical Research Letters*, **23**, pp1315-1318

52. Kagan, Y.Y. & Jackson, D.D. [1996]. Statistical tests of VAN earthquake predictions: Comments and reflections. *Geophysical Research Letters*, **23**, pp1433-1436.

53. Kanamori, H. & Anderson, D.L. [1975]. Theoretical Basis of some empirical relations in seismology. *Bull. Seism. Soc. Am.*, **65**, pp 1073-1095.

54. Kanamori, H. [1981]. The Nature of Seismicity Patterns before large earthquakes, Earthquake Prediction : An International Review.

55. Kearey, P. & Vine, F.J.[1996]. *Global Tectonics,* Blackwell Science, Edinburgh.

56. Korvin, G. [1992]. *Fractal Models in the Earth Sciences,* Elsevier Science Publishers, Amsterdam

57. Lapidus, D.F. [1990]. *Collins Dictionary of Geology*, Harper Collins, Glasgow

58. Lazarus, D. [1993]. Note on a possible origin for seismic electric signals. *Tectonophysics,* **224,** pp.265-267.

59. Lighthill, Sir J. [1996]. *A Critical Review of VAN*, World Scientific, Singapore

60. Main, I.G. [1995]. Earthquakes as Critical Phenomena: Implications for Probabilistic Seismic Hazard Analysis *Bull. Seism. Soc. Am.*, **85**, pp1299-1308.

61. Mandelbrot, B.B. [1967]. How long is the coast of Britain? Statistical self-similarity and fractional dimension. *Science*, **156**, pp636-638

62. Mandelbrot, B.B. [1982]. *The fractal Geometry of nature*, Freeman, San Fransisco.

63. Mandelbrot, B.B. [1989]. Multifractal Measures, especially for the Geophysicist, *Pure and Applied Geophysics*, **131**, pp5-42

64. Matsuzaki, M. & Takayasu, H. [1991]. Fractal features of the earthquake phenomenon and a simple mechanical model, *Journal of Geophysical Research*, **96 B12**, pp19925-1993

65. Mogi, K. [1968a]. Sequential Occurrence of recent great earthquakes. *Journal of Physics of The Earth*, **161**, pp30-36

66. Mogi, K. [1968b]. Some features of recent seismic activity in and near Japan. *Bulletin of the Earthquake Research Institute*, Univ Tokyo **46**, pp1225-1236

67. Mogi, K. [1979]. Two Kinds of Seismic Gap. *Pure and Applied Geophysics*, **117**, pp1171-1186

68. Mogi, K. [1985]. *Earthquake Prediction*, Academic Press, Tokyo

69. Mulargia, F. & Gasperini, P. [1992]. Evaluating the statistical validity beyond chance of VAN precursors. *Geophysical Journal International*, **111**, pp32-44

70. Mulargia, F. & Gasperini, P. [1996]. Precursor candidacy and validation: The VAN case so far. *Geophysical Research Letters*, **23**, pp1323-1326

71. Mulargia, F. & Gasperini, P. [1996]. VAN: Candidacy and validation with the latest laws of the game. *Geophysical Research Letters*, **23**, pp1327-1330

72. Nakanishi, H [1990]. Cellular Automaton model of earthquakes with deterministic dyanmics *Physical Review A*, **41**, pp7086-7089

73. Narkounskaia, G & Turcotte, D.L. [1992]. A cellular-automata, slider block model for earthquakes I. Demonstration of chaotic behaviour for a low-order system. *Geophysical Journal International*, **111**, pp250-258

74. Narkounskaia, G & Turcotte, D.L. [1992]. A cellular-automata, slider block model for earthquakes II. Demonstration of self-organised criticality for a 2-D system. *Geophysical Journal International*, **111**, pp259-269

75. Narkounskaia, G, Huang, J. & Turcotte, D.L. [1992]. Chaotic and Self-organised critical behaviour of a generalised slider-block model, *Journal of Statistical Physics*, **67**, pp1151

76. Nersesov, I.L.[1971]. *IZV Physics Solid Earth*, **15**, pp4

77. Nersesov, I.L.[1979]. *Experimental Seismology*, **1**, pp197

78. Nishenko, S.P. [1989]. Earthquake Hazrads and Predictions. In *Earthquake prediction Maurice Ewing Series IV (Editors Simpson, D.W. and Richards, P.G.)*, American Geophysical Union, Washington D.C.

79. Nishenko, S.P. & Sykes, L.R. [1993]. Comment on "Seismic Gap Hypothesis: Ten Years After". *Journal of Geophysical Research*, 98. pp9909-9916

80. Olami, Z. & Christensen, K. [1992]. Temporal correlations, universality, and multifractality in a spring-block model of earthquakes, *Physical Review A*, **46**, pp 1720-1723

81. Pepke, S.L. & Carlson, J.M. [1994]. Predictability of self-organising systems. *Physical Review E*, **50**, pp236-242

82. Peters, E.E. [1994]. *Fractal Market Analysis*, John Wiley & Sons Inc., New York

83. Rhoades, D.A. & Evison, F.F. [1996]. The VAN earthquake predictions. *Geophysical Research Letters*, **23**, pp1371-1375

84. Rikitake, T.[1968]. Geomagnetism and Earthquake Prediction, *Tectonophysics*, **6**, pp59-68

85. Rikitake, T. [1976]. *Earthquake Prediction*. Elsevier Science Publishers, New York

86. Rikitake, T. [1987]. Earthquake precursors in Japan: precursor time and detectability. *Tectonophysics*, **136**, pp265-282

87. Ritter, L. [1991]. *Earthquake Hazard Analysis: Issues and Insights*. Columbia University Press, New York

88. Rundle, J.B. [1988]. A Physical Model for Earthquakes, 1. Fluctuations and Interactions. *Journal of Geophysical Research*, **93 B6**, pp6237-6254

89. Rundle, J.B. [1988]. A Physical Model for Earthquakes, 2. Application to Southern California. *Journal of Geophysical Research*, **93 B6**, pp6255-6274

90. Rundle, J.B., Turcotte, D.L. & Klein, W. [1996]. *Reduction and Predictability of Natural Disasters*, Addison Wesley Publishing Company, New York.

91. Rundle, J.B. [1989]. A Physical Model for Earthquakes, 3. Thermodynamical Approach and its relation to nonclassical theories of nucleation, *Journal of Geophysical Research*, **94 B3**, pp2839-2855

92. Saleur, H., Sammis, C.G. & Sornette, D. [1996]. Discrete scale invariance, complex fractal dimensions and log-periodic fluctuations in seismicity, *Journal of Geophysical Research*, **101 B8**, pp17661-17677

93. Scholz, C.[1968]. The frequency magnitude relation of microfracturing in rock and its realtion to earthquakes. *Bulletin of the Seismological Society of America*, **58**, pp399-415

94. Schreider, S. Yu. [1990]. Formal Definition of Premonitory Seismic Quiescence. *Physics of the Earth and Planetary interiors*, **61**, pp113-127

95. Sears, F.W.[1987].. *University Physics*, Addison Wesley, Wokingham.

96. Silberschmidt, V.V. [1996]. Fractal approach in modelling earthquakes, *Geol. Rundsch.*, **85**, pp116-123.

97. Slifkin, L. [1993]."Seismic electric signals from displacement of charged dislocations. *Tectonophysics*, **224**, pp.149-152.

98. Sornette, A. & Sornette, D. [1989]. Self-Organised Criticality and Earthquakes. *Europhysics Letters*, **9**, pp197-202

99. Stavrakis, G.N. & Drakopoulos, J. [1996]. The VAN method: Contradictory and misleading results since 1981. *Geophysical Research Letters*, 23, pp1347-1350.

100.Suyehiro, S. [1966]. Difference between aftershocks and foreshocks in the relationship of magnitude to frequency of occurrence for the great Chilean earthquake of 1960. *Bulletin of the Seismological Society of America*, **56**, pp185-200

101.Turcotte, D.L. [1986]. Fractals and Fragmentation, *Journal of Geophysical Research*, **91**, pp 1921-1926

102.Turcotte, D.L. [1989]. A fractal approach to probabilistic seismic hazard assessment, *Tectonophysics*, **167**, pp 171-177.

103.Turcotte, D.L. [1986]. A Fractal model for crustal deformation, *Tectonophysics*, **132**, pp 261-269.

104.Utada, H., [1993]. "On the physical background of the VAN earthquake prediction method," *Tectonophysics*, **224**, pp.153-160.

105.Utada, H. [1996]. Difficulty of statistical evaluation of an earthquake prediction method. *Geophysical Research Letters*, **23**, pp1391-1395.

106.Utsu, T. [1969]. Aftershocks and Earthquake Statistics. *Fac. Sci., Hokkaido University,* Ser VII, **3**, pp129-195

107.Vallianatos, F. and K. Eftaxias, [1993]."A model for the influence of local inhomogeneities on the magnetotelluric variations at two VAN stations in Greece."*Tectonophysics*, **224**, pp.125-130.

108.Varotsos, P., Alexopoulos, K., Nomicos, K. & Lazaridou, M. [1988]. Official earthquake prediction procedure in Greece, *Tectonophysics*, **152**, pp 193-196.

109.Varotsos, P., K. Alexopoulos and M. Lazaridou, [1993a]. "Latest aspects on earthquake prediction in Greece based on seismic electric signals. II," *Tectonophysics*, **224**, pp.1-37.

110.Varotsos, P., K. Alexopoulos and M. Lazaridou, [1993b]. "A reply to 'Evaluation and interpretation of thirteen official VAN-telegrams for the period September 10, 1986 to April 28,1988, Ō by J. Drakopoulos, G. Stavrakakis and J. Latoussakis," *Tectonophysics*, **224**, pp.237-250.

111.Varotsos, P., K. Alexopoulos, M. Lazaridou and T. Nagao, [1993]. "Earthquake predictions issued in Greece since February 6, 1990," *Tectonophysics*, **224**, pp.269-288.

112.Varotsos, P., Eftaxias, K., Vallianatos,F. & Lazaridou, M.[1996]. Basic principles for evaluating an earthquake prediction method. *Geophysical Research Letters*, **23**, pp1295-1298

113.Varotsos, P., Eftaxias, K., Lazaridou, M., Dologlou, E. & Hadjicontis, V. [1996]. Reply to "Probability of chance correlations of earthquakes with predictions in areas of heterogeneous seismicity rate: The VAN Case." *Geophysical Research Letters*, **23**, pp1311-1314

114.Varotsos, P. & Lazaridou, M. [1991]. Latest aspects of earthquake prediction in greece based on seismic electric signals. *Tectonophysics*, 188, pp 321-347.

115.Varotsos, P. & Lazaridou, M. [1996]. Reply to "VAN earthquake predictions: An attempt at statistical evaluation" *Geophysical Research Letters*, **23**, pp1319-1322

116.Varotsos, P., Eftaxias, K. & Lazaridou, M. [1996]. Reply I to "VAN: Candidacy and validation with the latest laws of the game," and "Precursor candidacy and validation: The VAN case so far." *Geophysical Research Letters*, **23**, pp1331-1334.

117.Varotsos, P., Eftaxias, K. & Lazaridou, M. [1996]. Reply II to "VAN: Candidacy and validation with the latest laws of the game." and "Precursor candidacy and validation: The VAN case so far." *Geophysical Research Letters*, **23**, pp1335-1338.

118.Varotsos, P., Eftaxias, K. & Lazaridou, M. [1996]. Reply to "The VAN method: Contradictory and misleading results since 1981." *Geophysical Research Letters*, **23**, pp1351-1354.

119.Varotsos, P., Eftaxias, K. & Lazaridou, M. [1996]. Reply to "A false alarm based on electrical activity recorded at a VAN station in northern Greece in December 1990.". *Geophysical Research Letters*, **23**, pp1359-1362.

120.Varotsos, P., Eftaxias, K., Skordas, E., Hadjicontis, V. & Lazaridou, M.[1996]. Reply to "Rebuttal to replies I and II by Varotsos et al." *Geophysical Research Letters*, **23**, pp1341-1342.

121.Varotsos, P., Hadjicontis, V., Eftaxias, K., Skordas, E., & Lazaridou, M.[1996]. Reply to "Re-Rebuttal to the reply of Varotsos et al." *Geophysical Research Letters*, **23**, pp1345-1346.

122.Varotsos, P., Eftaxias, K., Lazaridou, M., Antonopoulos, G., Makris, J. & Poliyiannakis, J. [1996]. Summary of the five principles suggested by Varotsos et al.[1996]. and the additional questions raised in this debate. *Geophysical Research Letters*, **23**, pp1449-1452.

123.Weisenfeld, K. , Tang, C. & Bak, P. [1989]. A Physicist's Sandbox. *Journal of Statistical Physics*, **54**, pp1441-1458

124.Whitworth, W.A. [1886]. *Choice and Chance*, Cambridge (4th Edition)

125.Wyss, M. & Byerlee, J.D. [1978]. *Rock Friction and Earthquake Prediction,* Birkhauser Verlag, Basel & Stuttgart.

126.Wyss, M. [1996]. Inaccuracies in seismicity and magnitude data used by Varotsos and coworkers *Geophysical Research Letters*, **23**, pp1299-1302

127.Wyss, M[1997]. Second round of evaluations of proposed earthquake precursors. *Pure and Applied Geophysics*, **149**, pp3-16.

128.Wyss, M. & Allmann, A. [1996]. Probability of chance correlations of earthquakes with predictions in areas of heterogeneous seismicity rate: The VAN Case. *Geophysical Research Letters*, **23**, pp1307-1310

129.Yeats, R.S. , Sieh, K. & Allen, C.R. [1997]. *The Geology of Earthquakes*, Oxford University Press